AD-766 779

THE STUDY OF THE INTERACTION OF INTENSE PICOSECOND LIGHT PULSE WITH MATERIALS

Chi H. Lee, et al

Maryland University

Prepared for:

Army Research Office-Durham
Advanced Projects Research Office

26 July 1973

TECHNICAL
RESEARCH
REPORT

THE STUDY OF THE INTERACTION OF INTENSE PICOSECOND LIGHT PULSE WITH MATERIALS

A QUARTERLY TECHNICAL REPORT

SUBMITTED TO

THE U.S. ARMY RESEARCH OFFICE

PERIOD

March 22, 1973 to June 21, 1973

REPORTED BY

CHI H. LEE
and
Vutthi Bhanthumnavin

Approved for Public Release
Distributions Unlimited.

DEPARTMENT OF
ELECTRICAL ENGINEERING

UNIVERSITY OF MARYLAND

COLLEGE PARK, MARYLAND 20742

AR 70-31 Unclassified

Security Classification

3200.8 (Att 1 to Encl 1)
Mar 7, 66

DOCUMENT CONTROL DATA - R & D

(Security classification of title, body of abstract and indexing annotation must be entered when the overall report is classified)

1. ORIGINATING ACTIVITY (Corporate author)
Department of Electrical Engineering
University of Maryland
College Park, Maryland 20742

2a. REPORT SECURITY CLASSIFICATION
Unclassified

2b. GROUP

3. REPORT TITLE
The Study of the Interaction of Intense Picosecond Light-Pulse with Materials: Nonlinear Optical Interactions in KDP Prisms

4. DESCRIPTIVE NOTES (Type of report and inclusive dates)
A quarterly technical report. March 22, 1973 to June 21, 1973

5. AUTHOR(S) (First name, middle initial, last name)
Chi H. Lee and Vutthi Bhanthumnavin

6. REPORT DATE
July 26, 1973

7a. TOTAL NO. OF PAGES
~~137~~ 148

7b. NO. OF REFS
92

8a. CONTRACT OR GRANT NO.
DA-ARO-D-31-124-72-G82

b. PROJECT NO.
ARPA Order No. 675 Am. 9

c. Program Code No. 9E20

d.

9a. ORIGINATOR'S REPORT NUMBER(S)
TR-014

9b. OTHER REPORT NO(S) (Any other numbers that may be assigned this report)

10. DISTRIBUTION STATEMENT
Reproduction in whole or in part is permitted for any purpose of the United States Government.

11. SUPPLEMENTARY NOTES

12. SPONSORING MILITARY ACTIVITY
ARPA and U.S. Army Research Office

15. ABSTRACT

The intensity of the second harmonic light in total reflection and in transmission from uniaxial KDP crystals immersed in an optically denser liquid 1-bromonaphthalene have been measured as a function of angle of incidence of the fundamental beam from a mode locked Nd:glass laser. The results agreed well with the theoretical predictions of theory given by Bloembergen and Pershan. In particular, the existence of a Nonlinear Brewster's angle of a transparent medium (KDP), with nonlinear polarization in the plane of reflection, has been first demonstrated. The transmitted second harmonic intensity under noncollinear phase matched condition by means of two beam spatial mixing (TBSM) in the KDP crystal, using Q-switched Nd:glass laser pulses, was observed as a function of the angle of incidence. The result was in good agreement with the theory of Bloembergen and Pershan. As a consequence, this result was utilized to measure the second order intensity auto-correlation function of Nd:glass laser radiation.

DD FORM 1 NOV 68 1473

Unclassified

Security Classification

AGO 5698A

14 KEY WORDS	LINK A		LINK B		LINK C	
	ROLE	WT	ROLE	WT	ROLE	WT
Nonlinear optics						
KDP						
Second harmonic generation						
Nonlinear Brewster's angle						
Total internal reflection						
Picosecond pulses						
Mode-locked laser						

Quarterly Technical Report

for

Period March 22, 1973 to June 21, 1973

Submitted to the U.S. Army Research Office

ARPA:	675, Am 9
Program Code Number:	9E 20
Name of Grantee:	University of Maryland
Effective Date of Grant:	March 22, 1972
Grant Expiration Date:	March 21, 1973
Principle Investigator and Phone Number:	Dr. Chi H. Lee (301) 454-2443
Grant Number:	DA-ARO-D-31-124-71-G82
Research Assistants:	Mr. S. Jayaraman Mr. V. Bhanthumnavin Mr. S. Mak
Short Title of Work:	"The Study of the Interaction of Intense Picosecond Light Pulses with Materials"
Report by:	Chi-Hiung Lee Chi H. Lee

1b

NONLINEAR OPTICAL INTERACTIONS IN KDP PRISMS

by

Vutthi Bhanthumnavin
and
Chi H. Lee

ABSTRACT

The intensities of the second harmonic light in total reflection and in transmission from uniaxial KDP cyrstals immersed in an optically denser liquid 1-bromonaphthalene have been measured as a function of angle of incidence of the fundamental beam from a mode locked Nd:glass laser. In the experiment, various crystallographic orientations of the KDP crystal were used. The results agreed well with the theoretical predictions of Bloembergen and Pershan[12]. In particular, the existence of a nonlinear Brewster's angle of a transparent medium (KDP), with nonlinear polarization in the plane of reflection, has been first demonstrated. The transmitted second harmonic intensity under phase matched condition by birefringence[33, 34], in the oblique direction was found to vary more than ten orders of magnitude in the angular range of interest.

The transmitted second harmonic intensity under noncollinear phase matched condition by means of two beam spatial mixing (TBSM) in the KDP crystal, using Q-switched Nd:glass laser pulses, was observed as a function of the angle of incidence. The result was in good agreement with the theory of Bloembergen and Pershan[12]. As a consequence, this result was utilized to measure the second order intensity auto-correlation function of Nd:glass laser radiation. The picosecond pulsewidth of Nd:glass laser radiation was measured to be 5.29 picosecond.

TABLE OF CONTENTS

LIST OF FIGURES

CHAPTER I
INTRODUCTION

A. General Introduction

Since the advent of LASER[1] (Light Amplification by Stimulated Emission of Radiation) or optical maser, the coherent, high intensity and monochromatic light sources are available for nonlinear optical processes in materials. Franken and his co-worker[2], in 1961, performed an artfully devised experiment in which they proved that the ruby laser light of wavelength 6943Å focused within a quartz crystal contained on emerging a small admixture of a second harmonic of a wavelength 3471.5Å. The discovery of this phenomenon, which has its origin in the nonlinear optical properties of matter, became the starting point of vast development further enhanced by the rapid evolution of laser technique. This has led to the detection of a number of novel optical effects, which have since been discussed in various monographs[3, 4] and review articles[5-10]. Furthermore, the theoretical essentials of coherent nonlinear processes are to be found in the fundamental work of Armstrong et al[11], Bloembergen and Pershan[12], Akhamonov and Khokhlov[13] and certain other authors[14-17].

When low intensity light propagates in a transparent medium, it does not affect the optical properties of the medium because the electric polarization $\vec{P}(\vec{r},t)$ induced in it is a linear function of the electric field $\vec{E}(\vec{r},t)$ of the light wave. A linear relationship between $\vec{P}(\vec{r},t)$ and $\vec{E}(\vec{r},t)$ results immediately in Lorentz' s classical electron theory[18]. To a linear approximation, the solutions of Maxwell' s equations satisfy the principle of superposition, which states that the

electromagnetic waves simultaneously transversing a linear medium propagate independently without interacting upon one another. In linear, optically transparent medium, electromagnetic waves accordingly propagate without distortion, the refractive index n depending solely on the properties and thermodynamic state of the medium but not depending on the incident light intensity. All optical phenomena depend linearly on the electric field strength as long as the medium under investigation is probed by low intensity light wave and is not acted upon simultaneously by external field.

However, when a transparent medium is transversed by light of very high intensity, i.e. laser, its refractive index n and electric permitivity become dependent on the intensity of the incident light. This has indeed been directly observed, with the help of giant pulsed ruby lasers, by various authors[2, 19-21]. Lasers operating continuously or pulsed radiate a parallel and monochromatic light, coherent in space and time, and contain a flux of immense energy density. The very high light intensities of the beams, never achieved by ordinary light, cause the index of refraction to depend on the electric field $\vec{E}(\vec{r}, t)$ of the beam. An electromagnetic wave of such strength, inducing optical nonlinearity in the medium, itself undergoes distortion when propagating through the medium. By Fourier spectral analysis, the original wave of fundamental frequency ω is now additionally accompanied by harmonic components of double frequency 2ω, triple frequency 3ω and higher harmonics.[3-6, 11-13]. Furthermore, due to the availability of high

intensity and ultrashort light pulses, various nonlinear optical processes, e.g. self focusing phenomena, self induced transparency, stimulated Raman emission, photon echo, have been observed and well described in various articles[22-24] and reviewed article[9, 10, 17]. In the present work, which will be presented here thereafter, only second harmonic generation in reflection and transmission from an uniaxial crystal KDP using Nd:glass laser radiation as fundamental beam, will be described in detail, and to a lesser extense, an attempt to generalized the effect to third order is also included.

B. Review of Previous Experiments

1. Harmonic Generation in Reflection. Theory of interactions between light waves in a nonlinear media was given by Armstrong. Bloembergen, Ducuing and Pershan[11]. Consequently, the theory of light wave at the boundary of nonlinear media was given by Bloembergen and Pershan[12]. Second harmonic generation in reflection was first observed by Ducuing and Bloembergen in 1963[25, 26]. Both the directional and the polarization properties of second harmonic reflection from III-V semiconductor mirrors, e.g. GaAs, have been verified. Furthermore, Bloembergen has predicted[12] and demonstrated[26] SHG in reflection by using two fundamental beams of Q-switched ruby laser spatial mixing in GaAs mirror. Chang and Bloembergen[27] have verified the laws for the reflected intensity of second harmonic light. In the experimental verification they used various crystallographic cuts of cubic crystal GaAs mirrors upon which the fundamental beam of Q-switched ruby laser

was incident. In that experiment Chang and Bloembergen have first demonstrated the existence of Nonlinear Brewster Angle for the absorbing nonlinear medium. Bloembergen and Lee[28] observed the internal reflected second harmonic intensity (SHI) generated at 4860$\mathring{A}$ by an incident beam totally reflected by nonlinear medium $NaClO_3$ and KH_2PO_4 (KDP), immersed in an optically denser linear fluid (1-bromonaphthalene). The incident beam was the stimulated Stoke beam induced by Q-switched ruby laser in H_2 gas. In accordance with theory given by Bloembergen and Pershan[12], this experiment shows anomalously high reflected harmonic intensity because of the enhancement of the intensity by phase matching at the critical angle of incidence for total reflection. Furthermore, a detailed discussion and experimental verification to the theory[12] concerning total reflection and two beam spatial mixing on $NaClO_3$ has been given by Bloembergen, Simon and Lee[29].

The first experiment in obtaining an ultraviolet third harmonic generation in reflection was done by Bey, Giuliani and H. Rabin[30]. With the help of previous work of Bloembergen and Lee[28], they introduced in the experiment anomalous dispersion into normally unmatched medium. They obtained phase matched third harmonic generation (THG) at 3530$\mathring{A}$ of the Nd:glass laser line by introducing dye molecule of fuchsin red into the liquid medium of hexafluoroacetone sesquihydrate. Wang and Baarden[31] reported studies of THG reflected from the boundary of solids including metal, semiconductors, alkali

halides and glass. Recently, Burns and Bloembergen[32] used pico-second pulse from Nd:glass laser to study reflected THG in absorbing media of cubic or isotropic symmetry.

2. Harmonic Generation in Transmission. The first experiment of second harmonic generation was performed by Franken et al[2] in the transmitted direction. They used ruby laser beam focused in a piece of quartz and observed, after separation the fundamental by a prism, a second harmonic of wavelength 3471.5Å. Since then, the second harmonic of light has been observed in various piezoelectric and other nonlinear material. Giordmaine[33], Maker et al[34] in 1962, demonstrated independently the use of birefringence of uniaxial crystal to achieve phase matching condition under which the second harmonic of light is enhanced. Armstrong et al[11] and Kleinmann[14] introduced the concept of coherent length along which the fundamental and second harmonic beams will travel in step with respect to each other. Second harmonic generation with double refraction has been given in detailed by Boyd et al[35]. Miller[36] used Nd:$CaWO_4$ laser to observe second harmonic of light from $BaTiO_3$, KDP, ADP CdS and strongly nonlinear $LiNbO_3$ and $LiTa_3$[37]. Geusic et al[38] observed SHG at 5320Å in Ba_2NaNbO_{15} and $K_6Li_4NbO_3$ using slightly focused, continuously pumped, repetitively Q-switched Nd:YAG laser. Using ruby laser and Nd:glass laser Kurtz et al[39] and Nath[40] made a novel study of SHG from strongly nonlinear materials HIO_3 and $LiIO_3$ respectively. Askin et al[41] observed continuous SHG using the infrared transition 1.1526μ of the He-Ne

gas laser with a focused and a non-focused beam to measure the second order susceptibility component d_{36} of KDP. With the help of temperature tuning, phase matched SHG in $LiNbO_3$ without double refraction using infrared transition 1.1526μ of He-Ne gas laser was demonstrated by Miller[42]. Bloembergen et al[29] demonstrated two beam spatial mixing in $NaClO_3$ near critical angle of incidence and observed SHG in transmitted direction. The equation for the nonlinear phase matched condition which requires all three propagation vectors of the fundamental and of the second harmonic have to form a closed loop was first pointed out by Tien[43] and later by Boyd[44]. Phase matched SHG without double refraction (or noncollinear phase matched SHG) in ADP, KDP using He-Ne line of 1.1526μ was demonstrated by A. Askin et al[45]. Later noncollinear phase matched SHG in $LiIO_3$ was performed with Q-switched Nd:YAG laser by Shinsuke Umegaki et al[46]. Recently Aggarwal[47] achieved noncollinear phase matching in GaAs by using a carbon dioxide laser.

The first experiment in obtaining an ultraviolet third harmonic at 2314 Å using ruby laser is due to Terhune et al[20] in calcite and subsequently in cubic crystal LiF, KCl, CaF and liquids by Maker[48, 49]. Bey et al[50] provided the earliest experimental evidence that phase matching can be achieved in harmonic processes by the introduction of anomalous dispersion into a normally unmatched medium. They obtained phase-matched THG at 3530Å of the Nd:glass laser line by introducing dye molecule (fuchsin red) into a liquid medium (hexafluoroacetone

sesquihydrate). Their experiment was extended by Chang and Galbraith[57] to other solvents of different index mismatch and to another dye, methylene blue. Bey et al[52] reported interesting THG studies, which prove that a linearly polarized laser beam generates a third harmonic signal, while a circularly polarized beam does not, in accordance with theory. Ward and New[53] observed THG at 2314Å in gases He, Ne, Ar using a focused ruby laser beam. Harris et al[54] made a theoretical analysis and proposed THG in phase matched alkali metal vapors, e.g. Li, K, Na, Rb, Cs. Consequently Young[55], Miles[56] demonstrated THG in phase matched Rb vapor and in the alkali metal vapors respectively.

3. Measurement of Picosecond Pulsewidth by Means of Nonlinear Optical Method. The Nd:glass laser has recently become an important research tool. Not only does it constitute one of the most powerful sources of coherent radiation in terms of peak power, but it also distinguishes itself as a source of ultrashort light pulse. The emission of trains of short pulses produced by mode locking of this laser was first observed by DeMaria et al[56, 57]. Recent review articles of mode locked laser pulses and picosecond laser pulses have been given by DeMaria[58], DeMaria et al[59] and Smith[60]. In ruby laser[61], mode locking could be achieved by Q-switching the laser with a saturably absorbing dye. The duration mode locked laser pulses from Nd:glass laser was measured by Armstrong[62] by means of SHG in GaAs, and the result of pulsewidth measurement was about 4-6 pico-

seconds (ps). The introduction of another technique for measurement of the pulsewidth, so called two-photon fluorescence (TPF) method, was given by Giordmaine et al[63], Rentzepis[64]. In the TPF method care has to be taken in connection with the contrast ratio between the background and the overlapped region of the autocorrelation picture. Various theories were proposed to explain the picosecond substructure observed in Nd:glass laser. The simplest proposal made independently by several authors[65-69], was that the picosecond peaks observed in TPF arose from the short duration fluctuations present in spontaneous emission. The theory of two-photon fluorescence and another nonlinear optical coincidence technique (harmonic generation technique) has been treated in detail by several authors, particularly rigorous and exhaustive treatment, are given by Rowe and Li[70], and Picard and Schweitzer[71]. The difficulty in observating the contrast ratio 3:1 was removed, and the experimental result in pulsewidth measurement in agreement to the theory was performed, by means of TPF with very thin cell, by Shapiro and Duguay[72]. They obtained the pulsewidth of Nd:glass laser of 0.4 ps. The three photon fluoresence technique for measurement of ultrashort pulse was performed by P. M. Rentzepis et al[73], and the experimental result, in agreement to the theory, of the contrast ratio of 10:1 was obtained. The exhaustive review of study of the Nd:glass Laser Radiation was given by Duguay et al[74].

The optical harmonic generation technique, which gives background free in autocorrelation measurement of the ultrashort pulse, was first

performed by Armstrong[62]. In his experiment he utilized the unique polarization property of of GaAs, given by Chang et al[27], for SHG in reflection. Armstrong obtained the pulsewidth of Nd:glass laser radiation of 4-6 ps. Weber[75], using KDP in experimental set up similar to famous Michelson-Morley experiments, determined the pulsewidth of Nd:glass laser radiation. He obtained the pulsewidth of 8-12 ps. Giordmaine et al[76] introduced a new technique for determining of a narrow pulsewidth by using two beam spatial mixing on a crystal KDP. In their experiment employing an intense light burst in the stimulated Raman effect in CS_2 using Q-switched ruby laser, the backward Raman-Stoke wave was equally splitted into two parts with a proper delay time τ. Then the two beams were recombined in KDP crystal oriented to allow phase-unmatched second harmonic generation. The average Stoke pulsewidth was found to be 30 ps. Treacy[77], using a grating pair for pulse compression technique, obtained the pulsewidth of Nd:glass laser radiation of 0.44 ps, in agreement to theoretical limit. The unique polarization properties, reported by Bey et al[52], for THG from a phase matched solution consisted of dye fuchsin dissolved in hexafluoroacetone sesquihydrate, was promptly utilized by Eckardt and Lee[78] for third order autocorrelation measurement of Nd:glass laser. The result of their experiment yields the pulsewidth of Nd:glass laser radiation of 0.7 ps, in agreement to theoretical limit. Recently, Jayaraman and Lee[79,80] made an observation of two photon and three photon conductivity in GaAs, CdS and $CdS_{0.5}$-$Se_{0.5}$ using Q-switched and mode locked pulse from

Nd:glass laser, and demonstrated[81] the potentiality of multiphoton conductivity for measuring mode locked pulse from Nd:glass laser.

C. Aim of the Experiment

It is the purpose in this work to study and verify the theoretical prediction in the area of second harmonic generation given by Bloembergen and Pershan[12]. Furthermore, the experimental results concerning unique polarization properties and phase matched condition of uniaxial Potassium di Hydrogen Phosphate (KDP) crystal will be utilized for measurement of picosecond pulsewidth of Nd:glass laser radiation. During the course of study, Q-switched and mode locked Nd:glass lasers are employed as excitation sources and uniaxial KDP crystals of various crystallographic orientations served as nonlinear optical media. The angular dependence of relative second harmonic intensities in both reflection and transmission are measured and compared to theory.

The theory of wave propagation in a medium with nonlinear susceptibility and criteria of conventional phase matching and noncollinear phase matching are given in Chapter II. A concise account of picosecond pulsewidth measurement using phase matched second harmonic generation technique is also given. The experimental technique including crystal preparation and design of experiments is described in Chapter III. In Chapter IV detailed experimental results are given and discussed. The proposal and brief analysis for future experiments are given in Chapter V.

CHAPTER II
THEORY

Introduction

In the presence of very high intense electromagnetic radiation, the medium exhibits an electric polarization $\vec{P}(\vec{r},t)$, which is in general a nonlinear functions of electric field strength $\vec{E}(\vec{r},t)$. The relationship between $\vec{P}(\vec{r},t)$ and the applied field $\vec{E}(\vec{r},t)$ can be written in a tensorial form as (5)

$$\vec{P} = \overset{\approx}{\chi}_1 \vec{E} + \overset{\approx\approx}{\chi}_2 : \vec{E}\,\vec{E} + \overset{\approx\approx\approx}{\chi}_3 : \vec{E}\,\vec{E}\,\vec{E} + \ldots . \qquad (2.1)$$

where χ's are nonlinear susceptibility.

If the applied electric field is harmonically varying in time t with frequency ω, then the second term on the right hand side of (2.1) is the nonlinear source term at the second harmonic frequency $\omega_2 = 2\omega_1$. The nonlinear susceptibility χ of the medium will give rise to a polarization at the harmonic frequencies, which in turn radiates energy at these frequencies. The effective nonlinear source term at the second harmonic frequency $\omega_2 = 2\omega_1$ is given by

$$P^{NLS} = P^{NLS}(2\omega_1) = \overset{\approx\approx}{\chi}_2(\omega_2 = 2\omega_1) : E_1^T E_1^T \exp i(\vec{k}^s \cdot \vec{r} - 2\omega_1 t) \qquad (2.2)$$

where E_1^T is the amplitude of transmitted electric field in the medium

$\vec{k}^s$ is the wave vector of the source term and $\vec{k}^s = 2\vec{k}_1^T$

The nonlinear source term P^{NLS} was introduced by Armstrong et al[11]. In their paper the nonlinear susceptibility tensor χ was

shown quantum mechanically, to be related to the atomic properties of the medium. Furthermore, they also showed that the effective nonlinear source term can readily be incorporated in Maxwell's equations for the nonlinear medium. Since, during the course of study, a large number of harmonic photons are created by the interaction, the problems can be treated classically via Maxwell's equations. In this thesis, we shall recast the theory of Bloembergen in a form that direct comparison with the present experimental data can be readily made.

A. Wave Propagation in a Medium with Nonlinear Susceptibility

Maxwell's equations in c. g. s. units for nonlinear medium are

$$\begin{aligned} \nabla \cdot \vec{D} &= 4\pi \rho_f \qquad \nabla \cdot \vec{B} = 0 \\ \nabla \times \vec{E} &= -\frac{1}{c} \frac{\partial \mu \vec{H}}{\partial t} \\ \nabla \times \vec{H} &= \frac{1}{c} \frac{\partial}{\partial t} \vec{D} + \frac{4\pi}{c} \vec{J} \end{aligned} \tag{2.3}$$

where $\vec{D} = \epsilon \vec{E} + 4\pi \vec{P}^{NLS}$

For the cubic but noncentrosymmetric, nonconducting crystal, the wave equation, at the second harmonic frequency, obtained from (2.3), is given as

$$\begin{aligned} \nabla \times \nabla \times \vec{E}_2 + \frac{\epsilon(2\omega)}{c^2} \frac{\partial^2 \vec{E}_2}{\partial t^2} &= -\frac{4\pi}{c^2} \frac{\partial^2 \vec{P}^{NLS}}{\partial t^2} (2\omega) \\ \nabla^2 \vec{E}_2 - \frac{\epsilon(2\omega)}{c^2} \frac{\partial^2 \vec{E}_2}{\partial t^2} &= \frac{4\pi}{c^2} \frac{\partial^2 \vec{P}^{NLS}}{\partial t^2} (2\omega) \end{aligned} \tag{2.4}$$

Equation (2.4) is similar to the usual linear wave equation except it is augmented by a source term on the right hand side. The general solution of (2.4) consists of the solution of the homogeneous equation plus the particular solution of the inhomogeneous equation. The general equation for the transmitted and reflected second harmonic field created by the fundamental field incident on the medium from the vacuum (see Fig. 2-1) are given as,

$$\vec{E}_2^{\,T} = \hat{e}_T \, \mathcal{E}_2^{\,T} \exp i(\vec{k}_2^{\,T} \cdot \vec{r} - 2\omega_1 t) - \frac{4\pi \vec{P}^{NLS}(4\omega_1^2/c^2)}{(k_2^{\,T})^2 - (k^s)^2} \times$$

$$\left[\hat{p} - \frac{\vec{k}^s (\vec{k}^s \cdot \hat{p})}{(k^T)^2}\right] \exp i(\vec{k}^s \cdot \vec{r} - 2\omega_1 t) \tag{2.5}$$

$$\vec{H}_2^{\,T} = \frac{c}{2\omega_1} (\vec{k}_2^{\,T} \times \hat{e}_T) \, \mathcal{E}_2^{\,T} \exp i(\vec{k}_2^{\,T} \cdot \vec{r} - 2\omega_1 t)$$

$$\frac{-4\pi \vec{P}^{NLS}(4\omega_1^2/c^2)}{(k_2^{\,T})^2 - (k^s)^2} \; \frac{c}{2\omega_1} (\vec{k}^s \times \hat{p}) \exp i(\vec{k}^s \cdot \vec{r} - 2\omega_1 t)$$

$\hat{p}$ = unit vector along the $\vec{P}^{NLS}$ direction.

The reflected harmonic fields are

$$\vec{E}_2^{\,R} = \hat{e}_R \, \mathcal{E}_2^{\,R} \exp i(\vec{k}_2^{\,R} \cdot \vec{r} - 2\omega_1 t) \tag{2.6}$$

$$\vec{H}_2^{\,R} = \left(\frac{c}{2\omega_1}\right) (\vec{k}_2^{\,R} \times \hat{e}_R) \, \mathcal{E}_2^{\,R} \exp i(\vec{k}_2^{\,R} \cdot \vec{r} - 2\omega_1 t)$$

The direction of the wave vectors of the reflected wave $\vec{k}_2^{\,R}$ and the homogeneous transmitted wave $\vec{k}_2^{\,T}$, as well as the polarization unit vectors $\hat{e}_T$ and $\hat{e}_R$ and the magnitudes $\mathcal{E}_2^{\,R}$ and $\mathcal{E}_2^{\,T}$ have to be determined from the boundary conditions.

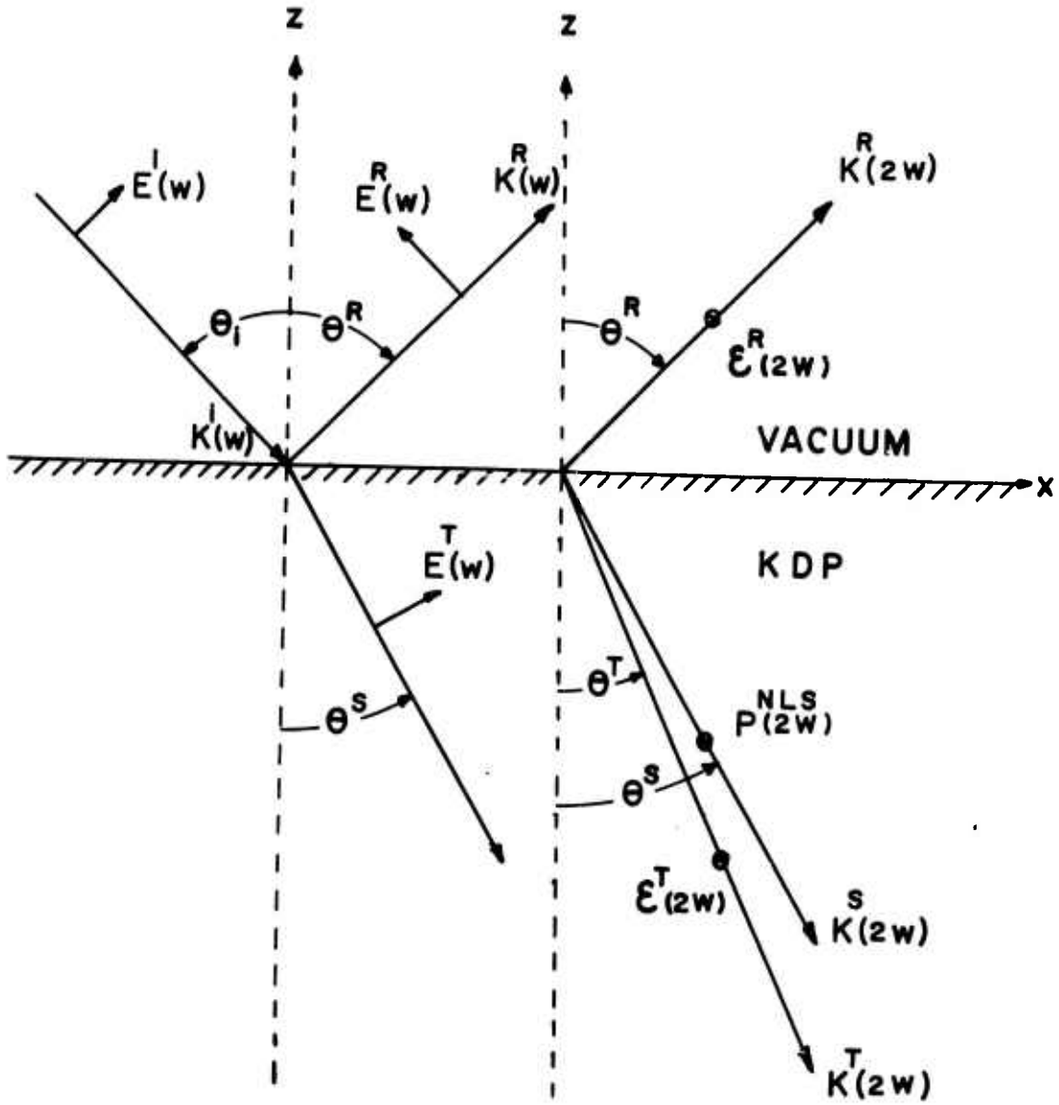
z
z
E^I(w)
E^R(w)
K^R(w)
K^R(2w)
θ_i
θ^R
θ^R
ℰ^R(2w)
K^I(w)
VACUUM
x
E^T(w)
KDP
θ^T
θ^S
NLS
P(2w)
θ^S
ℰ^T(2w)
K^S(2w)
K^T(2w)

FIGURE 2 - 1

The tangential components of $\vec{E}$ and $\vec{H}$ should be continuous everywhere on the boundary at all times. This requires that the individual frequency components at ω_1 and $2\omega_1$, are separately continuous across the boundary in order to satisfy this condition at all points on the boundary simultaneously . Thus for the fundamental frequency

$$k_{1x}^{i} = k_{1x}^{R} = k_{1x}^{T} \tag{2.7}$$

The polarization of electric fields at $2\omega_1$ are determined by the polarization of $\vec{P}^{NLS}$. Also it is required that

$$2k_{1x}^{T} = k_{2x}^{S} = k_{2x}^{R} = k_{2x}^{T} \tag{2.8}$$

Relations (2.7) and (2.8), in short, are the requirements of the conservation of tangential component of momentum.

1. General Laws of Reflection and Refraction. Consider two incident plane waves, $E_1 \exp i(\vec{k}_1^{\,i} \cdot \vec{r} - \omega_1 t)$ and $E_2 \exp i(\vec{k}_2^{\,i} \cdot \vec{r} - \omega_2 t)$, where $\omega_1 \neq \omega_2$ approaching the boundary between the linear and nonlinear media, from the side of the linear medium. The boundary is defined as the plane $z = 0$ as depicted in Fig. 2-2. The angles of incidence of the two waves are $\theta_1^{\,i}$ and $\theta_2^{\,i}$. The planes of incidence make an angle φ with each other, and φ varies between 0 and 2π. Choose the z and y direction of the coordinates system such that $k_{1y}^{\,i} = -k_{2y}^{\,i}$. In general, waves at all sum and different frequencies $m_1\omega_1 \pm m_2\omega_2$ will emanate from the boundary (m_1 and m_2 are integers). However, in case of second harmonic generation, the sum frequency $\omega_3 = \omega_1 + \omega_2$ ($\omega_1 = \omega_2$) will be considered explicitly.

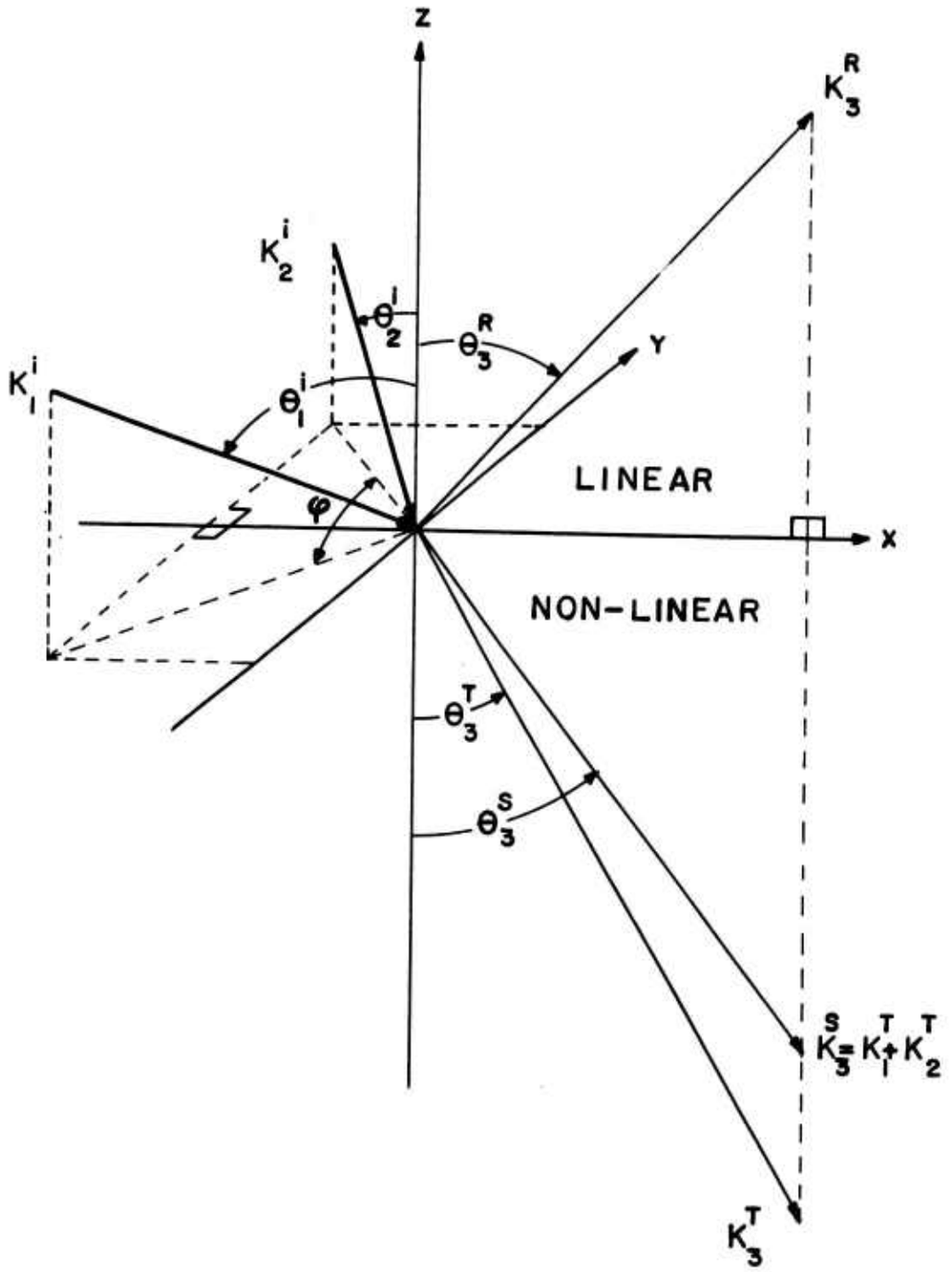
Z
K_3^R
K_2^i
θ_2^i
θ_3^R
Y
K_1^i
θ_1^i
LINEAR
φ
X
NON-LINEAR
θ_3^T
θ_3^S
$K_3^S = K_1^T + K_2^T$
K_3^T

FIGURE 2 - 2

A necessary and sufficient condition for the requirement that the boundary conditions will be satisfied simultaneously at all points in the plane $z = 0$ is that the x and y components of momentum wave vector remain conserved. For the sum wave, this gives the conditions.

$$k_{3x}^{R} = k_{3x}^{T} = k_{3x}^{S} = k_{1x}^{T} + k_{2x}^{T} = k_{1x}^{i} + k_{2x}^{i} \qquad (2.9)$$

$$k_{3y}^{R} = k_{3y}^{T} = k_{3y}^{S} = k_{1y}^{T} + k_{2y}^{T} = k_{1y}^{i} + k_{2y}^{i} = 0$$

Equation (2.9) suggests that the inhomogeneous source wave, the homogeneous transmitted and reflected waves and the boundary normal all lie in the same plane which is xz plane called "plane of sum reflection", as indicated in Fig. 2-2. The propagation of the inhomogenous wave, proportional to $\vec{P}^{NLS}(\omega_3)$, is given by $\exp i\{(\vec{k}_1^{\,T} + \vec{k}_2^{\,T}).r - (\omega_1+\omega_2)t\}$. Its angle with the normal into the nonlinear medium θ_3^{S} is determined by

$$\sin\theta_3^{S} = |\vec{k}_{1x}^{\,T} + \vec{k}_{2x}^{\,T}| \,/\, |\vec{k}_1^{\,T} + \vec{k}_2^{\,T}| \qquad (2.10)$$

The wave vectors $\vec{k}_1^{\,T}$ and $\vec{k}_2^{\,T}$ are given by Snell's law for refraction in the usual linear case. From Fig. 2-2 the relationship between $\vec{k}_3^{\,T}$, $\vec{k}_1^{\,i}$, $\vec{k}_2^{\,i}$ is given as

$$|\vec{k}_3^{\,T}|^2 \sin^2\theta_3^{T} = |\vec{k}_3^{\,R}|^2 \sin^2\theta_3^{R}$$

$$= |\vec{k}_1^{\,i}|^2 \sin^2\theta_1^{i} + |\vec{k}_2^{\,i}|^2 \sin^2\theta_2^{i} + 2|\vec{k}_1^{\,i}|\,|\vec{k}_2^{\,i}| \sin\theta_1^{i} \sin\theta_2^{i} \cos\varphi$$

(2.11)

Since $\epsilon = k^2 \frac{c^2}{w^2}$, equation (2.11) can be written as

$$\epsilon_3^T \omega_3^2 \sin^2\theta_3^T = \epsilon_3^R \omega_3^2 \sin^2\theta_3^R$$

$$= \epsilon_1^R \omega_1^2 \sin^2\theta_1^i + \epsilon_2^R \omega_2^2 \sin^2\theta_2^i$$

$$+ 2(\epsilon_1^R \epsilon_2^R)^{1/2} \omega_1 \omega_2 \sin\theta_1^i \sin\theta_2^i \cos\varphi \qquad (2.12)$$

Since $k^2 = \epsilon \frac{\omega^2}{c^2}$, and also from (2.9) we can arrange (2.12) as

$$\epsilon^S \sin^2\theta_3^S = \epsilon_3^T \sin^2\theta_3^T = \epsilon^R \sin^2\theta_3^R \qquad (2.13)$$

Equation (2.13) gives directional relationship between $\vec{k}_3^R$, $\vec{k}_3^T$ and $\vec{k}_3^S$. This relationship is the nonlinear counterpart of linear Snell's law.

The example of second harmonic generation follows from equation (2.12) if we put $\theta_1^i = \theta_2^i$ and $\varphi = 0$, and $\epsilon_1^R = \epsilon_2^R$, and $\omega_1 = \omega_2 = \omega$. This will lead to Snell' s law for nonlinear case

$$\epsilon_3^T \sin^2\theta_3^T = \epsilon_1^R \sin^2\theta^i$$

or in general (with the combination of (2.13)).

$$\sqrt{\epsilon_1^R} \sin\theta^i = \sqrt{\epsilon_3^T} \sin\theta_3^T = \sqrt{\epsilon_3^R} \sin\theta_3^R = \sqrt{\epsilon_3^S} \sin\theta^S \qquad (2.14)$$

The relationship (2.12) can be generalized further to the case of two beam spatial mixing (TBSM) second harmonic generation where two fundamental beams are incident from the opposite side of the face normal (z axis). Here we have $\theta_1^i = \theta_2^i$; $\varphi = 180^o$. From the equation (2.12) and (2.13) we get

$$\theta^T = \theta^S = \theta^R = 0 \ . \qquad (2.15)$$

This means that all three second harmonic waves travel along

facing normally inward for $\vec{k}_3^T$ and $\vec{k}_3^S$, and outward for $\vec{k}_3^R$ with respect to the boundary.

From the above analysis, one notices that the conditions of conservation of tangential component of momentum, equation (2.9), are very general. They can easily be used to derive the directional relationship for higher harmonics. They hold regardless of whether the harmonic radiation is of dipolar, electric or magnetic, or quadrupole origin.

2. Polarization and Intensities of the Harmonic Waves. In this section particular attention will be devoted for the polarization and intensities of harmonic waves at sum frequency $\omega_3 = \omega_1 + \omega_2 = 2\omega$. The nonlinear polarization induced in the medium is

$$\vec{P}^{NLS}(\omega_z) = \overset{\approx}{\chi}(2\omega) : \vec{E}_1^T \vec{E}_2^T \exp i\left[(\vec{k}_1^T + \vec{k}_2^T) \cdot \vec{r} - 2\omega t\right] \qquad (2.16)$$

The refracted waves at ω_1 and ω_2 are known in terms of incident waves by means of the formulas of Snell and Fresnel for the incident medium. Therefore the nonlinear source term, given in Equation (2.16), at ω_3 is known. The angular dependence of $\vec{P}^{NLS}$ itself is derived from the transmitted linear waves given by Fresnel equation. One must take proper account of this in analyzing the angular dependence of harmonic generation. As in the linear case, the second harmonic wave at $\omega_3 = 2\omega$ with electric field vector normal to the plane of reflection ($E_1(2\omega)$), as defined in the preceeding section, can be treated independently from that with electric field vector in the plane of reflection ($E_{11}(2\omega)$).

2a. Perpendicular Polarization ($E_\perp(2\omega)$) . ($E_y = E$, $E_x = E_z = 0$). Consider the case where the nonlinear polarization is normal to the plane of reflection, i.e. $P^{NLS} = P_y^{NLS}$ as shown in Fig. 2-3. The continuity of the tangential components of the solution in equation (2.5) and (2.6) at the boundary requires in this case

$$E_y = E_\perp^R = \mathcal{E}_\perp^T + \frac{4\pi P_\perp^{NLS}}{(\epsilon_S - \epsilon_T)} \tag{2.17}$$

$$H_x = -\sqrt{\epsilon}_R E_\perp^R \cos\theta_R = \epsilon_T \mathcal{E}_\perp^T \cos\theta_T + \frac{4\pi\sqrt{\epsilon_S}\, P_\perp^{NLS} \cos\theta_S}{(\epsilon_S - \epsilon_T)} \tag{2.18}$$

The continuity of the normal components of $\vec{D}$ and $\vec{B}$ follows automatically from the equations (2.17), (2.18), and (2.12).

By solving for $E_\perp^R$ and $E_\perp^T$ from equations (2.17) and (2.18), one obtains after algebraic manipulation.

$$E_\perp^R = \frac{-4\pi P_\perp^{NLS}}{\epsilon_T - \epsilon_S}\left[\frac{\sqrt{\epsilon_T}\cos\theta_T - \sqrt{\epsilon_S}\cos\theta_S}{\sqrt{\epsilon_T}\cos\theta_T + \sqrt{\epsilon_R}\cos\theta_R}\right] \tag{2.19}$$

$$E_\perp^T = -\frac{4\pi P_\perp^{NLS}}{\epsilon_T - \epsilon_S}\left[\exp i(\vec{k}^S \cdot \vec{r} - 2\omega t) - \frac{\sqrt{\epsilon_S}\cos\theta_S + \sqrt{\epsilon_R}\cos\theta_R}{\sqrt{\epsilon_T}\cos\theta_T + \sqrt{\epsilon_R}\cos\theta_R} \times \exp i(\vec{k}^T \cdot \vec{r} - 2\omega t)\right] \tag{2.20}$$

Since

$$\vec{k}^S - \vec{k}^T = \frac{\omega}{c}\left[\sqrt{\epsilon_S}\cos\theta_S - \sqrt{\epsilon_T}\cos\theta_T\right]\hat{Z} \tag{2.21}$$

Equation (2.20) can be transformed into a single plane wave with a propagation vector $\vec{k}^T$, with an amplitude

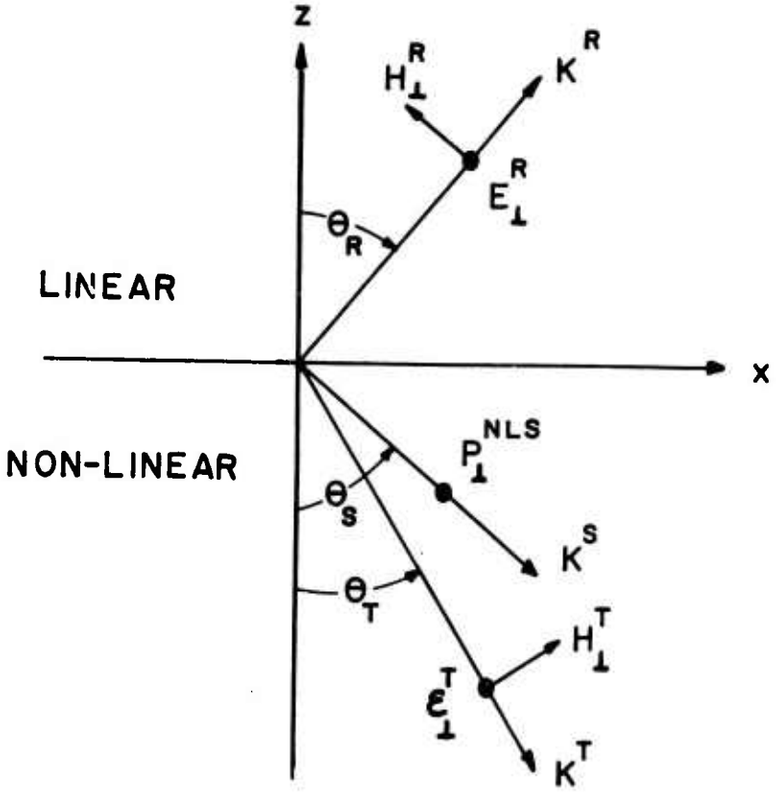

FIGURE 2 - 3

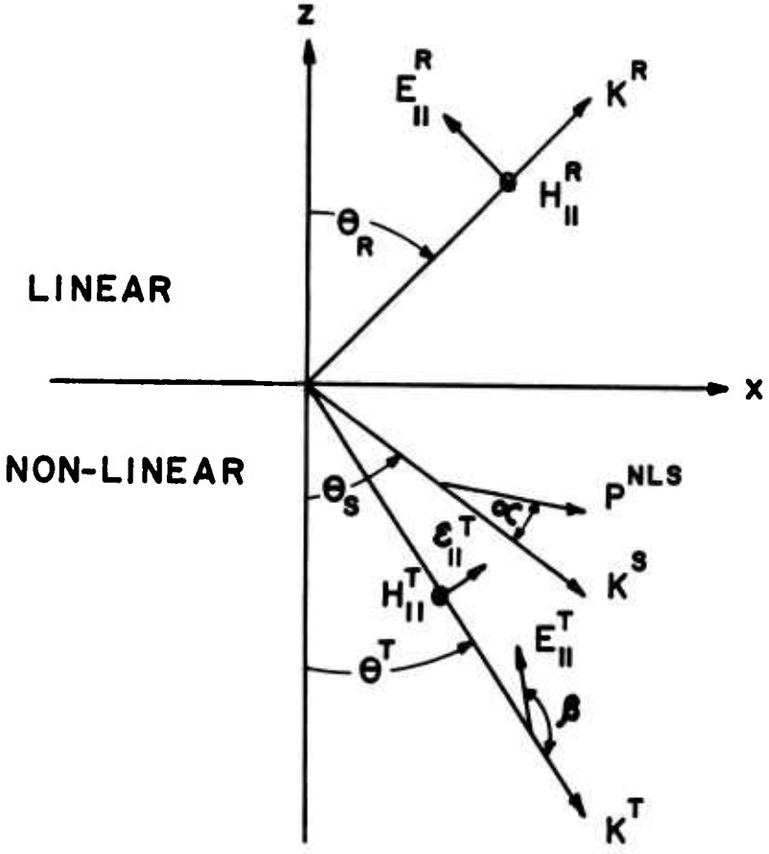

FIGURE 2 - 4

$$E^T = E_\perp^R + \frac{4\pi P_\perp^{NLS}}{\epsilon_S - \epsilon_T} \left\{ \exp\left[\frac{\omega}{c} (\sqrt{\epsilon_S}\cos\theta_S - \sqrt{\epsilon_T}\cos\theta_T) Z \right] - 1 \right\} \qquad (2.22\,a)$$

For the small values of z which satisfy the condition

$$\frac{\omega}{c} z \left(\sqrt{\epsilon_S}\cos\theta_S - \sqrt{\epsilon_T}\cos\theta_T \right) << 1 \qquad (2.22\,b)$$

The expansion of right hand side of equation (2.22) will give $E_\perp^T$ as a linear function of z. Then the intensity grows as z^2 from the boundary. This is precisely the effect of harmonic generation in the volume of an infinite medium, discussed by Armstrong et al[11].

2b. Parallel Polarization ($E_y = P_y^{NLS} = 0$). The nonlinear polarization $\vec{P}^{NLS}$ has only x and y components as indicated in Fig. 2-4.

It will be advantageous to describe the nonlinear polarization in the plane of reflection by its magnitude P_{11}^{NLS} and the angle α between its direction and the direction of propagation in the source $\vec{k}^S$. The continuity of the tangential componenets at z = 0 requires that from equations (2.5) and (2.6).

$$E_x = -E_{11}^R \cos\theta_R = \epsilon_{11}^T \cos\theta_T + \frac{4\pi P_{11}^{NLS} \sin\alpha \cos\theta_S}{\epsilon_S - \epsilon_T}$$

$$- 4\pi P_{11}^{NLS} \frac{\cos\alpha \sin\theta_S}{\epsilon_T} \qquad (2.23)$$

$$H_y = -\sqrt{\epsilon_R} E^R = -\sqrt{\epsilon_T}\, \epsilon_{11}^T - \sqrt{\epsilon_S} \frac{4\pi P_{11}^{NLS} \sin\alpha}{\epsilon_S - \epsilon_T} \qquad (2.24)$$

By solving for E_{11}^R from equation (2.23) and (2.24), one obtained the amplitude of the reflected wave E_{11}^R after arranging terms as

$$E_{11}^{R} = \frac{4\pi P_{11}^{NLS} \sin\theta_S \sin^2\theta_T \sin(\alpha + \theta_T + \theta_S)}{\epsilon_R \sin\theta_R \sin(\theta_T+\theta_S)\sin(\theta_T+\theta_R)\cos(\theta_T-\theta_R)} \tag{2.25}$$

With the introduction of the angle β between E_{11}^{T} and the direction of propagation $\vec{k}_T$ the transverse component of the total transmitted wave will be given with the help of equations (2.25), (2.26), (2.23) and (2.24), as

$$\begin{aligned} E_{11}^{T}\sin\beta = {} & \frac{4\pi P_{11}^{NLS}\sin\theta_S\sin\theta_T\sin(\alpha+\theta_T+\theta_S)}{\epsilon_T\sin(\theta_T+\theta_S)\sin(\theta_T+\theta_R)\cos(\theta_T-\theta_R)} \\ & - \frac{4\pi P_{11}^{NLS}\sin\alpha\sin\theta_S\cos\theta_S}{\epsilon_T\sin(\theta_T+\theta_S)} \\ & + \frac{4\pi P_{11}^{NLS}\cos\alpha\sin(\theta_T-\theta_S)\exp i\{\frac{\omega}{c} z(\sqrt{\epsilon}_S\cos\theta_S-\sqrt{\epsilon}_T\cos\theta_T)\}}{\epsilon_T} \\ & + \frac{4\pi P_{11}^{NLS}\sin\alpha\cos(\theta_T-\theta_S)\exp i\{\frac{\omega}{c} z(\sqrt{\epsilon}_S\cos\theta_S-\sqrt{\epsilon}_T\cos\theta_T)\}-1}{\epsilon_S-\epsilon_T} \end{aligned} \tag{2.26}$$

The longitudinal component of the electric field vector, parallel to $\vec{k}_T$, can be written in the form

$$\begin{aligned} E_{11}^{T}\cos\beta = {} & 4\pi P_{11}^{NLS}\sin\alpha\sin^2\theta_S - \cos\alpha\cos(\theta_T-\theta_S)\sin(\theta_T+\theta_S) \\ & \times \frac{\exp i\{\frac{\omega}{c} z(\sqrt{\epsilon}_S\cos\theta_S-\sqrt{\epsilon}_T\cos\theta_T)\}}{\epsilon_T\sin(\theta_T+\theta_S)} \end{aligned} \tag{2.27}$$

3. Nonlinear Brewster's Angle. For the case where P_{11}^{NLS} lies in the plane of reflection, the electric field of the reflected harmonic wave is given by equation (2.25). Equation (2.25) reveals the existence of Nonlinear Brewster's angle for harmonic waves, when $E_{11}^{R}=0$. Or in

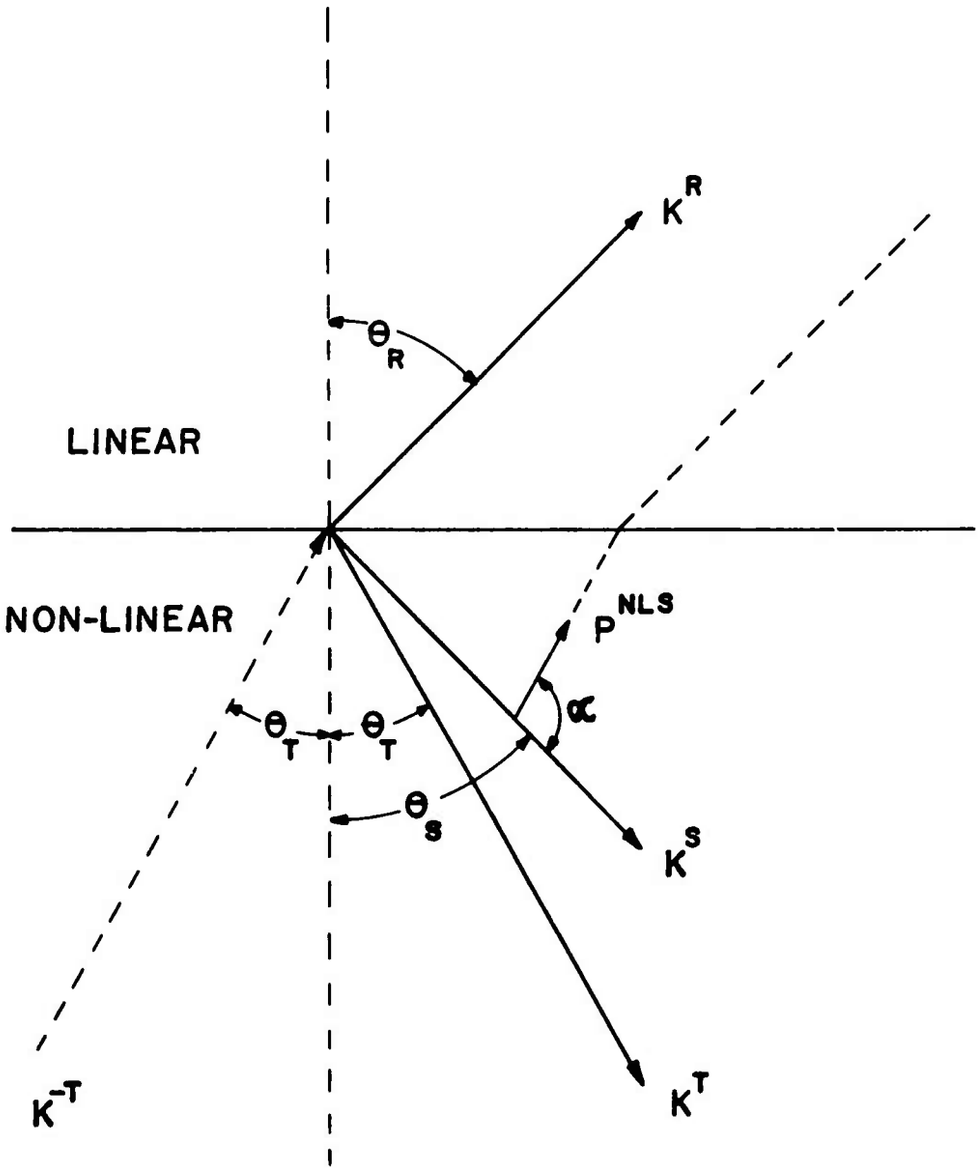

FIGURE 2 - 5

other words

$$E_{ll}^{R} = 0 \quad \text{implies} \quad \theta_T + \theta_S + \alpha = 0 \,, \pi \tag{2.28}$$

This condition implies that the nonlinear polarization P_{ll}^{NLS} is parallel to the direction of propagation of the harmonic wave in the nonlinear medium and hence it can not radiate. This nonradiating wave upon refraction back into the linear medium would otherwise give rise to the reflected ray in the direction θ_R . This is shown in Fig. 2-5.

In the present work, several KDP crystals of rectangular parallelepiped shape are used as the nonlinear media from which second harmonic waves are created and furthermore the optically dense fluid (1-Bromonaphthalene) is employed as the linear medium. It would be advantageous not only to depict wave vectors of fundamental and second harmonic waves at the boundary of KDP crystal immersed in the optically denser liquid (Fig. 2-6) but also to recast those fundamental equations given in the previous section into appropriate forms such that they are suitable for experimental comparison.

According to geometry of Fig. 2-6, the angles θ_R, θ_S and θ_T of the reflected, transmitted source and transmitted homogeneous waves, respectively, are given, with the aid of equation (2.14) and $n = \sqrt{\epsilon}$, by

$$n_{liq}(\omega)\sin\theta_i = n_{liq}(2\omega)\sin\theta_R = n(\omega)\sin\theta_S = n(2\omega)\sin\theta_T \tag{2.29}$$

The index without subscripts refers to the KDP crystal.

Since the liquid is optically denser than the KDP crystal, then there exist critical angles under which the fundamental and second

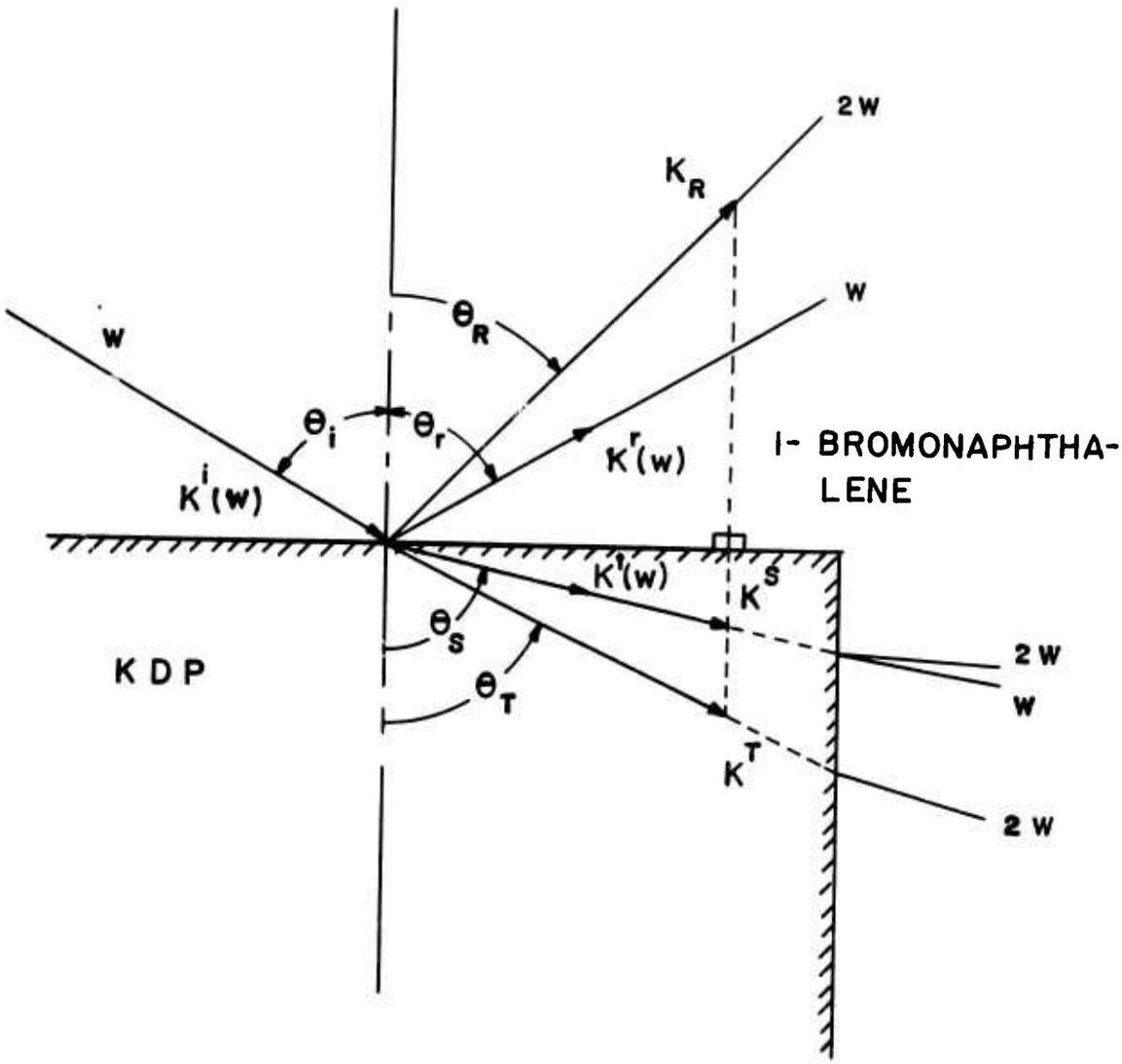
2W
K_R
θ_R
W
W
θ_i
θ_r
$K^r(w)$
$K^i(w)$
1- BROMONAPHTHA-
LENE
$K^t(w)$
K^S
θ_S
KDP
θ_T
2W
W
K^T
2W

FIGURE 2 - 6

harmonic waves are totally reflected. Those are given by

$$\sin\theta_{cr}(\omega) = n(\omega)/n_{liq}(\omega) < 1 \tag{2.30a}$$

$$\sin\theta_{cr}(2\omega) = n(2\omega)/n_{liq}(\omega) < 1 \tag{2.30b}$$

The components of the harmonic polarization $\vec{P}^{NLS}$ along the cubic axes of the nonlinear KDP crystal are given in terms of the fundamental field components at each point inside the crystal by

$$P_z^{NLS}(2\omega) = \chi_{36}^{NL} E_x^T(\omega) E_y^T(\omega) \tag{2.31a}$$

$P_x^{NLS}(2\omega)$, $P_y^{NLS}(2\omega)$ can be obtained by cyclic permutation of equation (2.31a).

Equation (2.31a) can be expressed in terms of the amplitude E_o of the incident fundamental wave by

$$P^{NLS}(2\omega) = \chi_{36}^{NL} \eta (F_T^L E_o)^2 \tag{2.31b}$$

Where η is a geometrical factor which depends on the orientation of the fundamental field vector and nonlinear polarization component with respect to the crystallographic cubic axes of the KDP. The linear Fresnel factor F_T^L describes the change in amplitude of the fundamental wave on transmission at the crystal surface. For the laser polarization perpendicular to the plane of incidence, it is given by

$$F_T^L = \frac{2\cos\theta_i}{\cos\theta_i + \sin\theta_{cr}(\omega)\cos\theta_S} \tag{2.32a}$$

and for the laser polarization in the plane of incidence it is

$$F_T^L = \frac{2\cos\theta_i}{\sin\theta_{cr}(\omega)\cos\theta_i + \cos\theta_S} \tag{2.32b}$$

The nonlinear polarization P^{NLS} is the source of the three harmonic waves. The amplitudes of electric field of second harmonic waves can be expressed in terms of P^{NLS} as follows:

$$E_R(2\omega) = 4\pi P^{NLS} F_R^{NL} \tag{2.33a}$$

$$E_S(2\omega) = 4\pi P^{NLS} F_S^{NL} \tag{2.33b}$$

$$E_T(2\omega) = 4\pi P^{NLS} F_T^{NL} \tag{2.33c}$$

where F^{NL}'s are the nonlinear Fresnel's factors.

From equations (2.19), (2.20), (2.22) and (2.33), the nonlinear Fresnel factors for the case of second harmonic polarization perpendicular to the plane of reflection are given by

$$F_{R,\perp}^{NL} = \frac{1}{\epsilon_T - \epsilon_S} \cdot \sqrt{\frac{\epsilon_T}{\epsilon_S}} \cdot \left(\frac{\sqrt{\epsilon_T}\cos\theta_T - \sqrt{\epsilon_S}\cos\theta_S}{\sqrt{\epsilon_T}\cos\theta_T + \sqrt{\epsilon_R}\cos\theta_R} \right) \tag{2.34a}$$

$$F_{S,\perp}^{NL} = \frac{1}{\epsilon_T - \epsilon_S} \tag{2.34b}$$

$$F_{T,\perp}^{NL} = \frac{1}{\epsilon_T - \epsilon_S} + F_{R,}^{NL} \tag{2.34c}$$

For the case of second harmonic polarization paralle to the plane of reflection the nonlinear Fresnel factor can be obtained from equations (2.23), (2.24), (2.25) and (2.33). They are given by

$$F_{R,11}^{NL} = \frac{\sin\theta_S \sin^2\theta_T \sin(\alpha + \theta_T + \theta_S)}{\epsilon_R \sin\theta_R \sin(\theta_T + \theta_R)\cos(\theta_T - \theta_R)\sin(\theta_T + \theta_S)} \tag{2.35a}$$

$$F_{S,11}^{NL} = \frac{\sin\alpha}{\epsilon_S - \epsilon_T} \tag{2.35b}$$

$$F_{T,11}^{NL} = \sqrt{\frac{\epsilon_S}{\epsilon_T}} \cdot \frac{\sin\alpha}{\epsilon_S - \epsilon_T} + \sqrt{\frac{\epsilon_R}{\epsilon_T}} \; F_{R,11}^{NL} \tag{2.35c}$$

The time average second harmonic power carried by the harmonic beams is given by the real part of Poynting vector multiplied by the cross-sectional area A of the respective beams. The intensities of harmonic beams are.

$$I_{R,S,T}^{(2\omega)} = \frac{c}{8\pi} \cdot \sqrt{\epsilon}_{R,S,T} \mid E_{R,S,T}^{(2\omega)}\mid^2 A_{R,S,T} \qquad (2.36)$$

where subscript R, S, and T refer to reflected, inhomogenous and homogeneous harmonic beams respectively. $A_{R,S,T}$ is the cross-section area of the beam and it can be written as

$$A_{R,S,T} = \frac{d\, d' \cos\theta_{R,S,T}}{\cos\theta_i} \qquad (2.37)$$

where $d\, d'$ are rectangular slit which defines the size of the incident laser beam.

Since the intensities of harmonic beams cannot be observed inside the crystal, it is preferable to relate the intensities of transmitted beams after they have reenterred the liquid at the side of the crystal. The transmitted power from the crystal to liquid is given by

$$T = \sqrt{\frac{\epsilon_R}{\epsilon_{S,T}}} \mid f_{S,T}^{L}\mid^2 \qquad (2.38a)$$

where $f_{S,T}^{L}$ is the linear Fresnel factor for transmission at the interface for crystal with right angle corner. It is given by

$$f_{S,T}^{L} = \frac{2}{1 + \{(\epsilon_R - \epsilon_{S,T})\, \epsilon(\omega) \sin^{-2}\theta_i + 1\}^{1/2}} \qquad (2.38b)$$

This factor is always close to unity, and $f_R^{L} = 1$ by definition.

Now the intensities given by equation (2.36) will be written in a rigorous form and are ready for direct comparison to the experiment.

$$I_{R,S,T}(2\omega) = (c/8\pi)\sqrt{\epsilon}_R\, |E_o|^4\, d\, d'\, (4\pi \chi_{36}^{NL})^2 \eta^2 (f_{R,S,T}^{L})^2 \times |F^L|^4\, |F_{R,S,T}|^2 \cos\theta_{R,S,T} (\cos\theta^i)^{-1} \qquad (2.39)$$

B. Criteria of Optimum Second Harmonic Generation

In this section, it is intended to point out general criteria for optimum harmonic generation, in particular, second harmonic generation. In the experiments, which verify the nonlinear optical laws for second harmonic generation (SHG), it is anticipated that the low level second harmonic intensity (SHI) will be encountered. Therefore it is worthwhile to utilize the condition for optimum SHG which is described below.

1. Phase Matching by Birefringence. When a fundamental wave of frequency ω propagating in a direction of $\vec{k}$ is incident on a nonlinear medium of piezoelectric crystal, the nonlinear polarization source $\vec{P}^{NLS}$ will be induced in the medium as

$$P_i^{NLS}(2\omega) = \chi_{ijk}(2\omega)\, E_j(\omega)\, E_k(\omega) \qquad (2.40)$$

The nonlinear polarization $P^{NLS}(2\omega)$ in turn will radiate SHI in transmission with electric field $E(2\omega)$ which is given by

$$E_i(2\omega) \approx \chi_{ijk}^{2\omega}\, E_j(\omega)\, E_k(\omega) \left\{ \frac{1 - \exp i\Delta k r}{\Delta k} \right\} \qquad (2.41)$$

where

$$\Delta k = k(2\omega) - 2k(\omega) = \frac{2\omega}{c}(n^{2\omega} - n^{\omega}) \qquad (2.42)$$

Consequently, the intensity of SHG will be given by

$$I(2\omega) \approx (\chi^{2\omega})^2 \left\{ \frac{\sin \frac{\Delta \vec{k}}{2} \cdot \vec{r}}{\frac{\Delta k}{2}} \right\}^2 I_o^2 \qquad (2.43)$$

where I_o is the intensity of the incident laser.

One possible method of increasing $I(2\omega)$, described in equation (2.43) is to set $\Delta k = 0$. This condition can be achieved by the utilization of double refraction of an uniaxial crystal, e.g. KDP, as pointed out independently by Giordmaine[33] and Maker et al[34]. This condition is called phase matching which is

$$\Delta k = 0 = \frac{2\omega}{c} (n^{2\omega} - n^{\omega}) \qquad (2.44)$$

Under this condition both fundamental and second harmonic beams travel in step inside the crystal with the same phase velocity. However, when $\Delta k \neq 0$, equation (2.41) shows $E(2\omega)$ to vary periodically as a function of distance r from the crystal surface. The period of variation is determined by the term so called "coherence length" ℓ_c, which is given by

$$\ell_c = \frac{2\pi}{\Delta k} = \frac{2\pi}{k^{2\omega} - 2k^{\omega}} = \frac{\lambda_o}{2(n^{2\omega} - n^{\omega})} \qquad (2.45)$$

The physical interpretation of ℓ_c is that it is the maximum crystal length which is useful in producing SHG. It is noted that under phase matching condition $(\Delta k = 0)$ ℓ_c is infinite, In practice, however, due to double refraction phenomena the maximum interaction length is limited because of the walk off effect[11,14].

The diagram showing how to obtain phase matching condition in KDP is shown in Fig. 2-7. In this diagram the angle θ_m, with respect

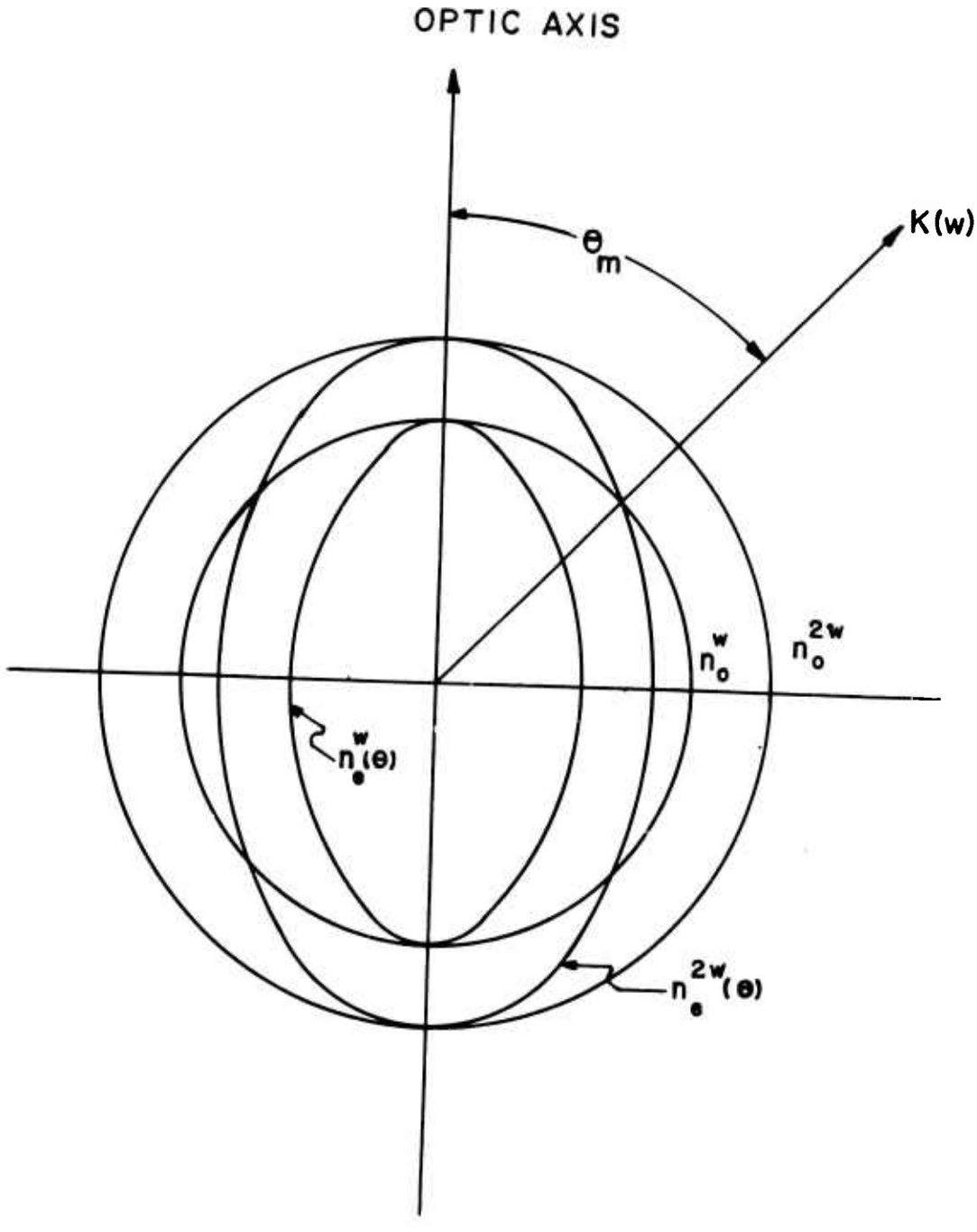

FIGURE 2 - 7

to z (optic) axis is called the phase matching angle. For KDP, if the fundamental beam is launched along θ_m as an ordinary ray, the second harmonic beam will be generated along the same direction as an extraordinary ray. The angle θ_m is determined by the intersection between the sphere corresponding to the normal index surface of the ordinary beam with the ellipsoidal surface corresponding to the normal index surface of the extraordinary ray. The angle θ_m is given by[82]

$$\sin^2\theta_m = \frac{(n_o^{\omega})^{-2} - (n_o^{2\omega})^{-2}}{(n_e^{2\omega})^{-2} - (n_o^{2\omega})^{-2}} \qquad (2.46)$$

Taking careful consideration to equation (2.43) the criteria for increasing second harmonic generation can be drawn as following.

1. By using laser systems that provide high peak power or large intensity I_o.

2. By selecting proper nonlinear crystal that possess large value of nonlinear susceptibility $\chi^{2\omega}$.

3. By utilizing phase matching condition ($\Delta k = 0$) as described above.

2. Noncollinear Phase Matching. According to the previous section, phase matching results in enhanced optical second harmonic generation (SHG). In certain bifringent crystal such as KDP this is accomplished by making the birefringence ($n_o^{2\omega} - n_e^{2\omega}$) equal to the dispersion ($n_o^{2\omega} - n_o^{\omega}$) at phase matching angle θ_m as shown in Fig. 2-7. However, SHG may still be limited by double refraction[11,14] which is describable by an angle ρ between the poynting vector of

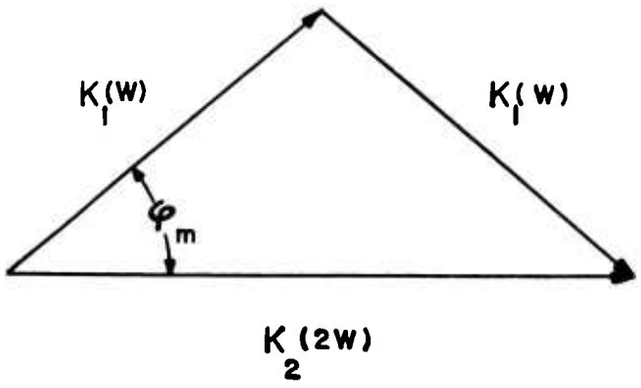

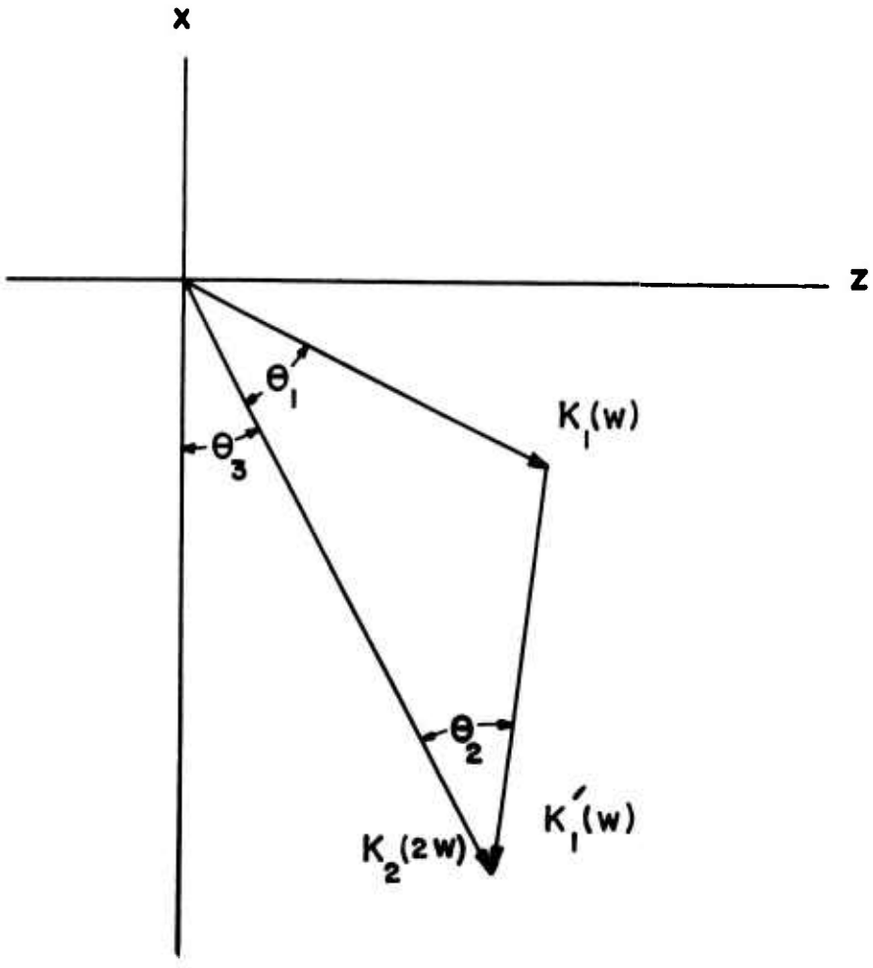

FIGURE 2 - 8

extraordinary harmonic wave and the ordinary fundamental wave. The angle ρ is given by[35]

$$\tan\rho = \frac{1}{2}\left(n_{e}^{2\omega}(\theta)\right)^{2}\left\{\frac{1}{\left(n_{e}^{2\omega}(\pi/2)\right)^{2}} - \frac{1}{\left(n_{o}^{2\omega}\right)^{2}}\right\}\sin 2\theta \qquad (2.47)$$

where θ is the angle between propagating vector of homogeneous second harmonic beam and the optic axis.

Consequently, the harmonic wave separates from the fundamental for a beam of finite diameter. The limitation of SHG from a gas laser due to double refraction[35] shows the reduced production of second harmonic beyond the aperture length ℓ_a which is given by

$$\ell_a = \sqrt{\pi}\,\frac{w_o}{\rho} \qquad (2.48)$$

where w_o is the minimum Gaussian spot size.

Increased SHG will result from $\ell_a \to \infty$ when $\rho = 0$. However, the divergence of the fundamental beam will then limit SHG instead of the aperture length ℓ_a (or double refraction). Phase matching with $\rho = 0$ has recently been achieved[42] in $LiNbO_3$ with $\theta_m = 90^{o}$ by varying the birefringence and dispersion via temperature tuning.

Another phase matching method with $\rho = 0$ is via noncollinear phase matching. This geometry is handy for application of ultrashort pulse measurement. However, one should point out that even when ρ is zero as in this case, the interaction length is not infinite. One normally does not adopt this scheme for maximum harmonic production.

The noncollinear phase matching employed in the present work, requires all three wave vectors $\vec{k}$'s forming a closed loop. The

condition is given by several authors[43, 33, 34] as shown in Fig. 2-8

$$\vec{k}_2(2\omega) = \vec{k}_1(\omega) + \vec{k}_1'(\omega) \tag{2.49}$$

where $\vec{k}_1$ and $\vec{k}_1'$ are wave vectors of two crossing fundamental beams, and $\vec{k}_2$ is the wave vector of second harmonic beam. According to equation (2.49), this vector relation can be satisfied only if $|\vec{k}_2| < 2|\vec{k}_1|$. This means that the birefringence must exceed dispersion. This condition is applicable to KDP crystal.

By using equation (2.49) and relationships $k_1(\omega) = \frac{n_o^{\omega}}{c} \cdot \omega$ and $k_2(\omega) = \frac{n_e^{2\omega}}{c} \cdot 2\omega$ one can get from Fig. 2-8 the conditions for noncolinear phase matching of the normal component :

$$\frac{n_o^{\omega}}{c} \cdot \omega \cos(\theta_1 + \theta_3) + \frac{n_o^{\omega}}{c} \cdot \omega \cos(\theta_2 - \theta_3) = \frac{n_e^{2\omega}}{c} \cdot 2\omega \cos\theta_3 \tag{2.50a}$$

For the tangential component :

$$\frac{n_o^{\omega}}{c} \cdot \omega \sin(\theta_1 + \theta_3) + \frac{n_o^{\omega}}{c} \cdot \omega \sin(\theta_2 - \theta_3) = \frac{n_e^{2\omega}}{c} \cdot \omega \sin\theta_3 \tag{2.50b}$$

For two beam spatial mixing (TBSM) in second harmonic generation, one can select the coordinates system and crystal orientation such that some parameters in equation (2.50a) and (2.50b) will be eliminated. Such configuration is illustrated in Fig. 2-9. According to equation (2.11) and the symmetry in Fig. 2-9. the net tangential component of the vector $\vec{k}_1 + \vec{k}_1'$ becomes zero. This in turn makes the tangential component of $\vec{k}_2(2\omega)$ zero, i.e. $\theta_3 = 0$. Under this condition the propagating vector $\vec{k}_2(2\omega)$ will be in the direction normal to the optic

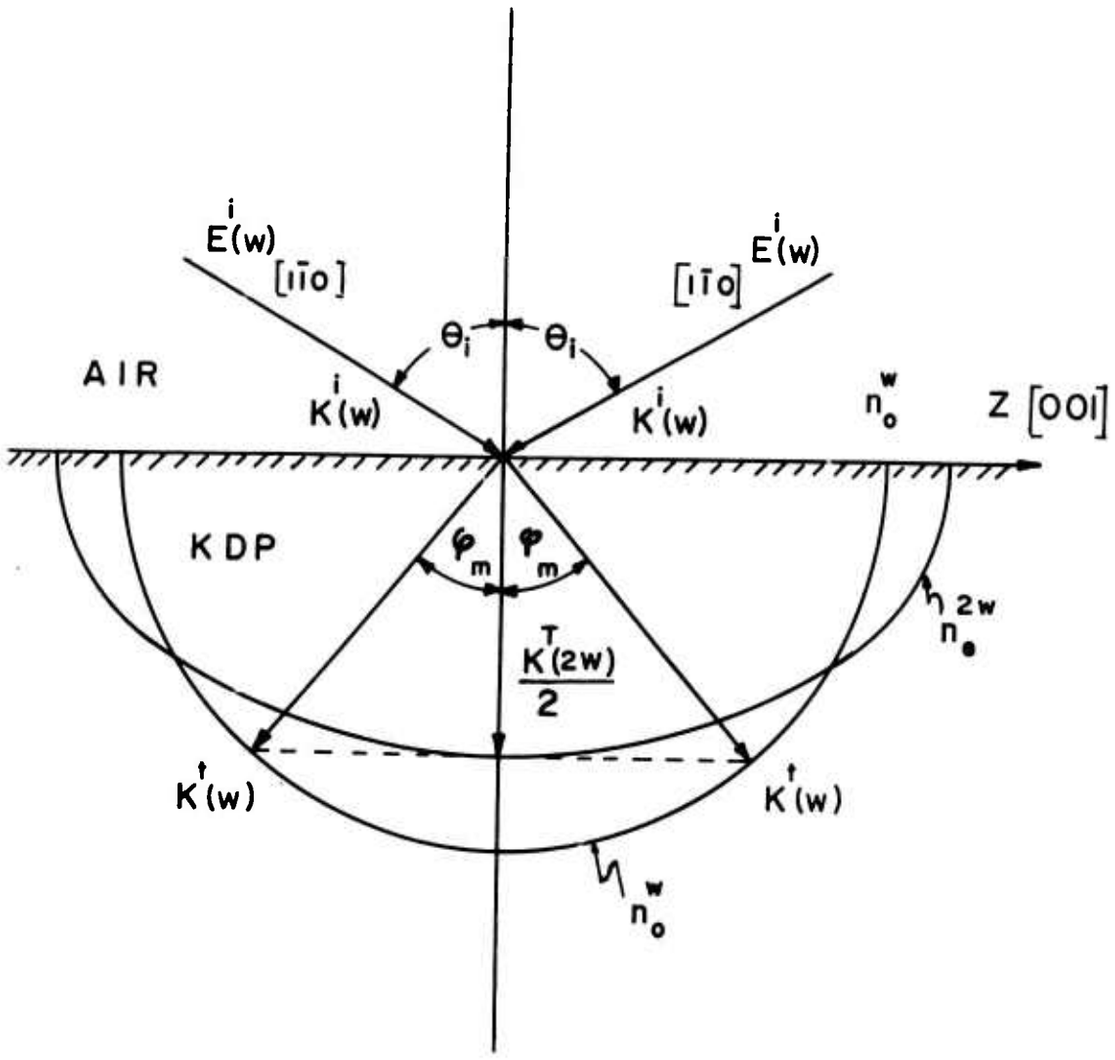
$E^i(w)$
[1$\bar{1}$0]
$E^i(w)$
[1$\bar{1}$0]
θ_i
θ_i
AIR
$K^i(w)$
$K^i(w)$
n_o^w
Z [001]
KDP
φ_m
φ_m
n_e^{2w}
$\frac{K^T(2w)}{2}$
$K^t(w)$
$K^t(w)$
n_o^w

FIGURE 2 - 9

(z) axis. Equation (2.50a), with $\theta_3 = 0$, can be reduced to

$$\frac{n_o^{\omega}}{c} \cdot \omega \cos\theta_1 + \frac{n_o^{\omega}}{c} \omega \cos\theta_2 = \frac{n_e^{2\omega}}{c} \cdot 2\omega \qquad (2.51)$$

By symmetry of Fig.2-9, $\theta_1 = \theta_2 = \varphi_m$, then (2.51a) turns out to be

$$n_o^{\omega} \cdot \cos\varphi_m = n_e^{2\omega} . \qquad (2.52)$$

Equation (2.52) is the condition for noncollinear phase matching for the experimental configuration shown in Fig.2-9. Having known the phase matching angle φ_m inside the crystal, the phase matching angle θ^i_{PM} for the incident beam can be computed via Snell's law given by equation (2.14).

$$\theta^i_{PM} = \sin^{-1}\left[n_{\omega}^{o} \sin\varphi_m \right] \qquad (2.53)$$

(taking $n_{air} = 1.0$).

C. Theory of Picosecond Pulsewidth Measurement

In this section, the theory involving the utilization of nonlinear optical methods for picosecond pulsewidth measurements will be discussed. Two photon fluorescence (TPF) method has been used for the measurement of picosecond pulsewidth by several authors[64, 72, 74]. However, particular treatment will be emphasized on harmonic generation method, which is utilized in this experiment.

Since KDP is a nonlinear crystal from which phase matchable SHG can be produced, then it is very convenient to use the square law intensity characteristics of KDP to measure the second order auto-correlation function of the laser light which, in this case, is a picosecond

pulse from Nd:glass laser. In the previous experiments[62, 75, 78], the harmonic intensities resulted from the spatial and temporal overlapping in the nonlinear media were weak such that they could be detected only by means of photomultiplier.

In the experiment KDP crystal of a special cut such that noncollinear phase matching can be achieved, is served as the source of SHI. Therefore, it is anticipated that there will be high SHI produced and the measurement of the pulsewidth can be done by means of both photomultiplier and photographic methods. The theory behind this measurement method for second order auto correlation is given below.

1. Second Order Auto-Correlation. The SHI radiating from the KDP crystal represents the variation of the auto-correlation function with respect to the degree of spatial and temporal overlapping of the light pulse onto itself. This can be performed by using a beam splitter and two 100% reflectors reflecting the two beams into the KDP crystal where in spatial and temporal overlapping occurrs . The schematic diagram is shown in Fig. 2-10. The incident electric field is $\vec{E}(\vec{r}, t)$. Then the resulting electric field $\vec{E}_R(\vec{r}, t)$ inside the KDP crystal is given by

$$\vec{E}_R(\vec{r}, t) = \vec{E}(\vec{r}, t) + \vec{E}(\vec{r}, t + \tau) \tag{2.54}$$

where $\tau = 2nd/c$ is the delay time of one of the reflected beams, and $2nd$ is the optical path difference between the two beams . The output, resulting from the overlapping of the two beam, is in the form of average second harmonic intensity $\langle SHI \rangle$ in the direction normal

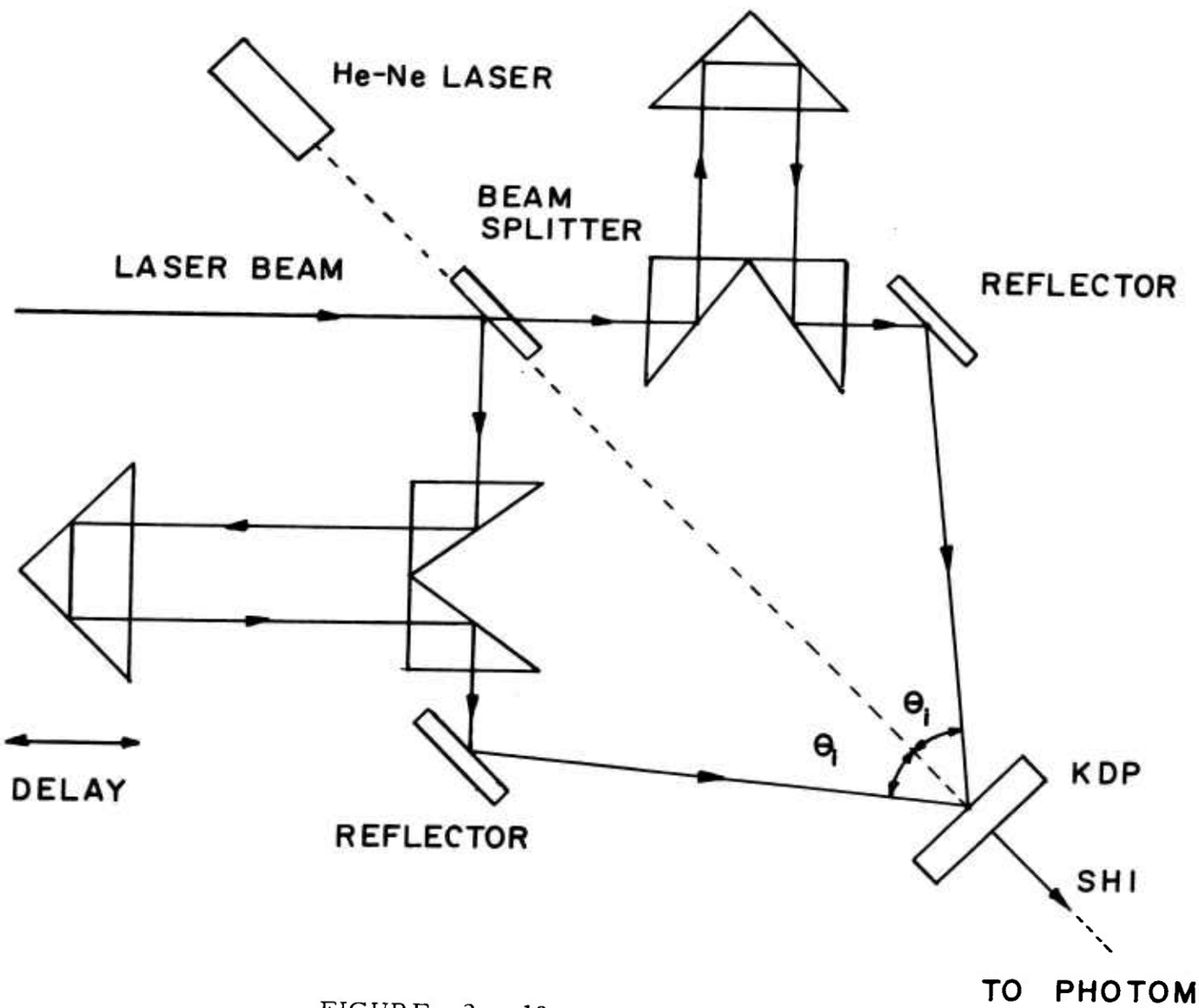
He-Ne LASER
BEAM
SPLITTER
LASER BEAM
REFLECTOR
DELAY
REFLECTOR
KDP
SHI
TO PHOTOMULT.

FIGURE 2 - 10

inward to the crystal. The $\langle SHI \rangle$ can be expressed in terms of the analytic signal $V_R(t, r)$ associated to the real field $E_R(t, r)$ as

$$\langle SHI \rangle \sim \langle V_R(t, r)\, V_R(t, r)\, V_R^*(t, r)\, V_R^*(t, r) \rangle \qquad (2.55)$$

where V_R^* is the complex conjugate of V_R.

The analytic signal is well known as the complex representation of an oscillating field. The real part of $V(t)$ is equal to the light field $E(t)$ and the imaginary part is its Hilbert transform. Since in the classical limit $V^*(t)$ corresponds to the quantum mechanical anihilation operator a and $V(t)$ to the creation operator a^+. One can view equation (2.55) as directly related to the quantum mechanical probability P for two photon absorption in the two photon fluorescence (TPF) method.

$$P \sim T_r \{ \rho\, a^+ a^+ a a \} \qquad (2.56)$$

where ρ is the density matrix describing the light field.

By using equation (2.54) and (2.55) the observed $\langle SHI \rangle_\tau$ at a certain position r corresponding to the delay τ is expressed by the incident light field $V(t)$ as

$$\begin{aligned} \langle SHI \rangle_\tau \sim & \langle (V - V_\tau)(V - V_\tau)(V^* - V_\tau^*)(V^* - V_\tau^*) \rangle \\ = & 2\langle V V V^* V^* \rangle + 4\langle V V_\tau V^* V_\tau^* \rangle \\ & - 2\langle (V V^* + V_\tau V_\tau^*)(V V_\tau^* + V^* V_\tau) \rangle \\ & - \langle V V_\tau^* V V_\tau^* + V^* V_\tau V^* V_\tau \rangle \end{aligned} \qquad (2.57)$$

where $V = V(t)$ and $V_\tau = V(t + \tau)$.

In equation (2.57), the first two terms are proportional to the

intensity correlation function $G^{(2)}$, known as Glauber's second order coherence function[83]. The last two terms describe the interference effects, giving spatial variation proportional to $\cos \omega_o \tau$ and $\cos 2\omega_o \tau$, respectively, where ω_o is the center frequency of the light field. These variation are averaged out to be zero since the average value of $\cos \omega_o \tau$ and $\cos 2\omega_o \tau$ over and interval $\Delta\tau$ corresponding to several wavelength vanish. The normalized intensity $\langle SHI \rangle$ is now expressed by intensity correlation function $G^{(2)}(\tau)$ of the incident field

$$\langle SHI \rangle_\tau = \frac{2\, G^{(2)}(0) + 4\, G^{(2)}(\tau)}{G^{(2)}(0)} \tag{2.58}$$

where $G^{(2)}(\tau)$ is defined as

$$G^{(2)}(\tau) = \frac{\langle V(t)\, V(t+\tau)\, V^*(t)\, V^*(t+\tau) \rangle}{\langle V(t)\, V^*(t) \rangle \langle V(t+\tau)\, V^*(t+\tau) \rangle} \tag{2.59}$$

The bracket indicates the time average or ensemble average. If only the time average is considered, we can use $I_R(t) = V_R(t)\, V^*(t)$ and arrange equation (2.59) into a new form as

$$G^2(\tau) = \frac{\int_{-\infty}^{\infty} I(t)\, I(t+\tau) dt}{(\bar{I})^2} \tag{2.60}$$

where $I(t)$ is actual intensity and $\bar{I}$ is the mean intensity.

In the experiment the KDP crystal is oriented in such a way that the noncollinear phase matching for SHI will be achieved if and only if the two beams have temporal and spatial overlapping inside the crystal. The nonlinear polarization P^{NLS} will be created and then it radiates at second harmonic frequency. In terms of those applied

electric fields the P^{NLS} is given by

$$P^{NLS} \sim E(t) \cdot E(t+\tau) \tag{2.61}$$

Further, P^{NLS} can be described by analytic signal V_{SH}. Using the analytic signal $V(t)$ associated with the real field $E(t)$, the analytic signal V_{SH} is directly obtained from

$$V_{SH} \sim V(t) \cdot V(t+\tau) \tag{2.62}$$

By using $I(t) = V(t)\, V^{*}(t)$ and equation (2.62). The average second harmonic intensity $\langle I_{SH} \rangle$ produced by two parts of the same signal $V(t)$ with spatial overlapped and time delay τ is given by

$$\langle I_{SH} \rangle \sim V(t)\, V(t+\tau)\, V^{*}(t)\, V^{*}(t+\tau) \sim G^{(2)}(\tau) \tag{2.63}$$

In this case the second harmonic intensity is a direct measurement of the second order auto-correlation function $G^{(2)}(\tau)$. Since neither one of the fundamental beams can produce SHI in the normal direction, then there will be a background free auto correlation function $G^{(2)}(\tau)$ and there is no contrast ratio, as in TPF method, to be considered.

Since the $G^{(2)}(\tau)$ obtained in the experiment is background free function, then by using the photographic method the exposure of the film will reveal the pulsewidth of the $G^{(2)}(\tau)$ function which in turns gives the direct measurement of the picosecond pulsewidth. Furthermore, the two fundamental beams are obliquely incident on the crystal as shown in the Fig. 2-11. Due to the finite size of the two beams, there will be a built-in time delay along different points on the surface of the very thin crystal. As shown in Fig. 2-11, at the central point of the

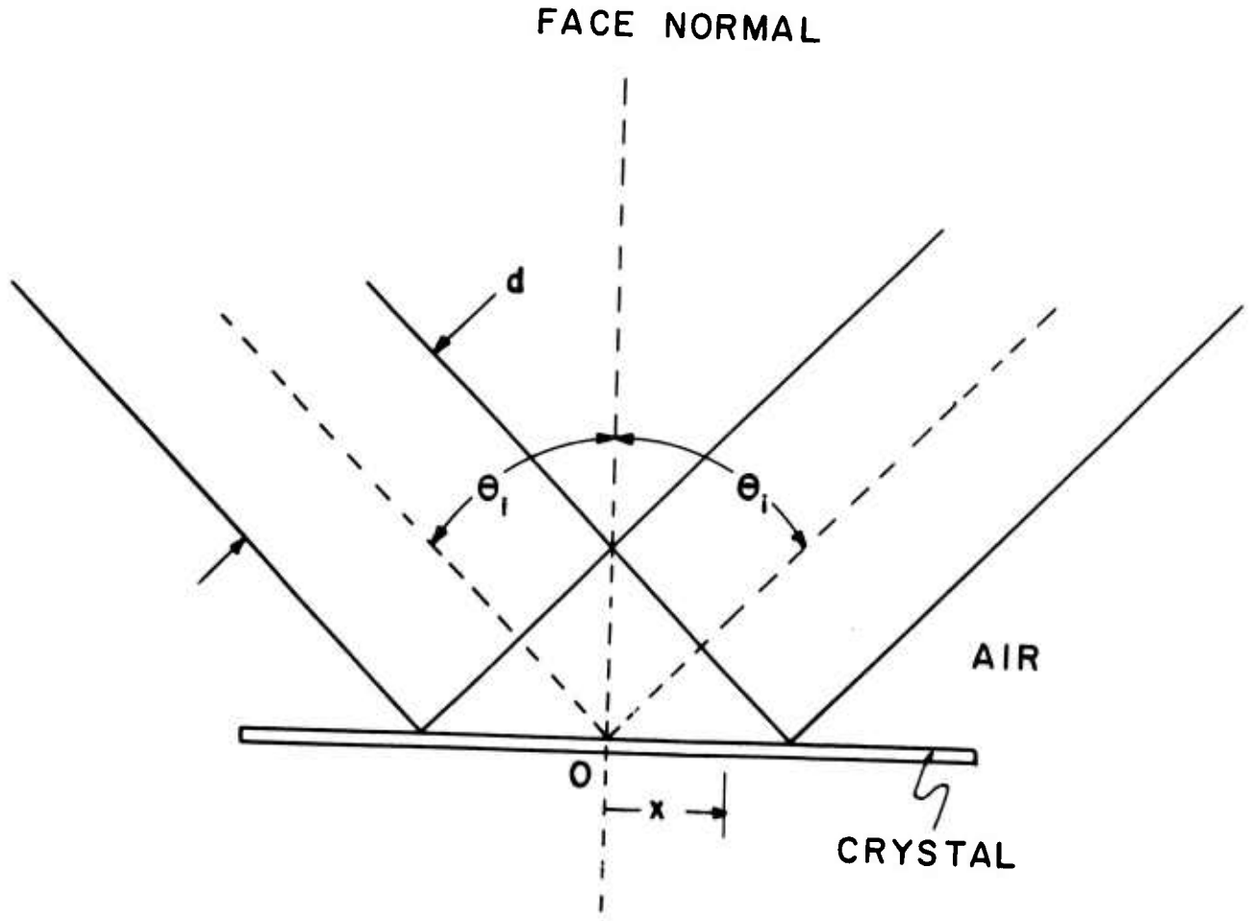

FIGURE 2 - 11

overlapping region, the light pulse of two beams arrive at the same time, thus there is no time delay. At the point x away from the center the light pulse from one beam will arrive at time $\Delta\tau$ earlier then the other beam. The delay is given by

$$\Delta\tau = \frac{2x \cos(90^{o} - \theta^{i})}{c/n}$$

$$\Delta\tau = \frac{2x \sin \theta^{i}}{c/n}$$

where c is the velocity of light,

θ^{i} the angle of incidence

n the refractive index of the linear medium.

For a beam of width d, the maximum delay τ across the entire overlapping region is

$$\Delta\tau)_{max} = \frac{d}{c} \sin \theta^{i} \qquad (2.64)$$

where n = 1.0 for air.

For d = 5 mm, $\theta^{i} = 15^{o}$ the maximum delay $\Delta\tau)_{max}$ is calculated to be about 5 picoseconds. This total built-in delay will be enought to cover a picosecond pulsewidth which has a theoretical value about 0.33 picosecond.

In order to cover the entire picosecond pulsewidth measured at the base, a crystal of larger birefringence is required.

Such a crystal will provide a relatively large noncollinear phase matching angle which in turn gives at higher value of $\Delta\tau)_{max}$ in (2.64) Another factor that will increase $\Delta\tau)_{max}$ is the index of refraction n of the linear medium. One can use a linear optically denser liquid called 1-Bromonaphthalene instead of air in the experiment.

CHAPTER III
EXPERIMENTAL TECHNIQUE

Since the present experimental work, by nature, involves nonlinear optical interaction in KDP crystal, it is appropriate to concisely describe the experimental arrangements and techniques including the laser systems that were used. The source of excitation was a Nd:glass laser which was operated in mode locked and Q-switched fashions. During the course of the experiment very high and low second harmonic intensities (SHI) were encountered and properly detected and subsequently they were compared to the theory. Furthermore, the experimental results concerning polarization properties and phase matched condition of KDP crystal were utilized for measurement of picosecond pulsewidth of Nd:glass laser. In this chapter major experimental preparations and techniques involved in setting up and detection second harmonic signal will be given. Since a Nd:glass laser was employed as the excitation source, and also to facilitate understanding the picosecond pulsewidth measurement, the Nd:glass laser operated in mode locked and Q-switched fashions will be briefly discussed below.

A. The Neodymium Glass Laser

The laser rod is made of glass in which the Nd^{+3} ions reside and act as impurities. The energy levels involved in the laser transition the excited states of Nd^{+3} ion. The laser action take place from the upper level $^4F_{3/2}$ to the lower level $^4I_{11/2}$ which

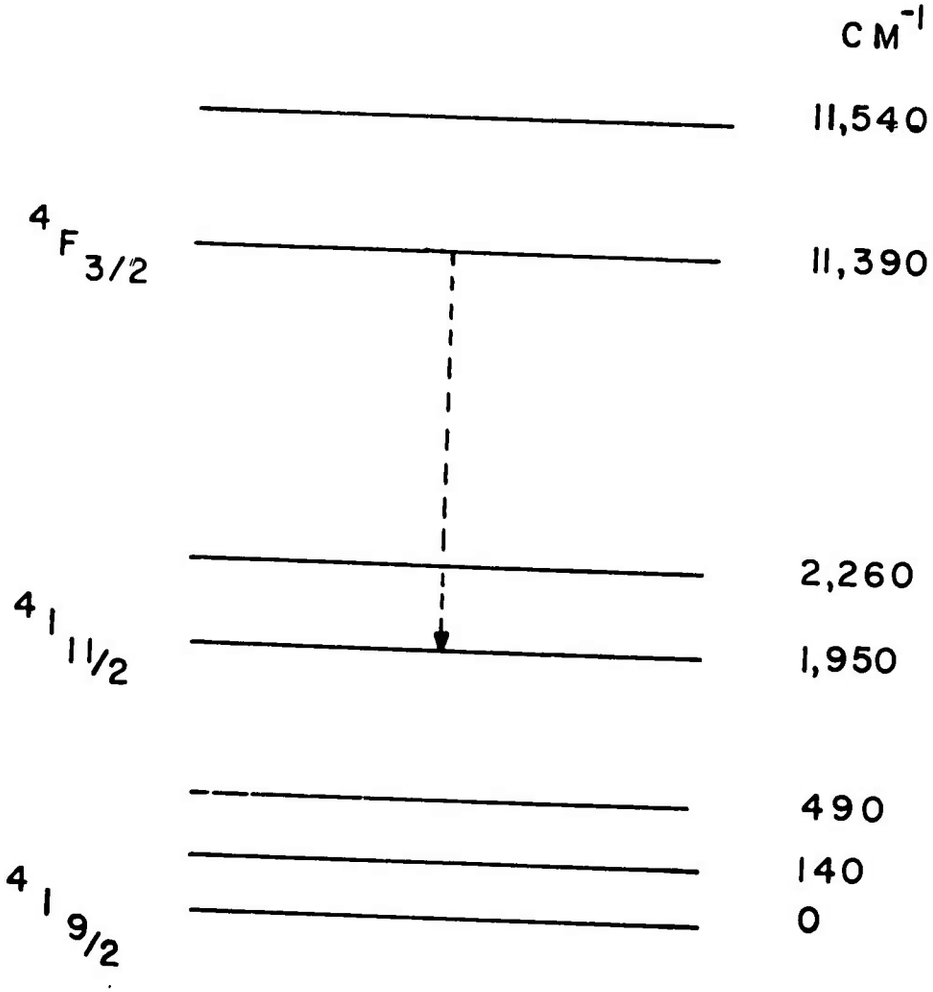

FIGURE 3 - 1

is approximately 1950 cm^{-1} above the ground state as shown in Fig. 3-1. The laser is classified as 4 level laser system from which the emission wavelength $\lambda_o = 1.06\mu m$ is radiated. The fluorescent linewidth can be measured directly and ranges around $300cm^{-1}$ (82). This width is rather broad. This is due to the amorphous structure of glass, which causes different Nd^{+3} ions to "see" slightly different surrounding. This causes their energy splitting to vary slightly. Different ions consequently radiate at slightly different frequencies, causing inhomogeneous broadening of the spontaneous emission spectrum. This larger bandwidth is advantageously utilized for mode locking the laser since it can support many axial modes , N , in the oscillation . For Nd:glass laser N is about 10^4.

1. <u>The mode locked Nd:glass laser.</u> The mode locked Nd:glass laser used in the experiment was a Korad Kl-system as shown in Fig. 3-2. It is consisted of Nd:glass rod having a Brewster - Brewster configuration to avoid reflection losses. The laser rod is of diameter 1.25 cm and of length 20cm. The two coated dielectric mirrors have at 1.06 μm reflectivities of 100% and 65%, respectively, and form a laser cavity having 75 cm length. In addition the contact dye cell of 0.078 cm thick, is attached to the mirror M_1 (100% reflectivity). The cell contains Kodak 9860 dye solution dissolved in dichloroethane . The solution serves as passive nonlinear absorber which is required to achieve mode locked pulse. Since the inhomogeneous linewidth ($\Delta\nu$) of the laser is $3x10^{12}$ Hz , then it is expected theoretically that the laser pulse will be of 0.33 picoseconds duration.

To generate ultra short pulses from the system, all the laser modes (axial modes) falling within the laser linewidth must be coupled together. This can be achieved by introducing the cell containing passive nonlinear absorber as described above. Despite of its wide use, passive mode locking is not well understood. However the mode locking by using saturable absorber can be explained on a qualitative basis in the time domain as follows:

The laser can be viewed as a quantum mechanical oscillator building up from spontaneous emission noises of various amplitude and intensity. The saturable absorber (dye solution) has a nonlinear absorption characteristic which for low light intensities acts as a strong absorber and for high light intensities is transparent. When the laser starts to build up, the low amplitude portions of the amplified fluctuating spontaneous emission noises are discriminated against the higher amplitude portion because of the nonlinear absorber. As a consequence, the lower intensity portion of the pulse is cut off and the peak portion is allowed to pass through the absorber. By the time the pulse is reflected back from the mirror, the absorber relaxes to the ground state and once again the pulse is sharpened and amplified by the laser rod. After many passes through the cavity, the pulse is narrowed to its limit, which is the inverse of the oscillating bandwidth of the laser system. The output will be a train of picosecond pulses contained in a single envelope. The characteristic length of the pulse train is about 300-600 nanoseconds.

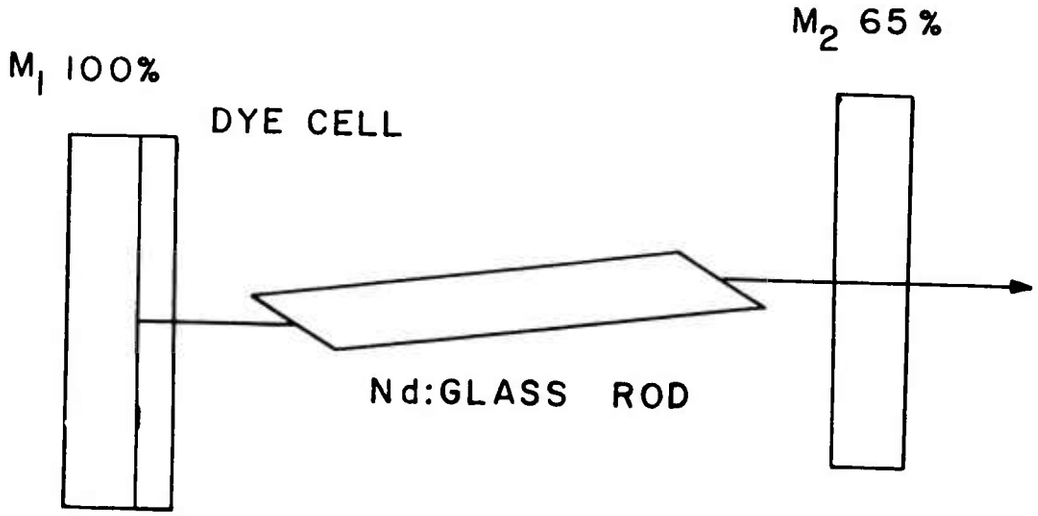

FIGURE 3 - 2

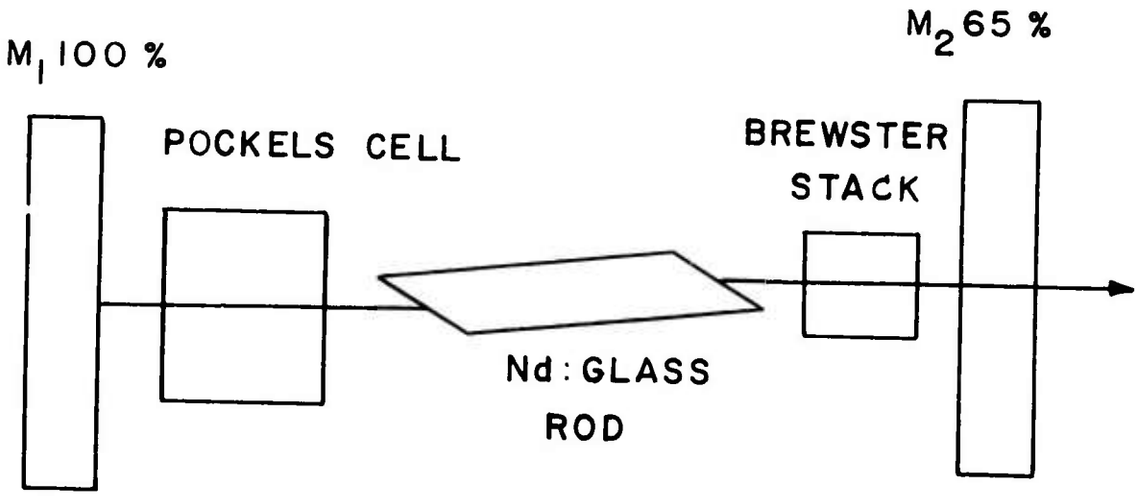

FIGURE 3- 3

The mode locked laser has two major advantages which are employed in the experiments. First, not like other lasers, it has a definite phase relationship among participating modes (axial modes). This causes the intensity of the laser output to have a temporal coherence and overall less fluctuation[87]. It is very important to the SHG experiment since it is a nonlinear optical process. Indeed, experimental data points are found to exhibit less fluctuation. Secondly, the laser system of this type has very high peak power. Therefore it is very useful for SHG when this effect is extremely small as in certain situation, e.g. Nonlinear Brewster's angle condition. Due to the ultrashort pulse duration the damage threshold to the crystal will be high; consequently crystal will not be easily damaged by the experiment.

2. The Q switched Nd:glass Laser. In the experimental investigation for two beam spatial mixing (TBSM) and for noncollinear phase matching in KDP, the Nd:glass Q-switched laser was utilized. Q-switched pulses were obtained by means of Korad Pockels cell model K-QS2 and polarizer stack consisting of glass plates oriented at Brewster's angle. The Q-switched Nd:glass laser system is depicted in Fig. 3-3. The Pockels cell and polarizer stack were oriented in such a way that their polarization axes were orthogonal to each other. A Pockels cell operation can be briefly described as follows. It serves as an optical shutter for Q-switched operation. While the laser rod is being pumped and the laser is building up the Pockels cell will be passive in the sense that it blocks or prevents the laser light from

reaching the cavity mirror M_1. This will introduce high losses into the system such that the laser oscillation is prevented at the low population inversions. When the population inversion in the laser rod reaches maximum value, the Pockels cell is triggered by means of the delay electronic circuit. At this moment a high voltage is applied across the crystal in the cell such that via electrooptical effects the axis of the polarization of the crystal is rotated by $\pi/2$. The laser light will pass through the cell reaching the mirror M_1 and be reflected back. Upon returning from mirror M_1 and passing through the cell again, the polarization of the light is suffered another $\pi/2$ rotation. The total change of the polarization of the light is π. Then the light can pass through the laser rod, the polarizer stag and reaches the mirror M_2. The essential role of polarizer stag is to enforce the polarization of the light and helps the Pockels to work efficiently. This will result in raising the Q of the system to a very high value in a short time. As a consequence the system will oscillate at the highest population inversion level. Then the laser will lase out from the mirror M_2 as a giant pulse having pulse duration about 30 nanoseconds. The Pockels cell for Q-switching is very effective and the Q-switched pulse is reproducible. Besides it is much easier to operate than the clumsy passive dye Q-switched cell used in the early day. The advantage of using a Q-switched pulse for two beam spatial mixing (TBSM) experiment is that its pulse duration is so long that the temporal overlapping is always achieved.

B. KDP Crystal

The nonlinear crystals used in the experimental investigation are all KDP (Potassium di Hydrogen Phosphate) of several crystallographic cuts. The orientation of crystallographic axes of the crystals are given along with the experimental results in chapter IV. The crystal KDP is a tetragonal crystal belonging to the symmetry class $\bar{4}2m$. It is piezoelectric and the second harmonic polarization in it is given by the equations (2.40) in Chapter II and its nonlinear susceptibilities has been given elsewhere[84].

The crystal is eminently suitable for the present experiment since it is phase matchable and has relative high value of the nonlinear susceptibility. Furthermore it is transparent at the fundamental and second harmonic wavelengths respectively. This will enable an investigation in transmission. In addition to possessing the intrinsic properties described above, its linear optical properties are isotropic so that the equations developed in chapter II are applicable. Because its linear index of refraction is relatively low, total reflection from it is possible via the optically denser linear fluid 1- Bromonaphthalene. From the tables for refractive dispersion[82] its indicies of refraction for the ordinary and the extraordinary rays at the fundamental and second harmonic wavelengths are deduced and given as

$$n_o^{\omega} = 1.4943$$

$$n_o^{2\omega} = 1.5131 \qquad n_e^{2\omega} = 1.4708$$

Where ω corresponds to the fundamental wavelength of 1.06μm.

The KDP crystals were ordered and prepared by Gould Inc. Tne typical dimensions of the crystals are 25 x 15 x 8 mm^3. The entrance and exist surfaces are polished optically flat to $\lambda/5$ at the D-line of sodium light. The other surfaces are see-through polished. The parallelism between opposite faces is better than 30 seconds, and none of surfaces are coated.

C. Optically Dense Fluid

In the experimental investigation of a phenomenon so-called total reflection and Nonlinear Brewster's angle are involved. The investigation under these conditions can be achieved only if the linear medium from which the laser beam is incident has a higher index of refraction than KDP. To observe the Nonlinear Brewster's angle of KDP in air would require an angle of incidence from air to KDP greater than 90°. This is impractical. Therefore, it is essential that the linear medium in contact with KDP, must possess a higher index of refraction. By using optically denser fluid 1-Bromonaphthalene, the angle of incidence which corresponds to the Nonlinear Brewster' s angle is in the vicinity of 43.0°.

In the experiment, the nonlinear crystal KDP was immersed in the optically denser fluid 1-Bromonaphthalene which has larger indices of refraction than KDP at both ω and 2ω The fluid is transparent from the range 0.4 - 1.06 μm. The index of 1-Bromonaphthalene has been tabulated at five different wavelengths[85]. The values at wavelengths of interest may be interpolated by means of the Cauchy relation[86].

This gives for the index of refraction of the fluid

$$n_{liq}(\omega) = 1.6260 \qquad n_{liq}(2\omega) = 1.6701$$

From Snell's law given in Chapter II one finds the critical angles for total reflection of the fundamental and second harmonic beams to be $\theta_{cr}^{i}(\omega) = 66.78^{o}$ $\theta_{cr}^{i}(2\omega) = 64.76^{o}$, respectively.

D. Experimental Arrangement

In the present study, the experimental arrangement can be divided into two major parts. One involves detection of SHG in the reflection and transmission using a single incident laser pulse and the other is two beam spatial mixing (TBSM) setup and measurement of a picosecond pulse. The experimental arrangements are described in the following.

1. Experimental Arrangement for SHG in Reflection and Transmission. The excitation source for this case was a Nd:glass laser operated in mode locked fashion. The laser system cavity mirrors M_1 and M_2, a contact dye cell with dye solution Kodak 9860 dissolved in dichloroethane and a water cooled laser head. The laser head consists of a Nd^{+3} doped glass rod. The rod was surrounded by a helical xenon flash lamp. The laser system is shown in Fig. 3-2 in the previous section. All optical alignment was performed with the help of He-Ne gas laser. The cavity length which was the optical path length between the mirrors M_1 and M_2 is about 75 cm. The entire laser system was covered with a wooden box, to

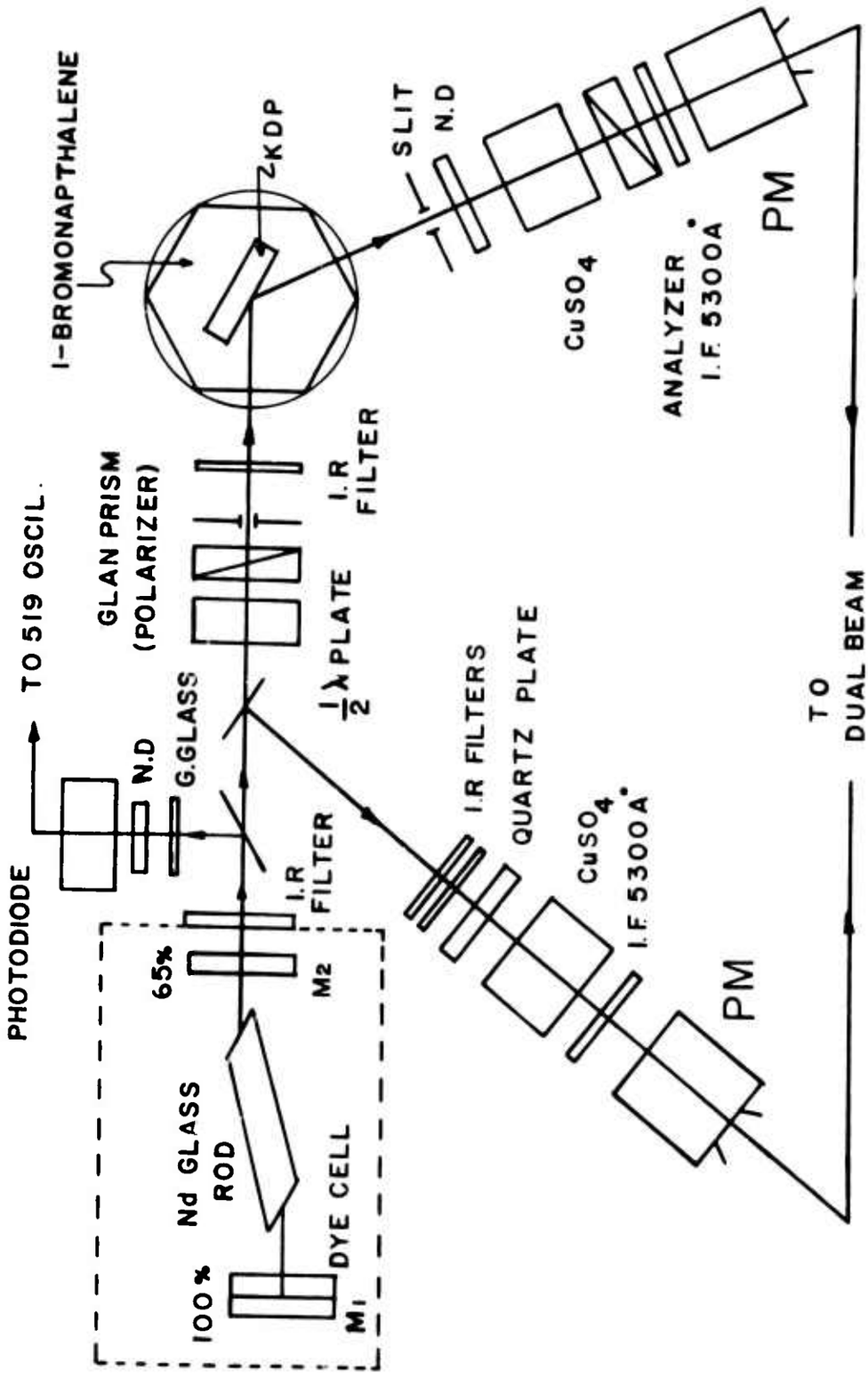
1-BROMONAPTHALENE
KDP
SLIT
N.D
CuSO4
ANALYZER
I.F 5300A°
PM
TO 519 OSCIL.
GLAN PRISM
(POLARIZER)
I.R
FILTER
½λ PLATE
G.GLASS
N.D
PHOTODIODE
65%
M2
I.R
FILTER
I.R FILTERS
QUARTZ PLATE
CuSO4
I.F 5300A°
PM
TO
DUAL BEAM
OSCILLOSCOPE
Nd GLASS
ROD
100%
M1
DYE CELL

FIGURE 3 - 4

prevent the flash lamp radiation during the pumping period from interfering with the SHI detection. Furthermore a Corning filter, no 2-64 (C. F. 2-64) was used at the exist of the wooden box to filter out the residual flash lamp light in the lasing direction. The experimental layout which will be described hereafter is depicted in Fig. 3-4. The fundamental beam was then partially deflected by an ordinary glass slide plate into a ITT photodiode F-400 (S-1) with ground glass and neutral density filter in front of it. The pulse from the ITT photodiode, displayed on a Tektronic 519 oscilloscope had an overall rise time of 0.7 nanosecond. In turn the Tektronic 519 oscilloscope also provided, upon registering the fundamental beam, the triggering signal to the Tektronic 557 dual beam oscilloscope, used for recording SHI from the monitor channel and from the KDP. A piece of z-cut quartz platelet was used in the monitor arm. The laser pulse causes the quartz to generate SHI which is used as a reference for reducing of statistical fluctuations in the SHG experiment The use of a monitor channel is a standard technique in nonlinear experimentation[27, 28].

The reason for using a z-cut quartz platelet quartz in the monitoring arm, rather than KDP, was that its surface did not deteriorate with time. The z-cut was chosen mainly because of the convenience in not having to worry about the orientation of the laser polarization with respect to the crystalline axis[27]. If the z axis is normal to the platelet, the second harmonic intensity from the quartz is proportional to

$$I(2\omega) \approx (\chi^{NL}(2\omega))^2 E^4_x(\omega) + 2E^2_x(\omega)E^2_y(\omega) + E^4_y(\omega))$$
$$(\chi^{NL}(2\omega))^2 E^4(\omega) \qquad (3.1)$$

Here $E_x(\omega)$ and $E_y(\omega)$ are the projection of the laser field on the X and Y axes of the quartz crystal. The second harmonic intensity was not changed when the quartz is rotated about the z axis. Another advantage of using a z-cut was that the crystal was far from the phase-matching condition. Thus accidental misalignment of the monitoring system would not effect the second harmonic conversion by a noticeable amount.

Corning filter CF 2-64 and 7-57 were used in front the quartz platelet in order to ensure that only the fundamental beam could strike the quartz. To discriminate the fundamental beam from the admixture of second harmonic signals from the quartz platelet, a copper sulphate solution ($CuSO_4$) was employed to filter out the fundamental. The remaining signal is then transversed through a Viard Atomic interference filter, having transmission peak at wavelength 5300$\mathring{A}$ corresponding to second harmonic of the fundamental. The signal was collected by a ten stage Amperex photomultiplier, model 56 AVP. The signal from the photo multiplier in the monitor channel was fed to the upper beam terminal of the Tektronic 551 dual beam oscilloscope.

The main fundamental beam was polarized in the vertical direction corresponding to the [110] direction of the KDP target.

The linear polarization of the fundamental beam was achieved by means of half waveplate and Glan-Kappa prism which were coated for

anti-reflection at the wavelength of 1.06μm. Before the fundamental beam entered a liquid cell, it transversed through Corning filters no. 2-64 and no. 7-56. This was to ensure that all spurious signals generated by the laser beam from various optical components were suppressed and only the fundamental beam of the wavelength $\lambda = 1.06\ \mu m$ would be incident on the KDP crystal.

The KDP crystal was mounted on an aluminum target holder which was connected to the angular rotator mounted on the platform above the liquid cell. The angular rotator was Kinematic model RT 200, with vernier scale permitting variation of rotation within accuracy of 0.01^{o}. The fundamental beam before entering the liquid cell was regulated by a rectangular slit 1 mm wide and 5 mm high. The liquid cell had a hexagonal shape with a circular flat fused quartz window on each side. Each window subtends an angle of 20^{o}. The cell contained optically denser fluid 1-Bromonaphthalene in which the KDP crystal was immersed. The KDP crystal was oriented in such a way that its nonlinear polarization source $\vec{P}^{NLS}$, in the direction of optic (z) axis, lay in the plane of reflection. The fundamental beam was polarized normal to the plane of reflection. In other words, the polarization of the fundamental beam was in the direction $[1\bar{1}0]$ with respect to the crystallographic axes of the KDP.

The detecting system for SHI produced from KDP was mounted on an aluminum arm pivoted underneath the liquid cell. The axis of rotation of the arm was common to the line passing through the center

of the cell and tangent to an entrance surface of the KDP. This will ensure that when the arm was rotated to change the angle of incidence θ^i, the SHI would be properly collected. Furthermore it helped to verify the directional property of SHI by rotating arm slightly off to both sides of the expected direction of the SH signal.

The detection system for SHI from the KDP was consisted of the following. A slit 4mm wide and 10 mm high was used to separate the reflected or transmitted SHI from the reflected or transmitted fundamental beam respectively. The slit was placed about 50 cm away from the liquid cell. For the case of total transmitted SHI where there were two transmitted beams of homogenous and inhomogeneous SHI, the larger slit was placed at 15 cm away from the cell to allow the two harmonic beams to pass through. Behind the slit a biconvex lense of 30 focal length was employed to ensure that all the harmonic signals would be properly collected by the photomultiplier which was about 75 cm away from the liquid cell. Between the lense and the photomultiplier a copper sulphate cell and Baird Atomic interference filter with transmission peak at 5300$\mathring{A}$ were employed in the manner as described previously for the monitor arm channel. Between the copper sulphate cell and the interference filter, a sheet of polariod was used for verifying the polarization orientation of second harmonic signal before passing through the interference filter. The photomultiplier in this channel was identical to that of the monitor channel so that the rise time of the two channels will be essentially the same and time correlation for SHG could be easily verified.

The signals from both channels were displayed on the dual beam oscillscope and photographed. The oscilloscope was triggered externally by a triggering signal from the Tektronic 519 oscilloscope which simultaneously monitored. To generate a data point, we took the ratio of the pulse heights corresponding to the signal and monitor intensity respectively and then averaged this ratio over five to ten laser firings. This was essential in order to improve the quantum statistical fluctuations of the SHG. The data points were plotted and compared to the computed theoretical curves.

2. Experimental Arrangement for Two Beam Spatial Mixing and Measurement of Picosecond Pulsewidth. When two fundamental beams have properly spatial and temporal overlapping inside a KDP crystal, second harmonic signal will be generated. This particular situation is well described previously in chapter II. To ensure the temporal overlapping inside the KDP crystal, Q-switched Nd:glass was used as a source of excitation since it had relatively long pulse duration. Q-switched pulse was produced by means of Pockels cell (Korad K-QS2) and polarizer stag inside the laser cavity. The arrangement for the monitor arm was exactly the same as described in the previous setup. The laser was again regulated by a slit of 2 mm wide and 5 mm high. A schematic of the experimental arrangement is shown in Fig. 3-5. After passing through the slit the fundamental beam was then reflected by a mirror having antireflection coating at $\lambda = 1.06\ \mu m$. The two fundamental beams were then made incident upon the KDP crystal. The

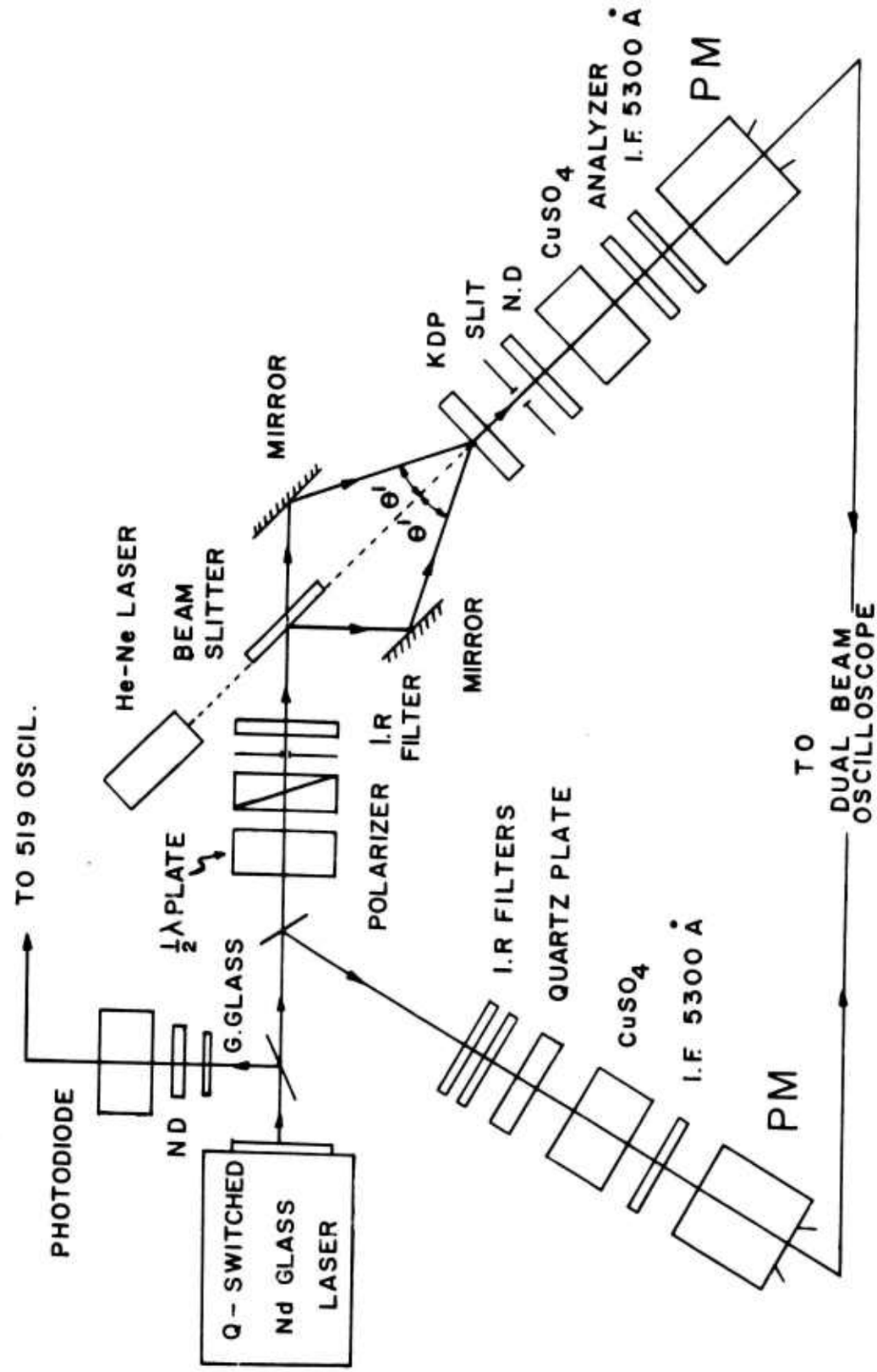
TO 519 OSCIL.
He-Ne LASER
BEAM SLITTER
MIRROR
KDP
SLIT
N.D
CuSO4
ANALYZER
I.F 5300 Å
PM
θ'
θ'
PHOTODIODE
ND
G.GLASS
½λ PLATE
POLARIZER
I.R FILTER
MIRROR
I.R FILTERS
QUARTZ PLATE
CuSO4
I.F 5300 Å
PM
TO DUAL BEAM OSCILLOSCOPE
Q-SWITCHED Nd GLASS LASER

FIGURE 3 - 5

KDP crystal and the detection arm for SHI from the KDP were fixed and aligned with the help of He-Ne gas laser which shone tangentially through the surface of the beam splitter (see the set up in Fig. 3-5). The KDP crystal is oriented in such a way that its optic (z) axis was parallel to the entrance surface and in the plane of reflection. This orientation of the KDP would yield the noncollinear phase matching condition, which was experimentally confirmed and will be discussed in Chapter IV. Angle of incidence ϑ^i of each fundamental beam was equal and regulated by the rotation of reflecting mirrors. The angular turning platforms on which both reflecting mirrors were situated had a 144:1 reduction gear ratio and a vernier scale permitting a variation of ϑ^i in step of 1 minute ($1/60^o$). The polarizations of both incident beams were in the direction normal to the plane of reflection. In another words they are in $[1\bar{1}0]$ direction with respect to KDP crystallographic axes. The detection arm was exactly the same as in the previous setup, however, it was fixed in a normal direction with respect to the exit surface of the KDP crystal. The Q-switched pulse shape of the fundamental beam was monitored by Tektronic 519 Oscilloscope which in turn provided triggering signal to the Tektronic dual beam oscilloscope on which both harmonic signals from the monitor and signal channel (from KDP) were displayed and photographed.

The experimental arrangement for measuring the picosecond pulsewidth was almost the same as in the TBSM experiment. However, the source of excitation was a mode locked Nd:glass laser which provided

FIGURE 3 - 6

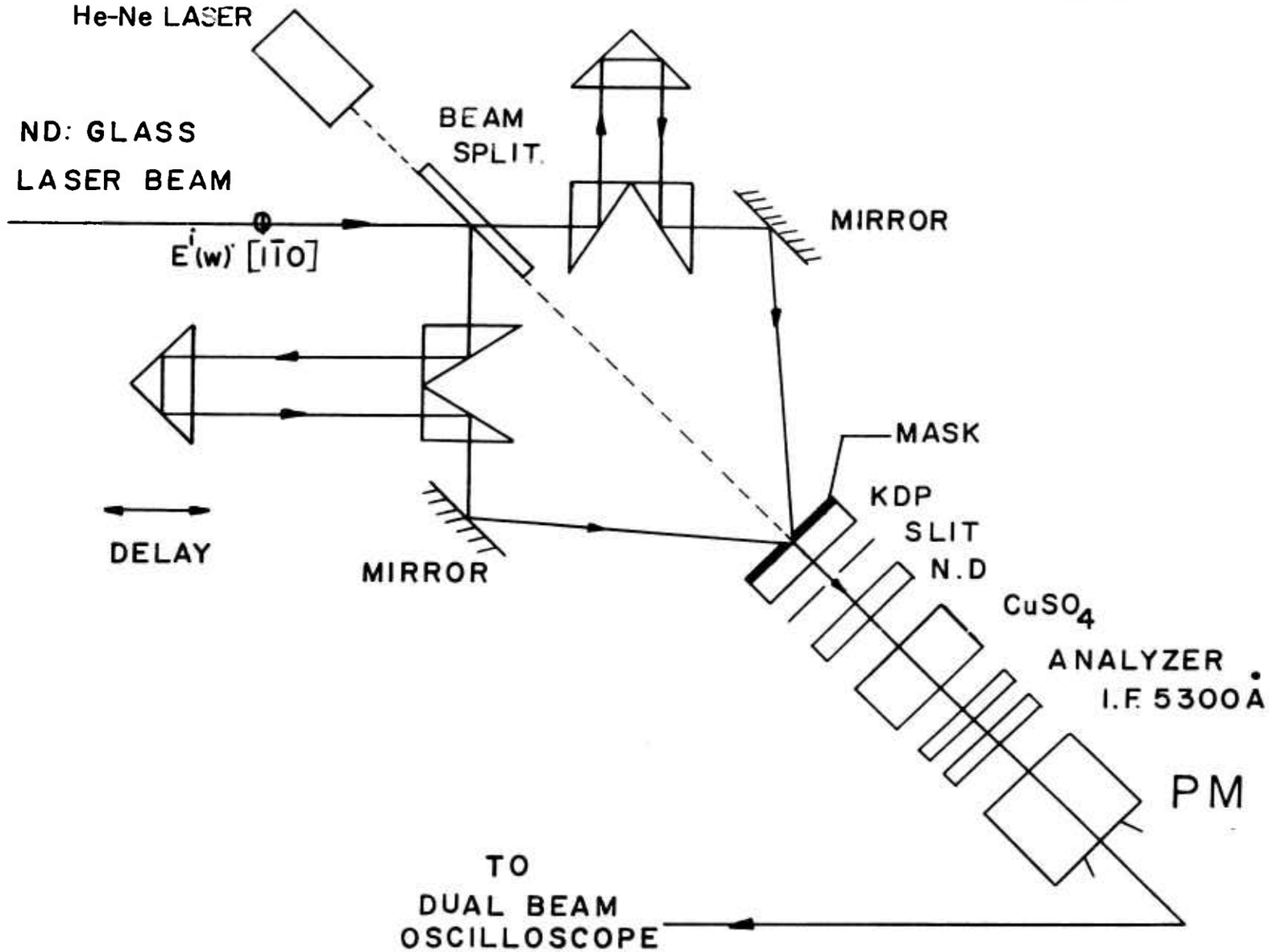
He-Ne LASER
ND: GLASS
LASER BEAM
BEAM
SPLIT.
MIRROR
$E^i(w)$ [ITO]
MASK
KDP
SLIT
N.D
$CuSO_4$
ANALYZER
I.F 5300Å
PM
DELAY
MIRROR
TO
DUAL BEAM
OSCILLOSCOPE

picosecond pulse trains. The experimental setup is shown in Fig. 3-6. Temporal delay for each beam was introduced between the beam splitter and the reflecting mirror. One delay was fixed and the other variable. A system of optical delay was composed of three right angle prisms as shown in Fig. 2-10. Variable temporal delay was achieved by mounting the prism on a very sensitive translational stage, which could translate in step of 1 mil (0.0254 mm), roughly equal to 1/10 picosecond. The KDP crystal with its orientation used in the investigation was the same as in TFSM case. In this experiment a single fundamental beam could not produce SHI in the normal direction to the exit face of the KDP crystal. It required both spatial and temporal overlapping of the two beams in the crystal. Spatial overlapping was easily arranged by properly rotating the two reflecting mirrors. However temporal overlapping could be achieved only by straight forward scanning the temporal delay until SHI was observed. By varying temporal delay and recording the corresponding SHI, the autocorrelation function was mapped out and the picosecond pulsewidth could be deduced.

CHAPTER IV
EXPERIMENTAL RESULTS

In this chapter, experimental results of second harmonic generation (SHG) in reflection and transmission from KDP crystal of various crystallographic orientations, using a mode locked and Q-switched Nd:glass lasers, are presented. Furthermore, an experimental technique of utilizing the polarization properties and phase matched condition in a KDP crystal for measurement of picosecond pulsewidth is reported and accounted for. The results of the present work are divided into four major parts namely the SHG in reflection, transmission, SHG by two beam spatial mixing (TBSM), and measurement of picosecond pulsewidth of Nd:glass laser. Those results are presented in the following paragraphs.

A. Second Harmonic Generation (SHG) in Reflection.

1. Nonphase Matchable SHG at Total Reflection. The KDP crystal used in this experiment has dimensions 25 x 15 x 8 $mm.^3$ The entrance surface is the 25 x 15 mm^2 face. The face normal of the entrance surface is along the optic axis which is [001] direction. The total reflection of the fundamental laser beam and for harmonic beam are achieved by means of optically denser linear fluid 1-bromonaphthalene as previously described. The polarization of the fundamental beam, as indicated in Fig. 4-1, is along the $[1\bar{1}0]$ direction.

The reflected second harmonic intensity generated from the crystal was observed as a function of the angle of incidence θ_i for the

crystallographic orientation shown in the inset of Fig. 4-1. The KDP crystal is a noncentrosymmetric cubic crystal and its linear susceptibility is a scalar. The theory developed by Bloembergen and Pershan[12], which is given in Chapter II, can be applied directly here. The reflected harmonic field polarized in the plane of reflection is given by equation (2.33a)

$$E_{R,ll} = 4\pi P^{NLS} F_{R,ll}^{NL} \tag{2.33a}$$

where the nonlinear Fresnel factor $F_{R,ll}^{NL}$ is given by equation (2.35a)

$$F_{R,ll}^{NL} = \frac{\sin\theta_S \sin\theta_T \sin(\alpha + \theta_S + \theta_T)}{\epsilon_R \sin\theta_R \sin(\theta_T+\theta_R)\cos(\theta_T-\theta_R)\sin(\theta_T+\theta_S)} \tag{2.35a}$$

The angles θ_R, θ_S and θ_T are related to θ_i by equation (2-29) which is recast into the forms

$$\begin{aligned} \sin\theta_R &= [n_{liq}(\omega)/n_{liq}(2\omega)] \sin\theta_i \\ \sin\theta_S &= [n_{liq}(\omega)/n_{cr}(\omega)] \sin\theta_i \\ \sin\theta_T &= [n_{liq}(\omega)/n_{cr}(2\omega)] \sin\theta_i \end{aligned} \tag{4.1}$$

where n_{cr} stands for reflective indicies of the KDP crystal whichare given in chapter III.

Using indicies of refraction for the liquid and the KDP, The critical angles of the fundamental and second harmonic beams can be found, according to equation (4.1) as

$$\begin{aligned} \theta^{cr}(\omega) &= \sin^{-1}\left(\frac{1.4943}{1.6260}\right) = 66.78^o \\ \theta^{cr}(2\omega) &= \sin^{-1}\left(\frac{1.4708}{1.6260}\right) = 64.76^o \end{aligned} \tag{4.2}$$

For $\theta_i > \theta^{cr}(\omega)$, θ_S becomes complex and one should use

$$\cos\theta_S = i[(\sin\theta_i/\sin\theta^{cr}(\omega))^2 - 1]^{1/2} \tag{4.3}$$

in equations (2.32b), (2.35a) and (2.39). Similarly, for $\theta_i > \theta^{cr}(2\omega)$, θ_T should be expressed as

$$\cos\theta_T = i[(\sin\theta_i/\sin\theta^{cr}(2\omega))^2 - 1]^{1/2} \tag{4.4}$$

According to the theory, the reflected second harmonic intensity $I_R(2\omega)$, given by equation (2.39), is

$$I_R(2\omega) = (c/8\pi)\sqrt{\epsilon_R}\,|E_o|^4\, dd'(4\pi\chi_{36}^{NL})^2\eta^2(f_R^L)^2 \times |F^L|^4\,|F_R^{NL}|^2\cos\theta_R(\cos\theta_i)^{-1} \tag{2.39}$$

The solid curve drawn in Fig. 4-1 is a plot of equation (2.39) on a relative scale and is calculated from the last five factors

$$|f_R^L|^2\,|F^L|^4\,|F_R^{NL}|^2\cos\theta_R(\cos\theta_i)^{-1}$$

This is appropriate since the remaining factors in equation (2.39) can be treated as constants in the experiment. The vertical scale in Fig. 4-1 is adjusted to the data. The experimental points are in striking agreement with the computed theoretical curve which displays nonanalytical singularities at angle of incidence $\theta_i = \theta^{cr}(\omega)$ and $\theta_i = \theta^{cr}(2\omega)$ respectively. These two singularities are expected since at these angle, $\cos\theta_S$ and $\cos\theta_T$ respectively, change from a real value to a pure imaginary value. We would like to point out specifically that the data points even reproduce two cusps in Fig. 4-1. This experimental features were not observed in the earlier measurements[28,29] of this sort. We attribute the

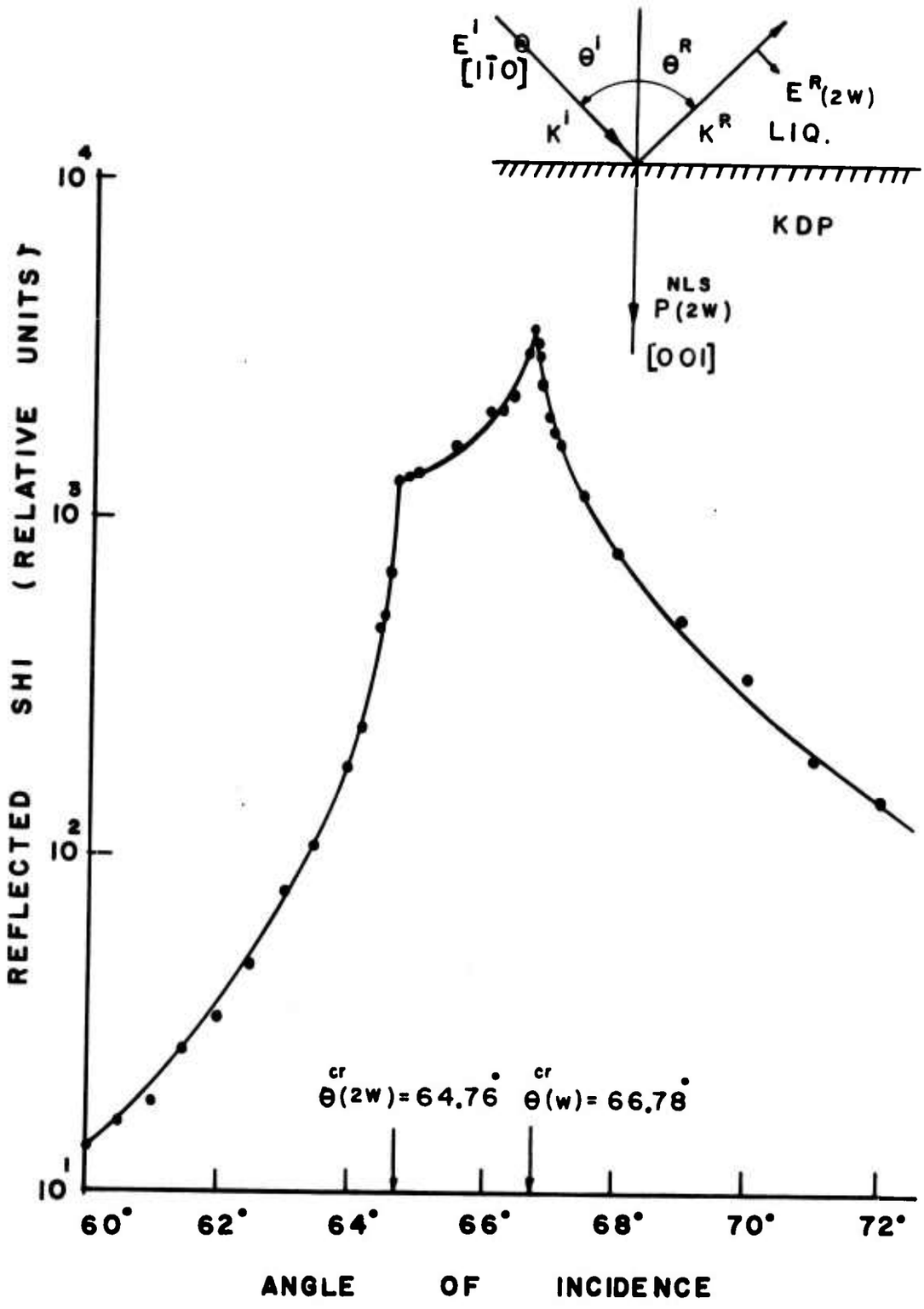
E^I
[1 1̄ 0]
θ
θ^I
θ^R
E^R(2w)
K^I
K^R
LIQ.
KDP
NLS
P(2w)
[0 0 1]
REFLECTED SHI (RELATIVE UNITS)
10^4
10^3
10^2
10^1
θ^cr(2w) = 64.76°
θ^cr(w) = 66.78°
60°
62°
64°
66°
68°
70°
72°
ANGLE OF INCIDENCE

FIGURE 4 - 1

success here to the fact that in our experiments the mode locked laser beam was used. The unique phase relationship among the axial modes in the fundamental beam eliminated most of the intrinsic quantum fluctuations which are typical of nonlinear optical experiments[87]. We thus emphasize once more the importance of using the mode locked laser in these experiments.

The enhancement of the reflected intensity arises mainly from two sources. First, the linear Fresnel factor F^{L} near the critical angle is larger than that away from this angle by about a factor of two. This will give a factor of sixteen in the reflected second harmonic intensity $I_R(2\omega)$. Second, the nonlinear Fresnel factor $F_{R,ll}^{NL}$ defined in equation (2.35a) in the neighborhood of these critical points as dominated by the term $[\sin(\theta_T+\theta_S)]^{-1}$ and it is larger than that away from these points by about a factor of three[88]. Therefore, after all factors are accounted for, the additional enchancement of $I_R(2\omega)$ in the neighborhood of the critical angles will be about two orders of magnitude. This result is in good agreement to the theoretical curve.

The physical interpretation of the enhancement of nonlinear Fresnel factor is that momentum matching[33, 34] for the wave propagating parallel to the surface inside the nonlinear medium is important in determining the reflected second harmonic intensity $I_R(2\omega)$ at the critical angle. The reflected second harmonic intensity near the critical angle is generated by the polarization in a surface layer with thickness of about $(\lambda \ell_{coh})^{1/2}$ where ℓ_{coh} is defined as the coherent

success here to the fact that in our experiments the mode locked laser beam was used. The unique phase relationship among the axial modes in the fundamental beam eliminated most of the intrinsic quantum fluctuations which are typical of nonlinear optical experiments[87]. We thus emphasize once more the importance of using the mode locked laser in these experiments.

The enhancement of the reflected intensity arises mainly from two sources. First, the linear Fresnel factor F^{L} near the critical angle is larger than that away from this angle by about a factor of two. This will give a factor of sixteen in the reflected second harmonic intensity $I_R(2\omega)$. Second, the nonlinear Fresnel factor $F_{R,\,ll}^{NL}$ defined in equation (2.35a) in the neighborhood of these critical points as dominated by the term $[\sin(\theta_T+\theta_S)]^{-1}$ and it is larger than that away from these points by about a factor of three[88]. Therefore, after all factors are accounted for, the additional enchancement of $I_R(2\omega)$ in the neighborhood of the critical angles will be about two orders of magnitude. This result is in good agreement to the theoretical curve.

The physical interpretation of the enhancement of nonlinear Fresnel factor is that momentum matching[33,34] for the wave propagating parallel to the surface inside the nonlinear medium is important in determining the reflected second harmonic intensity $I_R(2\omega)$ at the critical angle. The reflected second harmonic intensity near the critical angle is generated by the polarization in a surface layer with thickness of about $(\lambda \ell_{coh})^{1/2}$ where ℓ_{coh} is defined as the coherent

length. In general, the reflected second harmonic intensity at angles away from the critical angle is only generated from a layer about $\lambda_o / \sqrt{\epsilon_T}$ thick.

2. Phase Matched Second Harmonic Generation (SHG) at Total Reflection. The KDP crystal used in this case has dimensions of $25 \times 12 \times 18\ mm^3$. The entrance surface is $25 \times 12\ mm^2$ face and it has a face normal in the [111] direction. The crystal was immersed in the optically denser linear fluid 1-bromonaphthalene. The special cut was specially made for the crystal in such a way that the phase matching direction is along the entrance surface of the crystal. This can be done by cutting the crystal such that the optic (z) axis, which is in the same direction of nonlinear polarization $\vec{P}^{NLS}$, makes a phase matching angle θ_m to the surface. The angle θ_m was computed by using equation (2.46) and indices of refraction of KDP crystal. It was found that at the wavelength of interest the angle θ_m takes value of 41.2^o. The reflected second harmonic intensity $I_R(2\omega)$ generated by the crystal was observed as a function of the angle of incidence θ_i for the crystallographic orientation shown in the inset of Fig. 4-2. The fundamental field was polarized along the $[1\bar{1}0]$ direction and propagated as an ordinary ray. According to equation (2.31a) the nonvanishing nonlinear polarization was along the optic axis and therefore the harmonic field was polarized in the plane of reflection and propagated as an extraordinary ray.

The experimental result in Fig. 4-2 shows that the reflected second harmonic intensity increases by about three orders of magnitude when

the angle of incidence is changed by a few tenth of a degree in the vicinity of the critical angle. There is one maximum (peak) value of the reflected harmonic intensity and it is exactly at $\theta^{i} = \theta^{cr}(\omega) = 66.78^{o}$ in agreement to the theoretical prediction. The observed maximum reflected intensity is about 30 times of magnitude larger than reflected intensity in the nonphase matching case described in the previous section. This is due to more enhancement of the reflected harmonic intensity by nonlinear Fresnel factor in the phase matching case.

The enhancement can be mathematically explained in the view of equation (2.39) and (2.35a). According to the crystallographic cut of the crystal, the value of the nonlinear Fresnel factor $F^{NL}_{R,ll}$ tends to infinity when the angle of incidence $\theta^{i} = \theta^{cr}(\omega)$. At this condition we have $\theta_S = \theta_T = \pi/2$ where the phase matching condition prevails and thus $\sin(\theta_S + \theta_T) = 0$ in equation (2.35a). However, in practice, there are several factors, e.g. beam divergence, walk-off effect, that limit the reflected harmonic intensity from reaching infinite value. Furthermore, the singularity causing the divergence at critical total reflection predicted by the theory[12] for this situation has been removed by another treatment given by Shih and Bloembergen[91]. They used the Green's function technique to describe the generated harmonic field, with due attention being paid to the effects of the finite beam diameter. According to the theory based on this technique, the second harmonic intensity at the critical angle $\theta^{cr}(\omega)$ does have a finite value and it is in agreement to the experimental result that the enhancement of the reflected second

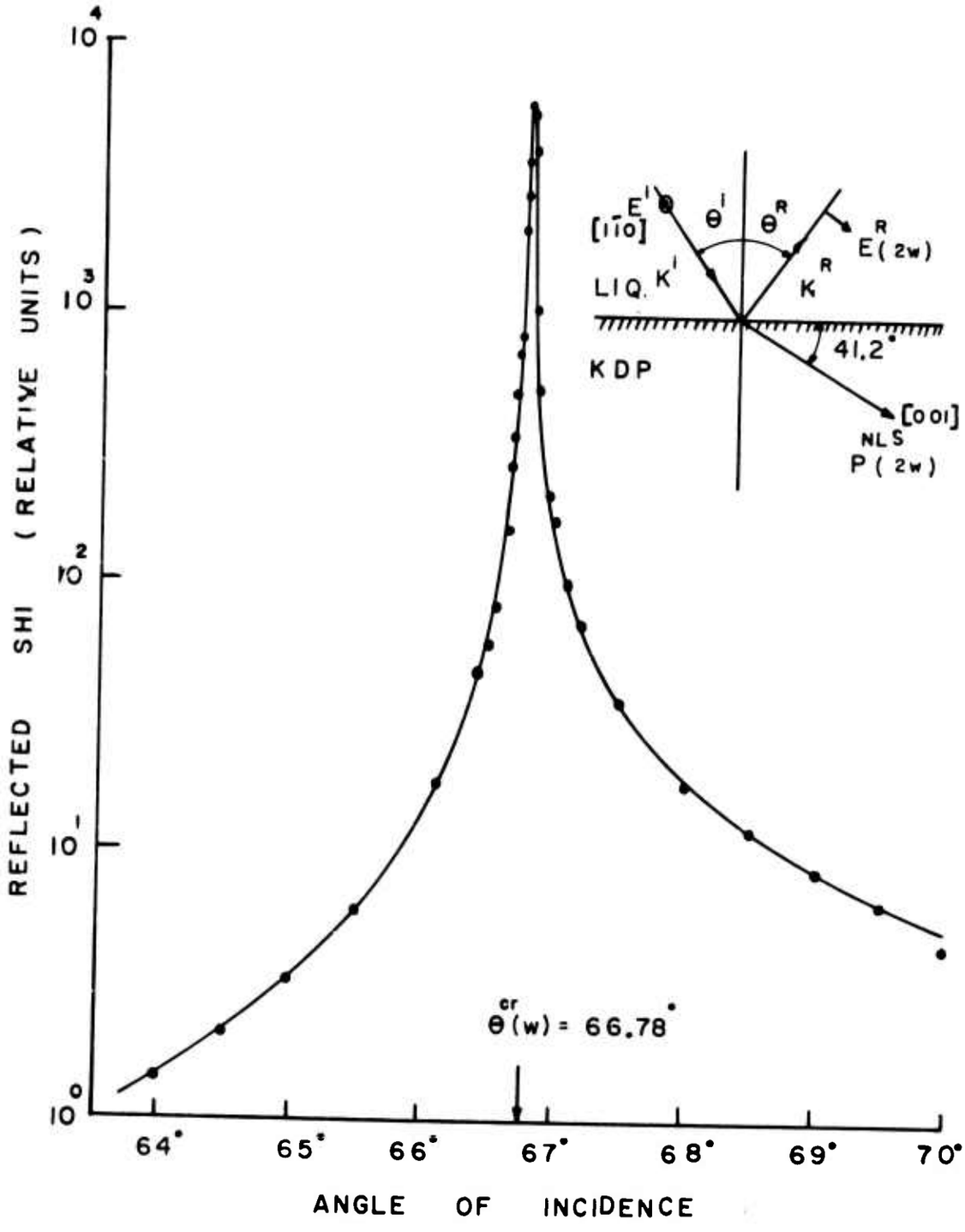
REFLECTED SHI (RELATIVE UNITS)
10^4
10^3
10^2
10^1
10^0
64°
65°
66°
67°
68°
69°
70°
ANGLE OF INCIDENCE
θ^cr(w) = 66.78°
[1̄10]
E^I
θ^I
θ^R
E^R (2w)
LIQ.
K^I
K^R
41.2°
KDP
[001]
NLS
P (2w)

FIGURE 4 - 2

harmonic intensity is three to four orders of magnitude when the angle of incidence is changed by a few tenth of a degree in the vicinity of $\theta^{cr}(\omega)$.

The theoretical curve in Fig. 4-2 has been calculated using again equation (2.39) with $\theta_S = \theta_T$ and $\alpha = \theta_m = 41.2^o$ and assuming $n_{cr}(\omega) = n_e(2\omega) = 1.4943$ without including angular variations for $\vec{k}_S$ and $\vec{k}_T$. This is justifiable that in the vicinity of the critical angle the extraordinary index of refraction for second harmonic frequency is slowly varying. A complete, but very involved expression, has been given by Fischer (89) for rigorous treatment. The theoretical curve is again calculated from the last five factors.

$$|f_R^{L}|^2 \, |F^L|^4 \, |F_{R,ll}^{NL}|^2 \cos\theta_R (\cos\theta_i)^{-1}$$

of equation (2.39). The vertical scale in Fig. 4-2 was adjusted to the data. Note the striking agreement between the experimental points and the theoretical curve, which predicts anomalously high reflected harmonic intensity at $\theta_i = \theta^{cr}(\omega)$. Furthermore, it is seen that the variation in the immediate neighborhood of the critical angle is rather well described by equation (2.39) for the geometry used. In the region where θ^i is greater than $\theta^{cr}(\omega)$, and also $\cos\theta_S$ and $\cos\theta_T$ take pure imaginary values, the reflected harmonic intensity is still comfortably detectable and it tends to decrease monotonously to zero value when θ_i approach 90^o. This can be understood physically because beyond the critical angle there is still evanescent wave of the fundamental beam whichwill create the nonlinear polarization $\vec{P}^{NLS}(2\omega)$ and will radiate back

into the linear medium the reflected harmonic beam. The enhancement due to phase matching at critical angle corresponding to this geometry is very useful for studying nonlinear optical properties of the medium which absorbs at the fundamental and/or second harmonic frequencies. Since all the information will be analyized via reflected harmonic intensity.

To facilitate better physical understanding in connection with reflected second harmonic phenomena, one can consider the drawn curve in Fig. 4-2 as a limiting case of that in Fig. 4-1. The separation between the two cusps in Fig. 4-1 depends upon the degree of phase mismatching in the neighborhood of the critical angle. As the condition for perfect phase matching is approached, the two cusps in Fig. 4-1 will move closer towards each other and the reflected harmonic intensity becomes larger until finally these two cusps collapse into one peak and the intensity tends to the highest value. This explanation was also carried out to reflected third harmonic generation (THG) by Bey et al[30].

Another experimental investigation in relation to phase matching at the critical angle was performed. Here the same KDP crystal of the same crystallographic cut was employed. However, the crystal was rotated 180^{o} about the face normal which is in $\lceil 111 \rceil$ direction as in the previous case. The reflected harmonic intensity $I_R(2\omega)$ generated from the crystal was observed as a function of the angle of incidence θ_i. The crystallographic orientation and the polarization of the fundamental beam are shown in the inset of Fig. 4-3. Again in this case the fund-

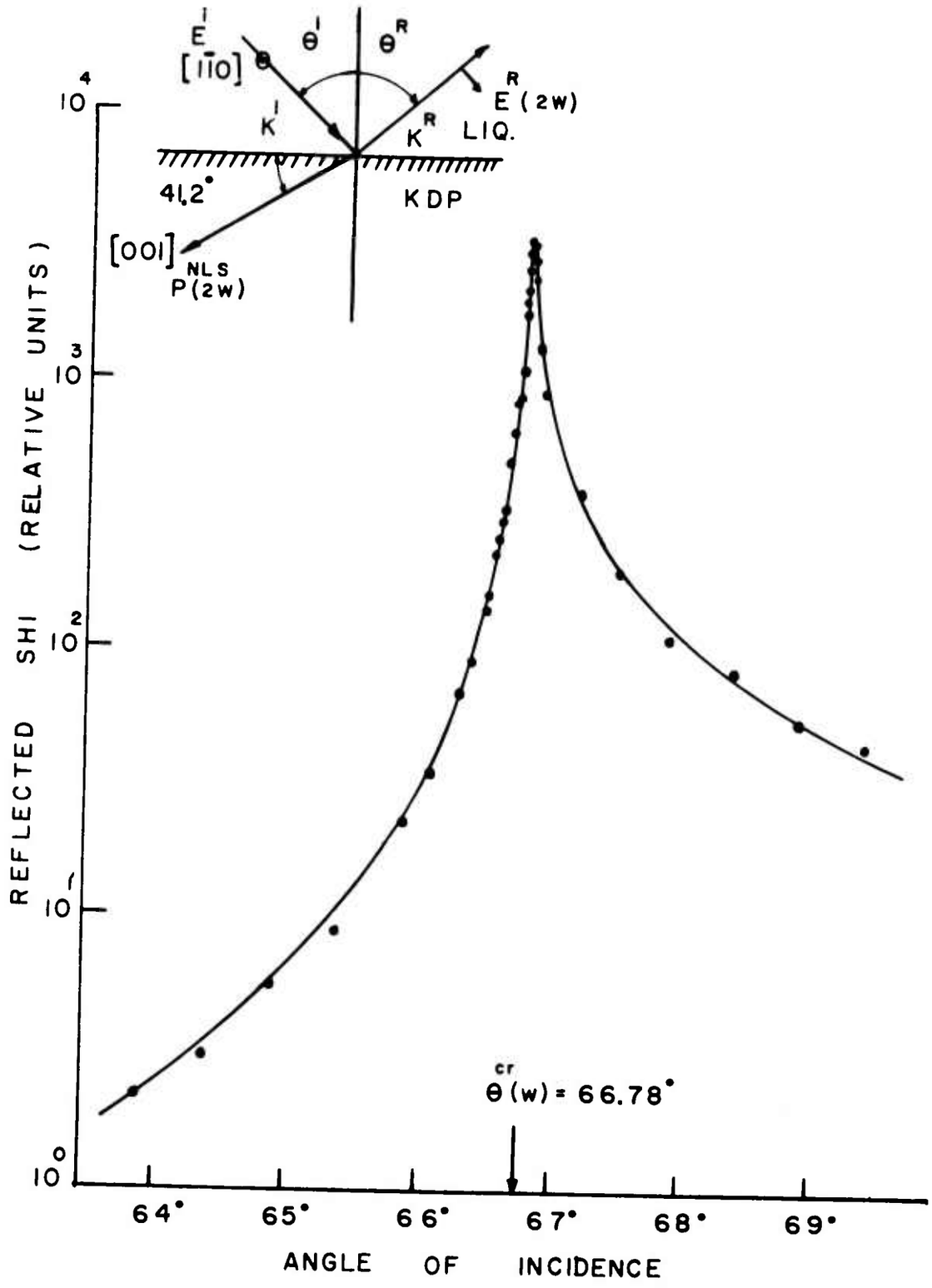
E^I
[1$\bar{1}$0]
θ^I
θ^R
E^R (2w)
K^I
K^R
LIQ.
41.2°
KDP
[001]
NLS
P(2w)
REFLECTED SHI (RELATIVE UNITS)
10^4
10^3
10^2
10^1
10^0
θ^cr(w) = 66.78°
64°
65°
66°
67°
68°
69°
ANGLE OF INCIDENCE

FIGURE 4 - 3

amental beam propagated as ordinary ray and the reflected harmonic beam polarized in the plane of reflection was extraordinary ray.

The experimental result in Fig. 4-3 shows that the reflected harmonic intensity increases by about two orders of magnitude when the angle of incidence changes by a few tenth of a degree from the critical angle. The maximum reflected harmonic intensity occurs at the critical angle as predicted by the theory. The theoretical curve in Fig. 4-3 was calculated in the same way as in Fig. 4-2. The vertical scale was adjusted to the data. Note the striking agreement between the experimental points and the theoretical curve, which predicts anomalously high reflected harmonic intensity at $\theta_i = \theta^{cr}_{(II)}$.

When the result from Fig. 4-3 is compared to that from Fig. 4-2, it is found out that the overall shape of the peak in Fig. 4-3 is broader and in addition the peak intensity is lower than that in Fig. 4-2 by about 13 times. This discrepancy can be well understood by the fact that KDP crystal is an uniaxial crystal possessing variable extraordinary index of refraction.

In general, one may expect different reflected harmonic intensities from the two geometries as shown in Fig. 4-2 and 4-3, respectively. These two geometries are identical except that in one case the KDP crystal has been rotated by 180^{o} about its face normal with respect to each other. The two situations corresponding to Fig. 4-2 and 4-3 can be shown in Fig. 4-4 where the normal (index) surfaces of ordinary ray and second harmonic extraordinary ray are fully indicated for both cases.

This is equivalent to an illumination by a beam of incident from a symmetric position on the other side of the face normal. In Fig. 4-4, where the drawing indicates the conservation of the tangential components of $\vec{k}$ vectors. The $\vec{k}$ vectors with subscripts a and b correspond to the geometries in the insets of Fig. 4-2 and 4-3, respectively. At total reflection, $\vec{k}_S^{\,a} = OA$, $\vec{k}_S^{\,b} = OC$. According to the normal (index) surfaces and boundary conditions of $\vec{k}$'s vectors, it is required that $\vec{k}_T^{\,a}$ may take two values, i.e. $\vec{k}_T^{\,a} = \vec{k}_S^{\,a} = OA$ or $\vec{k}_T^{\,a} = OB$. However, the former solution of $\vec{k}_T^{\,a} = OA$ would give a ray velocity propagating out of the nonlinear medium; i.e., the energy propagates out of the medium. This is not a physically allowed solution. Thus the only physically allowed solution is that $\vec{k}_T^{\,a} = OB$ and $\vec{k}_T^{\,b} = OC$. They correspond to the incident $\vec{k}_i^{\,a}$ and $\vec{k}_i^{\,b}$ waves, respectively.

In the formal treatment of the theory, Armstrong et al[11] and Kleinman[14] have represented the laser and second harmonic light by unbounded plane waves. Armstrong et al[11] pointed out that the interaction between light waves of finite aperture takes place along the direction of energy flow. In his paper, Kleinman[14] also showed that SHG will ultimately be limited by slightly different directions of propagation of the energy of the laser and second harmonic beams. The effect is called double refraction in a uniaxial crystals. In fact, the light wave in the nonlinear medium KDP in the two geometries have very narrow apertures near critical angle. Therefore, to examine the phenomena of SHG at phase matched condition in a uniaxial crystal, e.g.

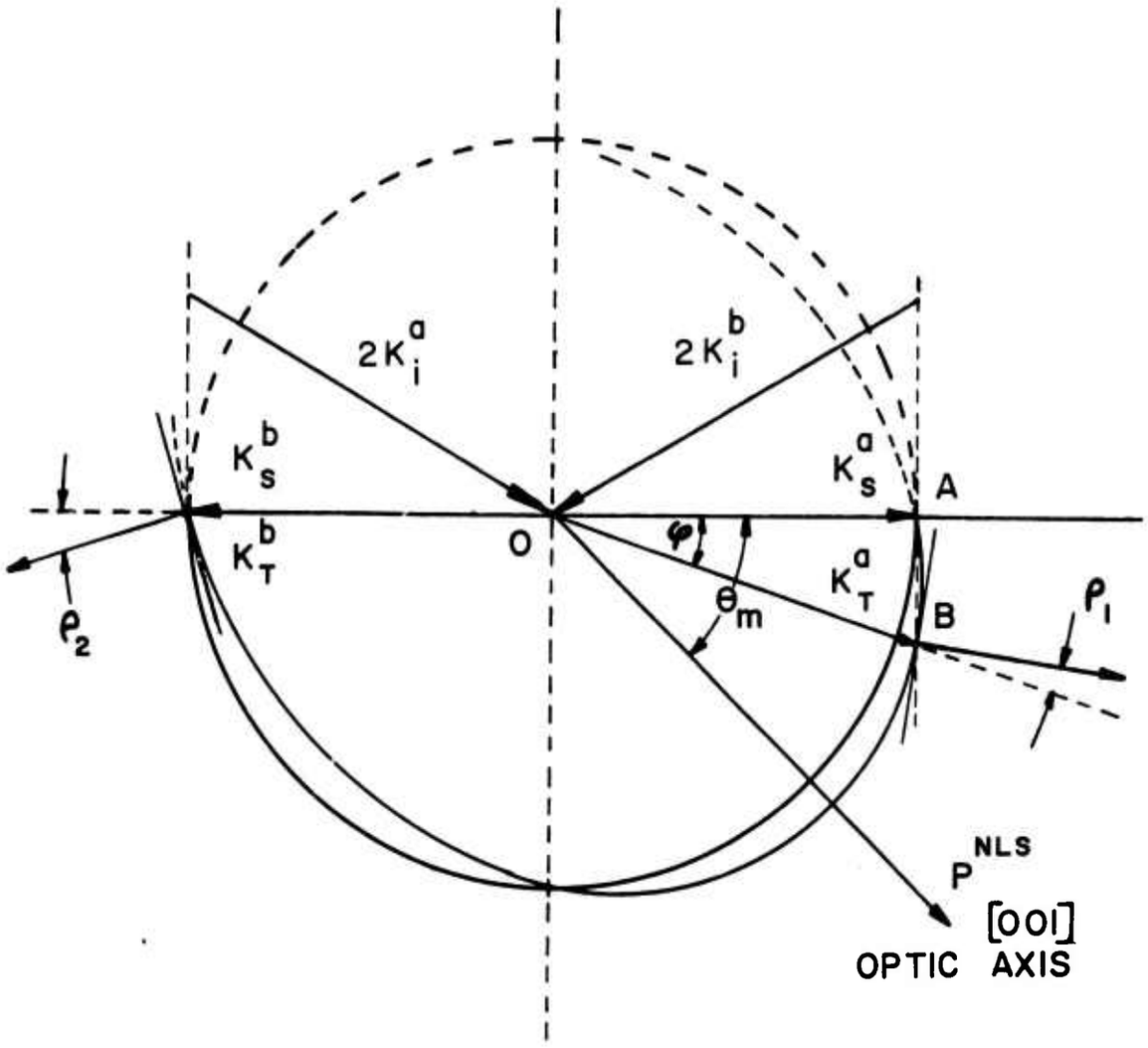
$2K_i^a$
$2K_i^b$
K_s^b
K_T^b
K_s^a
K_T^a
A
B
O
φ
θ_m
ρ_1
ρ_2
P^{NLS}
[001]
OPTIC AXIS

FIGURE 4 - 4

KDP, it is important to know the degree of overlapping between the direction of energy propagation of polarization wave $\vec{k}_S$ and radiation wave $\vec{k}_T$. It has been shown by Boyd et al[35] that for any direction of phase propagation the direction of energy propagation (Poynting vector) is given by the normal vector to the normal (index) surface. For the ordinary wave the propagation vector and the Poyting vector are parallel. However, for the extraordinary wave the Poynting vector deviates from the phase propagation direction by an angle ρ, called the angle of double refraction, the angle ρ is given by[35]

$$\tan\rho = \frac{1}{2} n^e_{2\omega}(\theta) \left\{ \frac{1}{[n^e_{2\omega}(\pi/2)]^2} - \frac{1}{[n^o_{2\omega}]^2} \right\} \sin 2\theta \qquad (4.5)$$

where θ is the angle between the phase propagation direction and the optic (z) axis. Furthermore, the angle φ in Fig. 4-4 can be obtained from

$$\frac{1}{[n^e_{2\omega}(\theta)]^2} = \frac{1}{[n^o_{2\omega}]^2} \cos\theta^2 + \frac{1}{[n^e_{2\omega}(\pi/2)]^2} \sin^2\theta \qquad (4.6a)$$

$$n^e_{2\omega}(41.2^o - \varphi)\cos\varphi = n^o_{\omega} \qquad (4.6b)$$

From (4.6a, b) the angle φ and as a consequence $n^e_{2\omega}(41.2^o - \varphi)$ were found as

$$\begin{aligned} \varphi &= 1.12^o \\ n^e_{2\omega}(41.2^o - 1.12^o) &= n^e_{2\omega}(40.08^o) = 1.49465 \end{aligned} \qquad (4.7)$$

The angle ρ_1 was found, upon substitution $n^e_{2\omega}(40.08^o)$ and appropriated value of indices of refraction of KDP, as

$$\rho_1 = 1.07^\circ \tag{4.8}$$

In the same way ρ_2 was calculated as

$$\rho_2 = 1.08^\circ \tag{4.9}$$

Therefore, the angle between the directions of energy propagation of $\vec{k}_S^a$ and $\vec{k}_T^a$ corresponding to the geometry of Fig. 4-2 is

$$\varphi - \rho_1 = 1.12^\circ - 1.07^\circ = 0.05^\circ$$

whereas the angle between the direction of energy propagation of $\vec{k}_S^b$ and $\vec{k}_T^b$ corresponding to the geometry of Fig. 4-3, is $\rho_2 = 1.08^\circ$. Thus in the former case, the polarization and radiation waves will have a larger interaction volume and hence will produce more intense second harmonic wave.

This qualitative analysis via double refraction phenomena explains the experimental results shown in Fig. 4-2 and 4-3. However, the double refraction effect corresponding to the idealized geometry of phase matching shown in Fig. 4-4 probably cannot account for the experimental factor of 13 times increase. The effect mentioned above depends very much on the actual value of the angle φ and the sizes of the fundamental and harmonic beams near the critical angle inside the nonlinear medium.

Another possible explanation of the different intensities when the KDP crystal is turned by 180° can be based upon the beating of different ordinary ray directions in the fundamental wave. This idea was first given by Maker et al[34]. In this explanation, we assume that the crystal was not cut precisely that the phase matching direction is not along its

surface and in addition the fundamental beam is allowed to have a slight divergence. The illustration is shown in Fig. 4-5 where symbols of subscripts a and b denote the same geometries as previously described in the early analysis. According to this case, the experimental maximum intensity is not obtained for the idealized geometry of Fig. 4-4, however, the maximum occurs when the phase matching direction 0 A make a small angle θ_A with the surface as shown in Fig. 4-5. The nonlinear polarization is created from the mixing of slightly divergent pairs of fundamental rays with wave vectors $\vec{k}_S^{a'}$ and $\vec{k}_S^{a''}$. The allowed perfect phase matching condition is

$$\vec{k}_T^{a} = \vec{k}_S^{a'} + \vec{k}_S^{a''}$$

This condition can be satisfied if $\theta_{k_T} \geq \theta_m$, as discussed by Maker et al[34], where θ_{k_T} is the angle between $\vec{k}_T$ and the optic (z) axis. When the crystal is turned by 180^o around its face normal, the wave vectors of the incident fundamental rays are represented by $\vec{k}_S^{b'}$ and $\vec{k}_S^{b''}$. For this situation the phase matched condition is not satisfied and as a consequence the reflected harmonic intensity will be lower. The analysis based on the discussion by Maker et al[34] seems to agree with the experimental data obtained in the case of nonphase matched and phase matched conditions described in Fig. 4-1 and 4-3, respectively. It was experimentally found that ratio of the harmonic intensities at the critical angle for phase matched to nonphase matched conditions is about 30 times, which is in the same order of magnitude (13 times) as obtained upon comparing Fig. 4-3 to Fig. 4-2 .

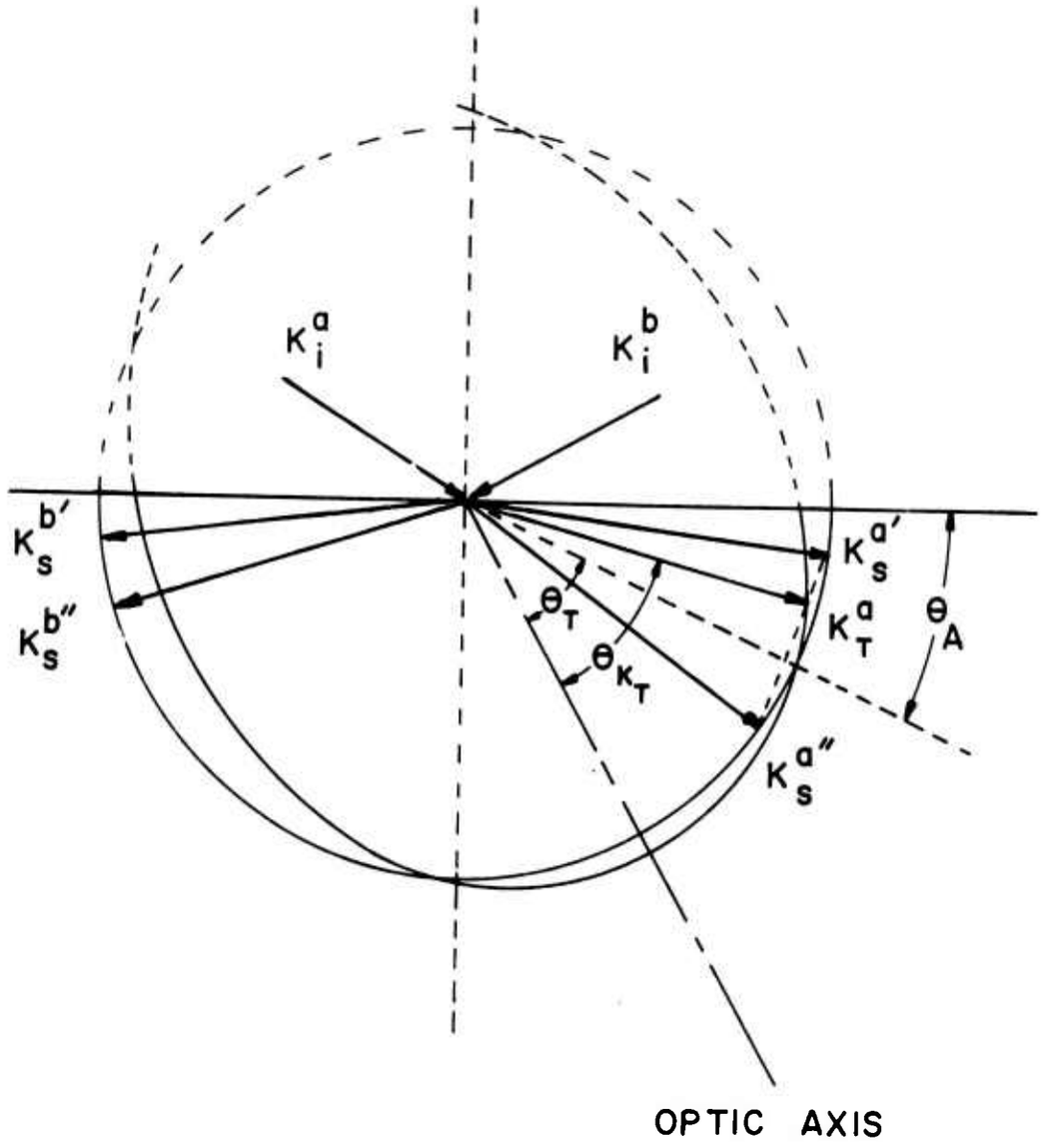

FIGURE 4 - 5

3. Nonlinear Brewster's Angle. The agreement of experimental data with theory for those separate experiments described in the previous sections encourages verification of a more subtle nonlinear optical postulate. In particular, we are led to ask if a nonlinear Brewster's angle for the nonlinear transparent medium can be found experimentally. Even though the nonlinear Brewster's angle for absorbing medium, e.g., GaAs, was first confirmed by Chang and Bloembergen[27], it is still important to carry the postulate to the transparent regime. An uniaxial KDP crystal is known to be transparent for both fundamental and second harmonic frequencies of Nd:glass laser. Besides its transparent property, it is also an ideal nonlinear material in the sense that it crystallographic, point group properties and nonlinear optical characteristics concerning SHG are well understood. The KDP crystal used in the investigation is the same as one used in the phase matching condition at total reflection described in Fig. 4-3. Again the crystal is immersed in the optically denser linear fluid 1-bromonaphthalene. The use of the liquid is to facilitate the achievement of observation of Nonlinear Brewster's angle since without optically denser linear medium from which the fundamental is incident, the condition for Nonlinear Berwster's angle will never be achieved. The face normal of the entrance surface of the crystal is in $\lceil 111 \rceil$ direction and the fundamental wave is polarized along $\lceil 1\bar{1}0 \rceil$ direction. According to (2.31a) the nonlinear polarization $\vec{P}^{NLS}$ will be in $\lceil 001 \rceil$ direction or optic (z) axis. The reflected harmonic intensity $I_R(2\omega)$ generated from the crystal was observed as

a function of the angle of incidence, which varies from 20^{o} to 75^{o}. The experimental result is shown in Fig. 4-6. In this particular geometry of the KDP crystal, we have the nonlinear polarization in the plane of reflection. The electric field of the reflected harmonic wave is given by equation (2.25). This equation reveals the existence of a Nonlinear Brewster's angle when $E_{ll}^{R}(2\omega) = 0$. Or in another words, we have

$$E_{ll}^{R}(2\omega) = 0 = \frac{4\pi P^{NLS} \sin\theta_S \sin^2\theta_T \sin(\alpha+\theta_T+\theta_S)}{\epsilon_R \sin\theta_R \sin(\theta_T+\theta_S)\sin(\theta_T+\theta_R)\cos(\theta_T-\theta_R)} \tag{4.10}$$

The equation (4.10) is true, if

$$\sin(\alpha+\theta_T+\theta_S) = 0$$

or

$$\alpha+\theta_S+\theta_T = 0, \pi \tag{4.11}$$

From the Fig. 4-6, one has $\alpha + \theta_S$, which is the angle between the nonlinear polarization and the face normal direction inside the crystal, equal to -48.78^{o}. Therefore, from equation (4.11) using the first condition which provides the realizable value of θ_T we have

$$\theta_T = 48.78^{o}$$

Having known the value of $\theta_T = 48.78^{o}$, the corresponding index of refraction of an extraordinary ray $n_{2\omega}^{e}(\theta_T = 48.78^{o})$ is found via equation (4.6a) to be

$$n_{2\omega}^{e}(\theta_T = 48.78^{o}) = 1.47125$$

Thus the Nonlinear Brewster's angle can be found via nonlinear Snell law (2.29) as

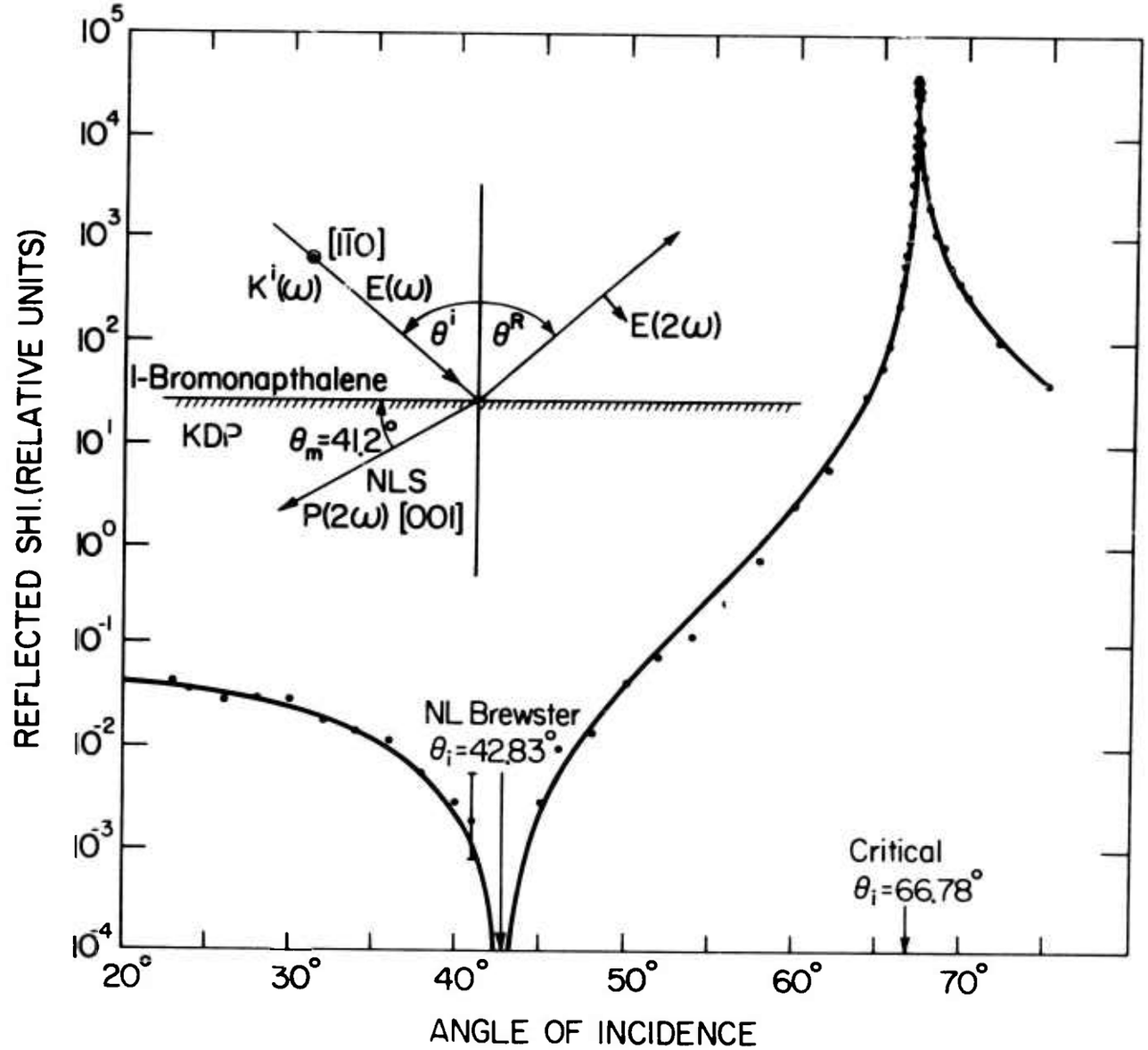
REFLECTED SHI.(RELATIVE UNITS)
10^5
10^4
10^3
10^2
10^1
10^0
10^{-1}
10^{-2}
10^{-3}
10^{-4}
[1$\bar{1}$0]
$K^i(\omega)$
$E(\omega)$
θ^i
θ^R
$E(2\omega)$
I-Bromonapthalene
KDP
θ_m=41.2°
NLS
P(2ω) [001]
NL Brewster
θ_i=42.83°
Critical
θ_i=66.78°
20°
30°
40°
50°
60°
70°
ANGLE OF INCIDENCE

FIGURE 4 - 6

$$\theta_i^{\text{NL. Brew.}} = \sin^{-1}\left\{\frac{n_{2\omega}^{e}(\theta_T=48.78^{o})}{n_{liq}(\omega)} \cdot \sin\theta_T\right\}$$

$$= \sin^{-1}\left\{\frac{1.47125}{1.6260} \cdot \sin 48.78^{o}\right\}$$

$$\theta_i^{\text{NL. Brew.}} = 42.83^{o}$$

Should the KDP be placed in the air instead of immersed in 1-bromonaphthalene, the calculated nonlinear Brewster's angle would be

$$\theta_i^{\text{NL. Brew.}} = \sin^{-1}\left\{\frac{1.47125}{1.0} \sin 48.78^{o}\right\}$$

$$= \sin^{-1}\{1.0896\}$$

This angle, of course, is nonphysical.

Note the striking agreement between experimental result and the theoretical prediction. One can see that in the vicinity of $\theta^{i} = 42.78^{o}$, there exists a pronounced dip of the reflected harmonic intensity $I_R(2\omega)$. This evidently confirms the existence of Nonlinear Brewster's angle. This is for the first time that Nonlinear Brewster's angle for transparent medium has been experimentally demonstrated. Notice that the reflected harmonic signal in the neighborhood of Nonlinear Brewster angle is very low level and at the angle it is expected no $I^{R}(2\omega)$ generated out of the crystal. By increasing the incident power density via a biconvex lense and using the low level signal detection method in which the reflected harmonic signal was collected and averaged over 25 to 50 laser firings, the pronounced dip at $\theta_i = 42.83^{o}$ was achieved. Other experimental points agree well with the theoretical curve which was calculated, as in previous case, from the last five factors of equation (2.39). In this case the

the angular variation of $n^{e}_{2\omega}(\theta)$ was taken into consideration in computing the theoretical curve since we are now dealing with much larger angular range. From Fig. 4-6, again the anomalously high reflected harmonic intensity $I^{R}(2\omega)$ at critical angle and overall agreement between data points and theory from $20^{o} \leq \theta^{i} \leq 75^{o}$ confirm the nonlinear optical theory developed by Bloembergen and Pershan[12].

The physical interpretation of the existence of a Nonlinear Brewster's angle can be understood in terms of classical dipole radiation. When the fundamental beam is incident on the KDP crystal at the Nonlinear Brewster's angle, it will setup a nonlinear polarization $\vec{P}^{NLS}$ in direction parallel to the direction of propagation of the reflected harmonic wave inside the nonlinear medium. According to the classical dipole radiation theory, there would be no radiation seen in this direction. This nonradiating wave upon refraction back into the linear medium would otherwise give rise to the reflected ray in the direction of θ_{R}.

The experimental points and the corresponding theoretical curve in the vicinity of Nonlinear Brewster's angle have a pronounced dip, in contrast to the case of GaAs irradiated by ruby laser, performed by Chang et al[34]. This can be explained that for the KDP case, the crystal has real and small value of $\varepsilon(\omega)$ and $\varepsilon(2\omega)$ in contrast to the case of GaAs which has large and complex values of $\varepsilon(\omega)$ and $\varepsilon(2\omega)$ at the ruby laser line. Maxwell's equations and the boundary conditions derived for a transparent medium can all be extended to an absorbing medium, provided that the dielectric constants are replaced by their complex values. Then, in that case, one can see

that the condition for $E_{11}^{R}(2\omega) = 0$ can never be satisfied, as $\sin\theta_i = [\varepsilon(2\omega)/\varepsilon_{liq}(\omega)]^{1/2} \sin 48.78^{o}$ can never be achieved physically if $\varepsilon(2\omega)$ is complex. This fact was confirmed when a Nd:glass laser was used instead of a ruby laser, and the pronounced dip at the Nonlinear Brewster's angle for GaAs was observed by Chang et al[34]. This is because the second harmonic emission of the Nd:glass laser is absorbed much less by GaAs since the imaginary part of its linear dielectric constant is 1.50.

The conclusion to be drawn, in relation to the reflected intensity of the harmonic wave from a nonlinear medium KDP crystal immersed in a optically denser linear fluid 1-bromonaphthalene, is that the observed angular dependence of the reflected harmonic intensity and, in particular, the existence of Nonlinear Brewster's angle of a transparent medium are in good agreement with the theory of Bloembergen and Pershan[12]. The regime of an evanescent fundamental wave and reflected second harmonic wave have been demonstrated.

B. Second Harmonic Generation (SHG) in Transmission.

1. Homogeneous and Inhomogeneous Second Harmonic Waves in the Neighborhood of Critical Angles. Having obtained a good agreement between the experimental data and theoretical prediction in the case of the nonphase matchable reflected SHI described in section A-1, it was encouraging to investigate the SHG in transmission near the critical angles $\theta^{cr}(2\omega)$ and $\theta^{cr}(\omega)$, respectively. The result obtained in this investigation, according to the theoretical prediction, will complement that of section A-1. The gemetrical situation just

before total reflection occurs was shown in Fig. 2-6 in chapter II. The primary fundamental beam is transmitted almost parallel to the surface in the nonlinear KDP crystal. There are two transmitted harmonic beams[12]. The driven polarization wave propagates in the same direction as the transmitted laser beam. It has a wave vector $\vec{k}_S = 2\vec{k}_{Laser}(\omega)$ and represents the particular solution of the inhomogeneous wave equation. In addition, there is a homogeneous solution with wave vector $\vec{k}_T(2\omega)$. In the present study the KDP crystal has a right angular corner and the two transmitted harmonic beams are spatially distinct and readily observed separately. According to the particular crystallographic cut, which will be described later, it is clear that the beam with wave vector $\vec{k}_T$ will disappear first at $\theta_i = \theta^{cr}(2\omega)$ and the ray with wave vector $\vec{k}_S$ will disappear at the same time as the transmitted fundamental since $\theta^{cr}(\omega)$ is found to be greater than $\theta^{cr}(2\omega)$. As the angle of incidence θ_i becomes larger than $\theta^{cr}(\omega)$ the inhomogeneous wave will disappear.

The KDP crystal used has dimensions of 25 x 15 x 8 mm^3. Its face normal is in the [001] direction (optic axis). The homogeneous and inhomogeneous transmitted harmonic intensity were observed separately as a function of angle of incidence. The polarization of the fundamental beam and the orientation of the crystal are shown in the inset of Fig. 4-7.

The homogeneous and inhomogeneous harmonic intensities are given by equation (2.39), respectively, as

$$I_T(2\omega) = (c/8\pi)\sqrt{\epsilon_R}\,|E_o|^4 dd'(4\pi\chi_{36}^{NL})^2\eta^2(f_T^L)\,|F^L|^4 \times |F_T|^2\cos\theta_T(\cos\theta_i)^{-1} \qquad (4.12)$$

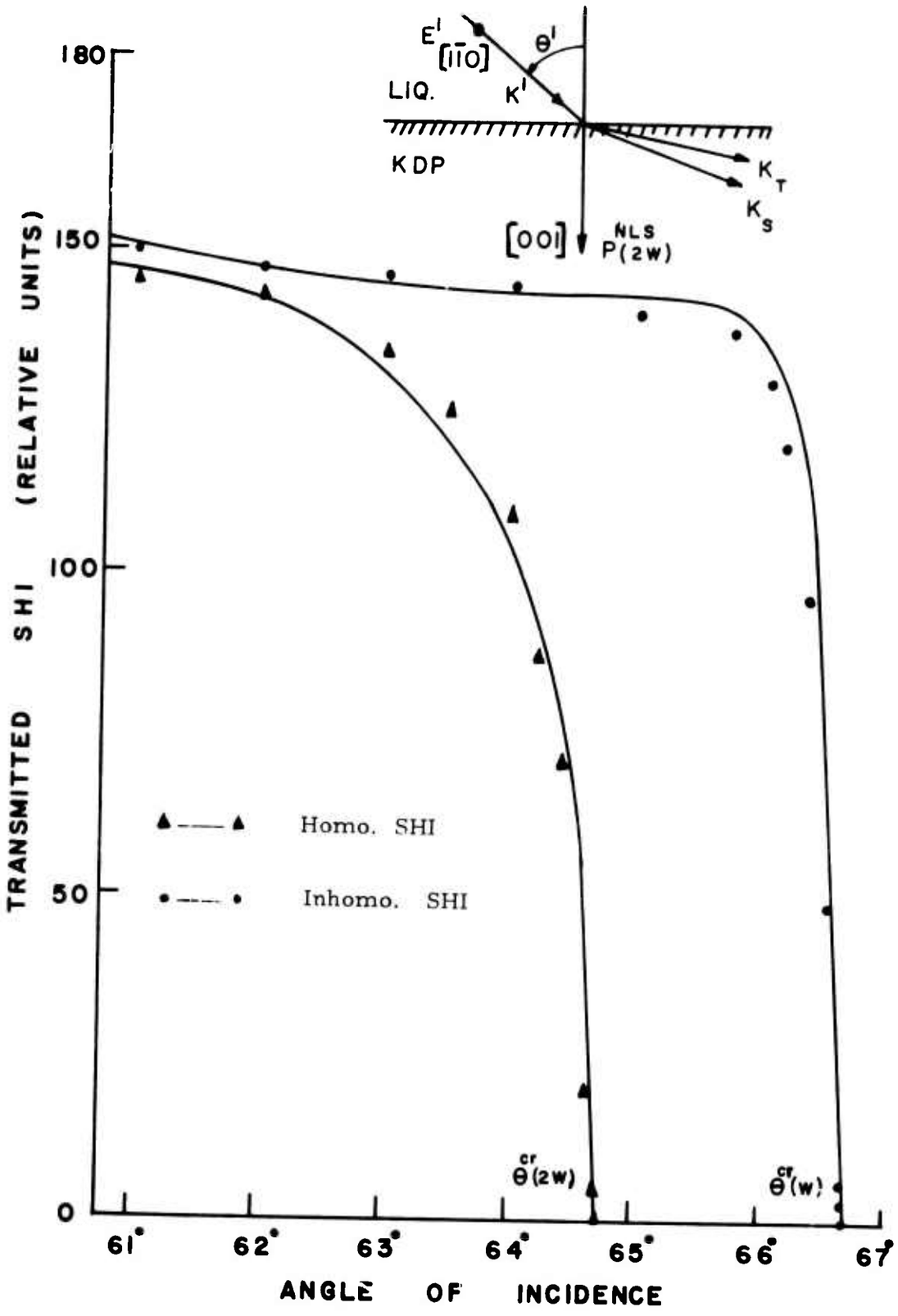
E'
[1$\bar{1}$0]
θ'
LIQ.
K'
KDP
K_T
K_S
[001]
NLS
P(2w)
180
150
100
50
0
TRANSMITTED SHI (RELATIVE UNITS)
Homo. SHI
Inhomo. SHI
$\theta^{cr}_{(2w)}$
$\theta^{cr}_{(w)}$
61°
62°
63°
64°
65°
66°
67°
ANGLE OF INCIDENCE

FIGURE 4 - 7

$$I_S(2\omega) = (c/8\pi)\sqrt{\epsilon_R}\,|E_o|^4\, dd'\, (4\pi\chi_{36}^{NL})^2\eta^2(f_T^L)|F^L|^4$$
$$|F_S|^2 \cos\theta_S(\cos\theta_i)^{-1} \qquad (4.13)$$

The drawn solid curves in Fig. 4-7 are plots of equations (4.12) and (4.13) for homogeneous and inhomogeneous SHI and are calculated from the last five factors, respectively,

$$|f_{T,S}^L|^2\, |F^L|^4\, |F_{T,S}^{NL}|^2 \cos\theta_{T,S}(\cos\theta_i)^{-1}$$

The linear vertical scale in Fig. 4-7 is adjusted to the data as appropriat for each case. The experimental points are in good agreement with the computed theoretical curve. They are in excellent agreement to the theoretical prediction that the homogeneous and inhomogeneous SHI will be terminated at $\theta^{cr}(2\omega)$ and $\theta^{cr}(\omega)$, respectively. The critical angles $\theta^{cr}(2\omega)$ and $\theta^{cr}(\omega)$ from the experiment are the same as found in the previous cases. The behavior of the two SHI near the critical angles as shown in Fig. 4-7 can be explained in the following. The two transmitted SHI are the net result of the competing effects of the increasing linear Fresnel factor to the fourth power, the decreasing nonlinear Fresnel factor squared, and the rapidly decreasing cross section of the fundamental inside the medium near the total reflection. As to these competing factors the homogeneous and inhomogeneous harmonic intensities fall down rapidly toward $\theta^{cr}(2\omega)$ and $\theta^{cr}(\omega)$. The reason for the homogeneous and inhomogeneous SHI terminated at $\theta^{cr}(2\omega)$ and $\theta^{cr}(\omega)$ respectively is that when θ_i is greater than $\theta^{cr}(2\omega)$ and $\theta^{cr}(\omega)$ the value of $\cos\theta_T$ and $\cos\theta_S$ become

pure imaginary respectively. As a consequence the two transmitted harmonic intensities will become imaginary which are not physically allowable. Furthermore, one can see from Fig. 4-7 that the homogeneous SHI disappears at $\theta^{cr}(2\omega)$ while inhomogeneous SHI still persists for 2.02^{o} more and finally is terminated at $\theta^{cr}(\omega)$. In the region between $\theta^{cr}(2\omega) \leq \theta_i \leq \theta^{cr}(\omega)$ which is 2.02^{o} interval, one can comfortably observe inhomogeneous SHI. One can apply the result from this investigation, particularly in the region $\theta^{cr}(2\omega) \leq \theta_i \leq \theta^{cr}(\omega)$ to other nonlinear crystal which is appropriately cut. Since in this region one will obtain only inhomogeneous SHI which has direct association with the nonlinear polarization source term $\vec{P}^{NLS}$ and the nonlinear susceptibility χ^{NL}. The knowledge of inhomogeneous SHI in this particular region will directly facilitate the study of $\vec{P}^{NLS}$ and χ^{NL} of a nonlinear medium.

2. Phase Matched Second Harmonic Generation (SHG) in Transmission.

SHG under phase matched conditions and in a normally incident direction was performed by several authors[33, 34]. However in the present work the phase matched direction is no longer in the normal incident direction. The SHG in transmission under this phase matched condition, and away from it, were experimentally investigated and compared to the prediction of the theory. This will verify the theoretical prediction and check the theory for other conditions aside from previous confirmations.

The KDP crystal used in the experiment was the same one as in section B-1. The total transmitted second harmonic intensity due to the sum of homogeneous and inhomogeneous transmitted harmonic intensities

is observed as a function of angle of incidence which varied from -15^{o} to 50^{o}. The fundamental beam is polarized in the $[1\bar{1}0]$ direction and the KDP crystallographic orientation are shown in Fig. 4-8. The phase matching angle θ_m according to this geometry can be computed by using equation (2.46) and indices of refraction of KDP crystal given in Chapter III. The phase matched direction was found to be $\theta_m = 41.2^{o}$ away from the crystal face normal direction (optic axis). Thus the angle of incidence corresponding to this direction is given by

$$\theta_i = \sin^{-1}\left\{\frac{n^{e}_{2\omega}(\theta_m)}{n_{liq}(\omega)} \cdot \sin\theta_m\right\}$$

where $n^{e}_{2\omega}(\theta_m) = n^{o}_{\omega} = 1.4943$

Hence $\theta_i = \sin^{-1}\left\{\frac{1.4943}{1.626\upsilon} \cdot \sin 41.2^{o}\right\}$

$$\theta_i = 37.27^{o}$$

The theoretical curve for total transmitted second harmonic intensity is the sum of homogeneous and inhomogeneous intensities given by (4.12) and (4.13), respectively

$$I_{total}(2\omega) = I_S(2\omega) + I_T(2\omega) \qquad (4.14)$$

The thereotical curve shown in Fig. 4-8 was computed from the sum of the last five factors in equation (4.12) and (4.13) and it can be mathematically expressed as

$$I_{Total}(2\omega) \approx (f^{L}_{T})\,|F^{L}|^{4}(\cos\theta_i)^{-1}\left\{|F^{NL}_{T,11}|^{2}\cos\theta_T + |F^{NL}_{S,11}|^{2}\cos\theta_S\right\} \qquad (4.15)$$

The expression for $I_{Total} = I_S + I_T$ given by equation (4.14) is justified for the present investigation. For this geometry, the transmitted

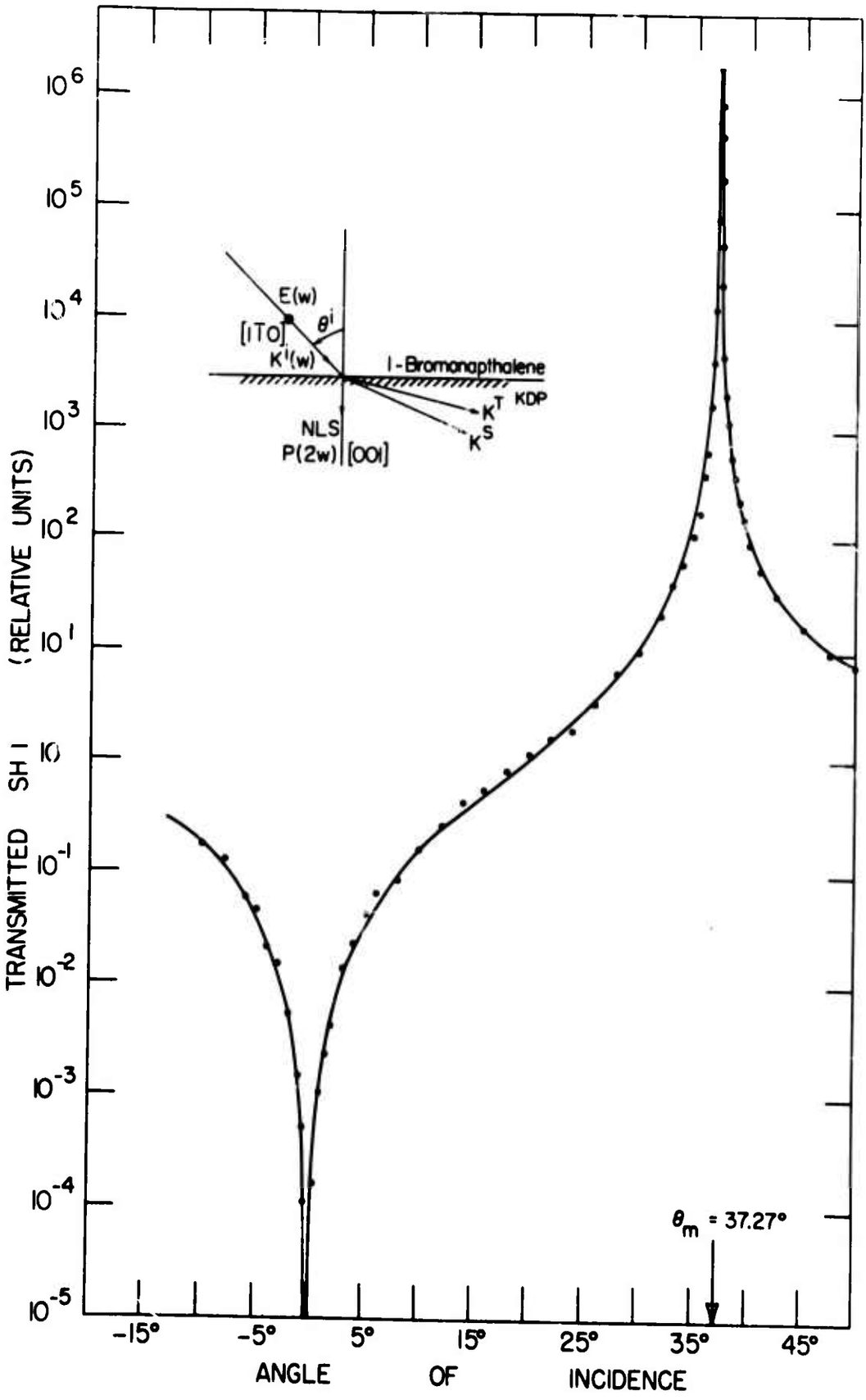
E(w)
[ITO]
θ^i
K^1(w)
1-Bromonapthalene
K^T KDP
K^S
NLS
P(2w) [001]
TRANSMITTED SH I (RELATIVE UNITS)
10^6
10^5
10^4
10^3
10^2
10^1
10
10^-1
10^-2
10^-3
10^-4
10^-5
θ_m = 37.27°
-15°
-5°
5°
15°
25°
35°
45°
ANGLE OF INCIDENCE

FIGURE 4 - 8

intensities were measured by observing the transmitted harmonic waves emerging from the back face of the crystal. Since the two harmonic beams now overlap and interfere, the harmonic intensity is a function of the path length of the beam inside the crystal. If the entrance and exit faces are not parallel over the entire cross sectional area of the beam, the interference must be integrated over this area. The result of this integration gives three terms. The first two terms are exactly the separate homogeneous and inhomogeneous intensities given by (4.12) and (4.13) respectively. The third term retains an oscillatory dependence of the length of crystal and has an amplitude determined by the angle of parallelism of the two faces. If the two faces are exactly parallel, the magnitude of the third term equals to the sum of the first two terms[90]. If the path lengths of the two harmonic beam differed by several coherence lengths, the amplitude of the third term is negligible compare to the first two. Since the KDP crystal used in the experiment is an uniaxial crystal in which a double refraction phenomena is intrinsic. Therefore the magnitude of the third term corresponding to the interference of the two harmonic beams is negligible and thus the expression of $I_{Total}(2\omega)$ given by (4.14) is valid.

According to the theory for general crystallographic orientation, it is anticipated that the total harmonic intensity will exhibit the oscillatory feature in the heighborhood of very small angle of incidence. However, this effect has not been observed. Instead, the total harmonic intensity near normal incidence is falling rather monotonically toward zero value

at $\theta_i = 0^o$. This behavior can be understood in terms of two physical reasons. First, for the region of small angle of incidence, the double refraction still persists and it reduces the effectiveness of the interference between the two harmonic beams as described in the previous paragraph. Second, according to particular crystallographic orientation of the crystal used in this experiment, it is noted that the $\vec{P}^{NLS}$ is in the same direction of the crystal face normal. In terms of the dipole radiation point of view, the nonlinear polarization $\vec{P}^{NLS}$ cannot radiate harmonic waves in the direction of its oscillation. Therefore it is anticipated that no harmonics intensities are observed in the direction of the crystal face normal i.e., $\theta_i = 0^o$. Furthermore, the total harmonic intensity will be small in the neighborhood of $\theta_i = 0^o$. Thus the trend of monotonic decrease of the total harmonic intensity dominates the anticipated oscillatory behavior in this region.

The total harmonic intensity, collected by means of the technique described in details in chapter III, is observed as a function of the angle of incidence which varies from -15^o to 55^o. Note the striking agreement between experimental data points and computed theoretical curve of $I_{Total}(2\omega)$ given by (4.14). In particular, the theoretical prediction concerning the phase matching angle $\theta_i = 37.27^o$ and zero total harmonic intensity at $\theta_i = 0^o$ are confirmed. In addition, by using a KDP crystal and a mode locked Nd:glass laser, the dynamical range of the dectable harmonic intensity is of about 10 orders of magnitude.

Another investigation of phase matched SHG in transmission was

performed by using a KDP crystal of different crystallographic cut. The KDP used in this investigationhas an optic axis , which is $\lceil 001 \rceil$ directed making an angle 41.2^{o} to the crystal entrance surface. The normal to the crystal face is in $\lceil 111 \rceil$ direction. The crystal is immersed as usual in a linear optically denser liquid 1-bromonaphthalene. The fundamental beam is polarized in the $\lceil 1\bar{1}0 \rceil$ direction. The total harmonic intensity $I_{Total}(2\omega)$ was observed as a function of angle of incidence which varied from 0^{o} to 52.5^{o}. The crystallographic orientation of the crystal and the result obtained from the investigation is depicted in Fig. 4-9. , The theoretical curve of total harmonic intensity $I_{Total}(2\omega)$ is again given by equation (4-14) on the same assumption explained in the previous section. The theoretical curve drawn in Fig. 4-9 was computed from equation (4-15) and the vertical scale is adjusted to the experimental data.

The angle of phase matching θ_m could be found in the usual way by using equation (2.46) and indices of refraction of KDP given in Chapter III. The phase matching angle was found to be $\theta_m = 41.2^{o}$. According to the present geometry, there exist two possible phase matched directions. The first direction is along the entrance surface of the crystal. This direction is associated with phase matched SHG at total reflection and has been investigated in section A-2 previously. The second direction which is still 41.2^{o} away from the other side of optic (z) axis. It makes an angle θ_T, inside the KDP crystal, to the direction of the face normal. The angle θ_T is given by

$$\theta_T = 90^{o} - (41.2^{o} + 41.2^{o}) = 7.6^{o}$$

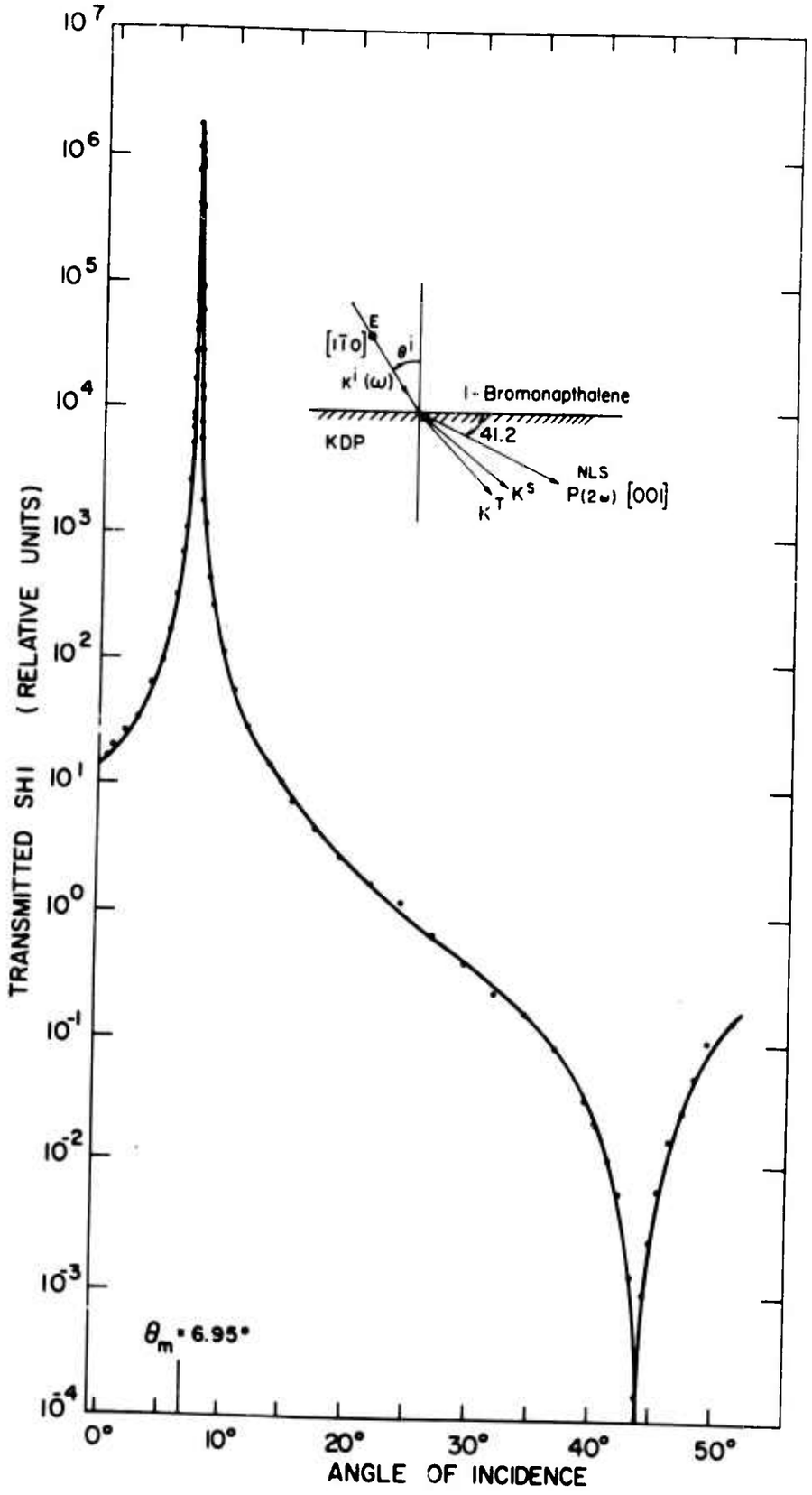
TRANSMITTED SHI (RELATIVE UNITS)
10^7
10^6
10^5
10^4
10^3
10^2
10^1
10^0
10^{-1}
10^{-2}
10^{-3}
10^{-4}
$\theta_m = 6.95°$
0°
10°
20°
30°
40°
50°
ANGLE OF INCIDENCE
[1$\bar{1}$0]
E
θ^i
$K^i(\omega)$
1-Bromonapthalene
41.2
KDP
NLS
P(2ω) [001]
K^T
K^S

FIGURE 4 - 9

The corresponding angle of incidence θ_i is given by

$$\theta^i = \sin^{-1}\left\{\frac{n^e_{2\omega}(\theta_m)}{n_{liq}(\omega)} \cdot \sin\theta_T\right\}$$

where $n^e_{2\omega}(\theta_m) = n^o_{\omega} = 1.4943$

Thus

$$\theta_i = \sin^{-1}\left\{\frac{1.4943}{1.6260} \cdot \sin(7.6^o)\right\}$$

$$\theta_i = 6.95^o$$

The rapid increase of the total harmonic intensity at the phase matching angle θ_m is due to an enhancement of the nonlinear Fresnel factors $F^{NL}_{S,ll}$ and $F^{NL}_{T,ll}$ given by (2.35b) and (2.35c) for polarization and radiative harmonic waves respectively. This rapidly monoton increase of the total harmonic intensity dominates the oscillatory pattern in the region of small angle of incidence so that no oscillatory pattern of interference between the homogeneous and inhomogeneous harmonic beam has been observed. The experimental data points are in striking agreement to the computed theoretical curve shown in Fig. 4-9. It is noted that the prominent dip of the curve occurs in the neighborhood of $\theta_i = 44^o$ as expected in theory. According to classical dipole radiation, the inhomogeneous or homogeneous harmonic intensity will become minimum when the propagating vector $\vec{k}_S$ or $\vec{k}_T$ parallel to the direction of $\vec{P}^{NLS}$ which is in the [001] direction. This situation occurs when θ_S or θ_T is $(90^o - 41.2^o) = 48.8^o$. The corresponding angle of incidence θ_i is thus given by

$$\theta_i' = \sin^{-1}\left\{\frac{n^o_{(\omega)}}{n_{liq}(\omega)} \cdot \sin\theta_S\right\}$$

$$= \sin^{-1}\left\{\frac{1.4943}{1.6260} \cdot \sin(48.8^o)\right\}$$

$$\theta_i' = 43.73^o \qquad (4.16)$$

For the situation that $\vec{k}_T$ is parallel to $\vec{P}^{NLS}$, one has $\theta_T = 48.8^o$ and the corresponding $n^e_{2(\omega)}$ can be computed by equation (4.69) as

$$n^e_{2(\omega)}(0) = n^o_{2(\omega)} = 1.5131$$

Thus the corresponding angle of incidence θ_i'' is given by

$$\theta_i'' = \sin^{-1}\left\{\frac{n^o_{2(\omega)}}{n_{liq}(\omega)} \cdot \sin\theta_T\right\}$$

$$\theta_i'' = \sin^{-1}\left\{\frac{1.5131}{1.6260} \cdot \sin(48.8^o)\right\}$$

$$\theta_i'' = 44.42^o \qquad (4.17)$$

Due to the intrinsic birefringent phenomena in KDP crystal the two harmonic beams have larger spatial separation when θ_i become large. Furthermore, information from equations (4.16) and (4.17) indicate that homonogeneous and inhomogeneous harmonic intensities will never be simultaneously zero value at the same angle of incidence θ_i. Therefore the value $I_{Total}(2\omega)$ given by equation (4.14) will never become zero as in the previous case where the nonlinear polarization $\vec{P}^{NLS}$ is parallel to the face normal direction, i.e., $\theta_S = \theta_T = 0$. The experimental points are indeed in good agreement to the theoretical

prediction given by the above analysis. It is noted that the dynamical range of the total harmonic intensity for this case is about 10 orders of magnitude which is the same as in the previous case.

The investigation relating to SHG in transmission emanating from a KDP crystal immersed in an optically denser linear liquid 1-bromonaphthalene can be concluded that the experimental results of individual as well as the total harmonic intensity are in good agreement with the theory developed by Bloembergen and Pershan[12]. The regime of transmitted second harmonic waves corresponding to an angular range from normal incidence to critical angle has been demonstrated.

C. Second Harmonic Generation (SHG) by Two Beam Spatial Mixing (Noncollinear Phase Matched Experiment).

The theory developed by Bloembergen and Pershan[12] has also predicted the possibility of SHG using two fundamental beam mixing inside the nonlinear medium. The first demonstration of SHG by two beam spatial mixing (TBSM) technique was performed with Q-switched ruby laser radiation incident on GaAs by Ducuing and Bloembergen.[25] Later Bloembergen, Simon and Lee[28] performed TBSM experiment using Raman laser of wavelength 9770$\mathring{A}$ incident upon $NaClO_3$. Those previous experiments were performed without phase matched condition. In the present study of TBSM experiment, an uniaxial KDP crystal prepared for noncollinear phase matched condition was employed and the fundamental beam was Q-switched pulse from the Nd:glass laser. The purpose is to extend the theory into the domain of noncollinear phase

matched condition from an uniaxial KDP crystal and as a consequence the knowledge of polarization and SHG by TBSM technique will be utilized for picosecond pulsewidth measurements of the Nd:glass laser.

The KDP crystal used in the experiment has dimensions of 25 x 15 x 8 mm^3. It has crystallographic orientation that its optic (z) axis is parallel to the entrance surface. The two equal intensity fundamental beams are incident from opposite sides of the face normal which is in [110] direction. The angles of incidence of each beam are equal to θ_i.

The fundamental beams are polarized in $[1\bar{1}0]$ direction and according to equation (2.31a) the nonlinear polarization $\vec{P}^{NLS}$ is in the [001] direction (optic axis). The polarization and crystallographic orientation of the crystal are shown in the inset of Fig. 4-10. The overall experimental arrangement and the transmitted SHI in this experiment have been in Fig. 3-6 of Chapter III.

When the two fundamental beams of equal intensity impinge on the nonlinear KDP crystal with equal angle of incidence θ_i from the opposite sides of the face normal, a nonlinear polarization P^{NLS} is created in the plane of incidence with zero tangential component of the wave vector. Since the polarization has the same phase at all points along the surface, it radiates second harmonic waves in the normal inward and outward direction. According to this situation, equation (2.15) can be applied directly and one has

$$\theta_T = \theta_S = \theta_R = 0 \tag{4.18}$$

The value of ϵ_S inside the KDP is determined by the length of the source wave vector $\vec{k}_S$;

$$\vec{k}_S = \frac{2\omega}{c}\sqrt{\varepsilon_S}\,\hat{a} = \frac{2\omega}{c} n_\omega^o \cos\theta_t \hat{a} \tag{4.19}$$

where θ^t is the refracted angle for the individual transmitted fundamental beam.

By using equation (2.30a) and $n_{air} = 1.0$, the $\vec{k}_S$ given by equation (4.19) can be expressed in term of θ_i as

$$\vec{k}_S = \frac{2\omega}{c} n_\omega^o \left[1-\sin^2\theta_i/\sin^2\theta^{cr}(\omega)\right]^{1/2} \hat{a} \tag{4.20}$$

where $\theta^{cr}(\omega)$ is 66.78^o.

According to equation (4.20), $\vec{k}_S$ has maximum value at $\theta_i = 0^o$ and vanishes when $\theta_i = \theta^{cr}(\omega)$. This is in agreement to the fact that when the two fundamental beams are incident at critical angle $\theta^{cr}(\omega)$ the fundamental beam will be along the boundary of the interfaces and their normal component with respect to the interface is zero.

From equation (4.20), one can vary the length of $\vec{k}_S$ which is along the face normal direction such that it is equal to the length of $\vec{k}_T$ in the same direction. Thus the noncollinear phase matched condition is achieved.

The physical description which described this condition has been given in chapter II. According to the noncollinear phase matched condition, one has for normal component condition given by equation (2.51) as

$$n_o^\omega \cdot \omega\cos\alpha + \frac{n_o^\omega}{c} \cdot \omega\cos\alpha' = \frac{n_e^{2\omega}}{c} (\pi/2) \cdot 2\omega$$

$$n_o^\omega \cos\alpha' = n_e^{2\omega}(\pi/2) \tag{4.21}$$

Thus

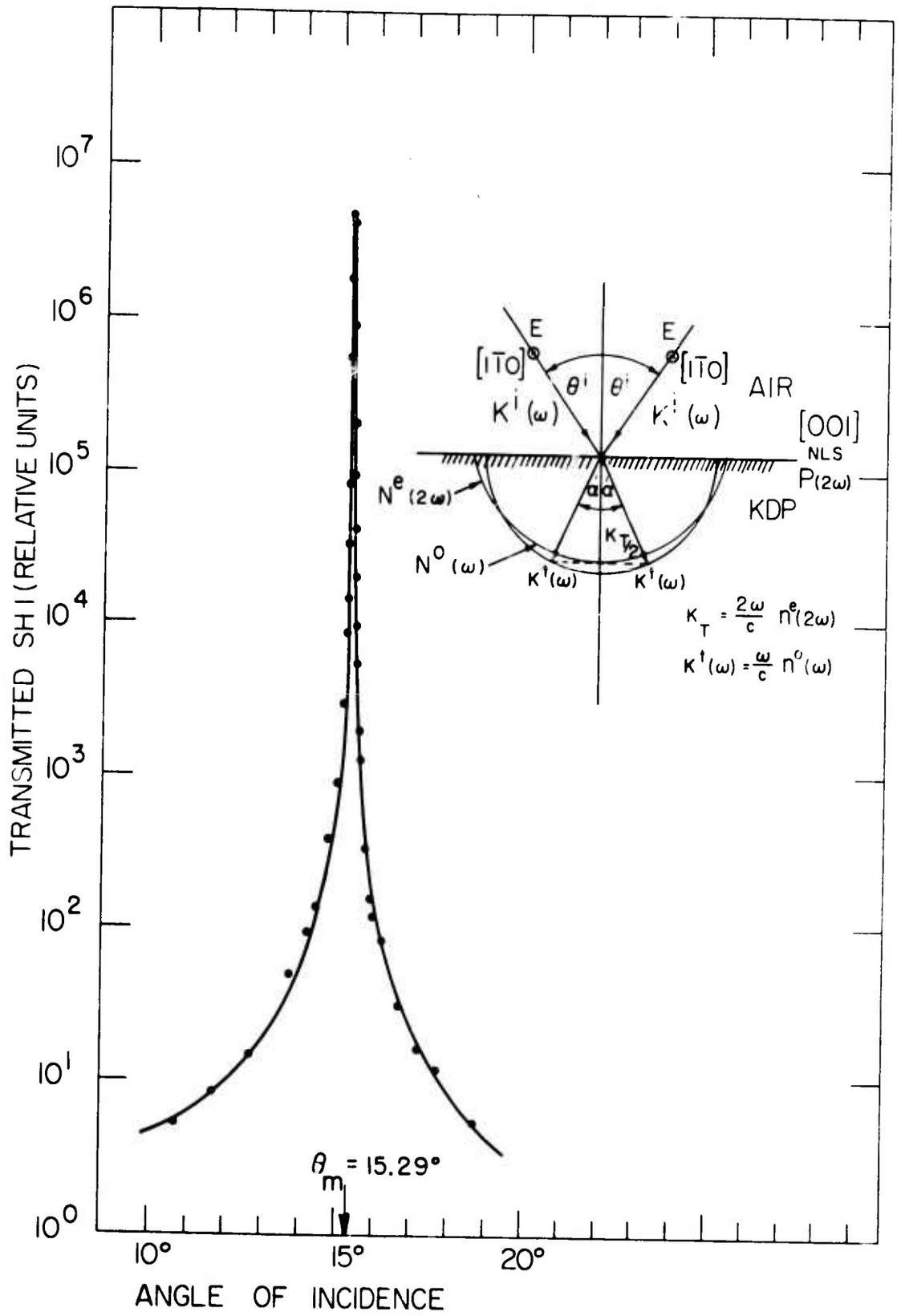
TRANSMITTED SH I (RELATIVE UNITS)
10^7
10^6
10^5
10^4
10^3
10^2
10^1
10^0
$\theta_m = 15.29°$
10°
15°
20°
ANGLE OF INCIDENCE
E
E
[1$\bar{1}$0]
[1$\bar{1}$0]
θ^i
θ^i
$K^i(\omega)$
$K^i(\omega)$
AIR
[001]
NLS
$P(2\omega)$
KDP
$N^e(2\omega)$
$N^o(\omega)$
$K_{T/2}$
$K^t(\omega)$
$K^t(\omega)$
$K_T = \frac{2\omega}{c} n^e(2\omega)$
$K^t(\omega) = \frac{\omega}{c} n^o(\omega)$

FIGURE 4 - 10

$$\alpha' = \cos^{-1}\left[\frac{n_e^{2\omega}(\pi/2)}{n_o^{\omega}}\right]$$

$$= \cos^{-1}\left[\frac{1.4708}{1.4943}\right] \qquad (4.22)$$

$$\alpha' = 10.17^{o}$$

The corresponding angle of incidence or the noncollinear phase matched angle, is given by equation (2.53) as

$$\theta_i^{m} = \sin^{-1}\left[n_{\omega}^{o} \sin\alpha'\right]$$

$$= \sin^{-1}\left[1.4943 \sin 10.17^{o}\right]$$

$$\theta_i^{m} = 15.29^{o}$$

The total transmitted harmonic intensity $I_{Total}(2\omega)$ was observed in the direction of face normal of the exist face of the crystal. It was measured as a function of angle of incidence and compared to the computed theoretical curve. The theoretical curve shown in Fig. 4-10 was computed by using equation (4.15). The justification of using equation (4.15) for $I_{Total}(2\omega)$ is the same as given in the previous section. The anomalously high total harmonic intensity $I_{Total}(2\omega)$ in Fig. 4-10 is due to the enhancement of nonlinear Fresnel factors $F_{S,ll}^{NL}$ and $F_{T,ll}^{NL}$ at $\theta_i = \theta_i^{m}$. This can be mathematically shown in the following.

From equation (2.35b), one has

$$F_{S,ll}^{NL} = \frac{\sin\alpha}{\epsilon_S - \epsilon_T} \quad ; \text{where } \alpha = 90^{o}$$

Thus

$$F_{S,\perp}^{NL} = \frac{1}{\left[n_{\omega}^{o}\cos\theta^{t}\right]^{2} - \left[n_{2\omega}^{e}(\pi/2)\right]^{2}} \tag{4.23}$$

Furthermore, since $\theta_S = \theta_T = \theta_R = 0$ and $\alpha = 90^{o}$ for this case the nonlinear Fresnel factor $F_{T,\perp}^{NL}$ given by equation (2.35c) is reduced to

$$F_{T,\perp}^{NL} = \frac{\varepsilon_S}{\sqrt{\varepsilon_T}} \frac{1}{(\varepsilon_S - \varepsilon_T)} + \frac{1}{\sqrt{\varepsilon_R \varepsilon_T}}$$

where $\varepsilon_R = 1.0$ for air, thus

$$F_{T,\perp}^{NL} = \frac{n_{\omega}^{o}\cos\theta_S}{n_{2\omega}^{e}(\pi/2)} \left\{\frac{1}{\left[n_{\omega}^{o}\cos\theta^{t}\right]^{2} - \left[n_{2\omega}^{e}(\pi/2)\right]^{2}}\right\} - \frac{1}{n_{2\omega}^{e}} \tag{4.24}$$

Here θ^{t} in equations (4.22) and (4.23) is the same parameter used in equation (4.19). It is noted that both $F_{S,\perp}^{NL}$ and $F_{T,\perp}^{NL}$ given by equations (4.23) and (4.24) respectively have the term in their denominators satisfied the phase matched condition given by equation (4.12). In other words $F_{S,\perp}^{NL}$ and $F_{T,\perp}^{NL}$ become infinite at $\theta^{t} = \alpha' = 10.17^{o}$. Therefore upon substituting equation (4.23) and (4.24) into equation (4.15) one has a singularity point for $I_{Total}(2\omega)$ at the noncollinear phase matched condition.

Note the striking agreement between experimental points and the computed theoretical curve shown in Fig. 4-10. The noncollinear phase matched angle θ_i^{m} is indeed equal to 15.29^{o} as predicted by the theory. The total harmonic intensity $I_{Total}(2\omega)$ changes by about four orders of magnitude when the angle of incident changes by a few tenth of a degree

from θ_i^m. This is for the first time that the theoretical prediction of the enhancement of the nonlinear Fresnel factors $F_{S,11}^{NL}$ and $F_{T,11}^{NL}$ for a uniaxial KDP crystal at noncollinear phase matched condition has been demonstrated.

D. Measurement of Picosecond Pulsewidth

The agreement of experimental data with the theory for the TBSM experiment described in the previous section encourages us to utilize the results for measurement of picosecond pulsewidth of mode locked Nd:glass laser. Since KDP is a nonlinear crystal from which phase matchable SHG can be produced, then it is very convenient to use its square law intensity characteristic to measure the second order auto-correlation function of Nd:glass laser radiation.

In the experiment the KDP crystal used in the TBSM experiment in the previous section served as the nonlinear medium. The KDP crystal was in the air and its crystallographic orientation was the same as indicated in the inset of Fig. 4-10. The fundamental beam were mode locked pulse trains of 300-600 nanoseconds duration as shown in Fig. 4-11 and their polarizations were in the $[1\bar{1}0]$ direction. The two fundamental beams were incident upon the crystal at noncollinear phase matched angle θ_i^m. The detail of experimental setup was given in Fig. 3-6 of Chapter III. According to the result of TBSM experiment, it required both spatial and temporal overlapping of the two fundamental beams inside the crystal. The temporal overlapping was critical and could be achieved only by straight forward scanning of the temporal delay of one beam with respect to the other until SHI was observed. From equation (2.62) one can

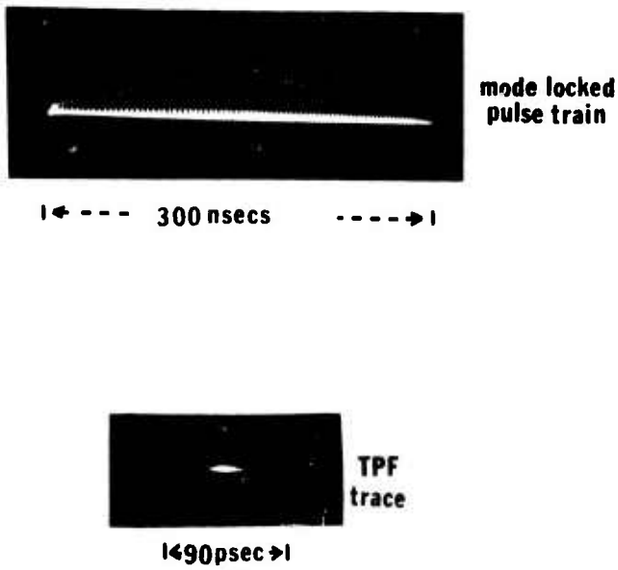

FIGURE 4 - 11

see that the transmitted harmonic intensity $I_{Total}(2\omega)$ is directly proportional to the second order auto-correlation function $G^{(2)}(\tau)$. The $G^{(2)}(\tau)$ obtained from this experiment is a background free function since a single fundamental beam cannot generate SHI in the normal direction to the exit face of the crystal. In the experiment the transmitted harmonic intensity was observed as a function of temporal delay τ and as a consequence the $G^{(2)}(\tau)$ was directly mapped out as shown in Fig. 4-12 .

The resolution in the picosecond pulsewidth measurement is strongly dependent on the thickness of the KDP crystal used in the experiment. The used crystal thickness of 8mm, can give a relatively large volume of interaction between the two fundamental beams inside the crystal. The depth of the interacting volume inside the crystal was reduced to a minimum value such that the SHI could be comfortably observed for the entire scanning delay τ . This was done by means of masking the entrance surface of the crystal by a 0. 2 mm wide slit , which would give a depth of interaction of about 0. 6 mm corresponding to a time duration of 3. 0 picosecond for the light travelling inside the KDP crystal. From the experimental result given in Fig. 4-12, the full width at half height of the curve $G^{(2)}(\tau)$ gives about 2. 67 picoseconds for the width of the auto-correlation curve. Since the scanning introduces a factor of two for the temporal delay of one pulse in relation to the other, thus the measured pulsewidth is about 5 picoseconds.

The accuracy of this measurement can be improved by using the same crystallographic orientation of a KDP crystal with a thickness

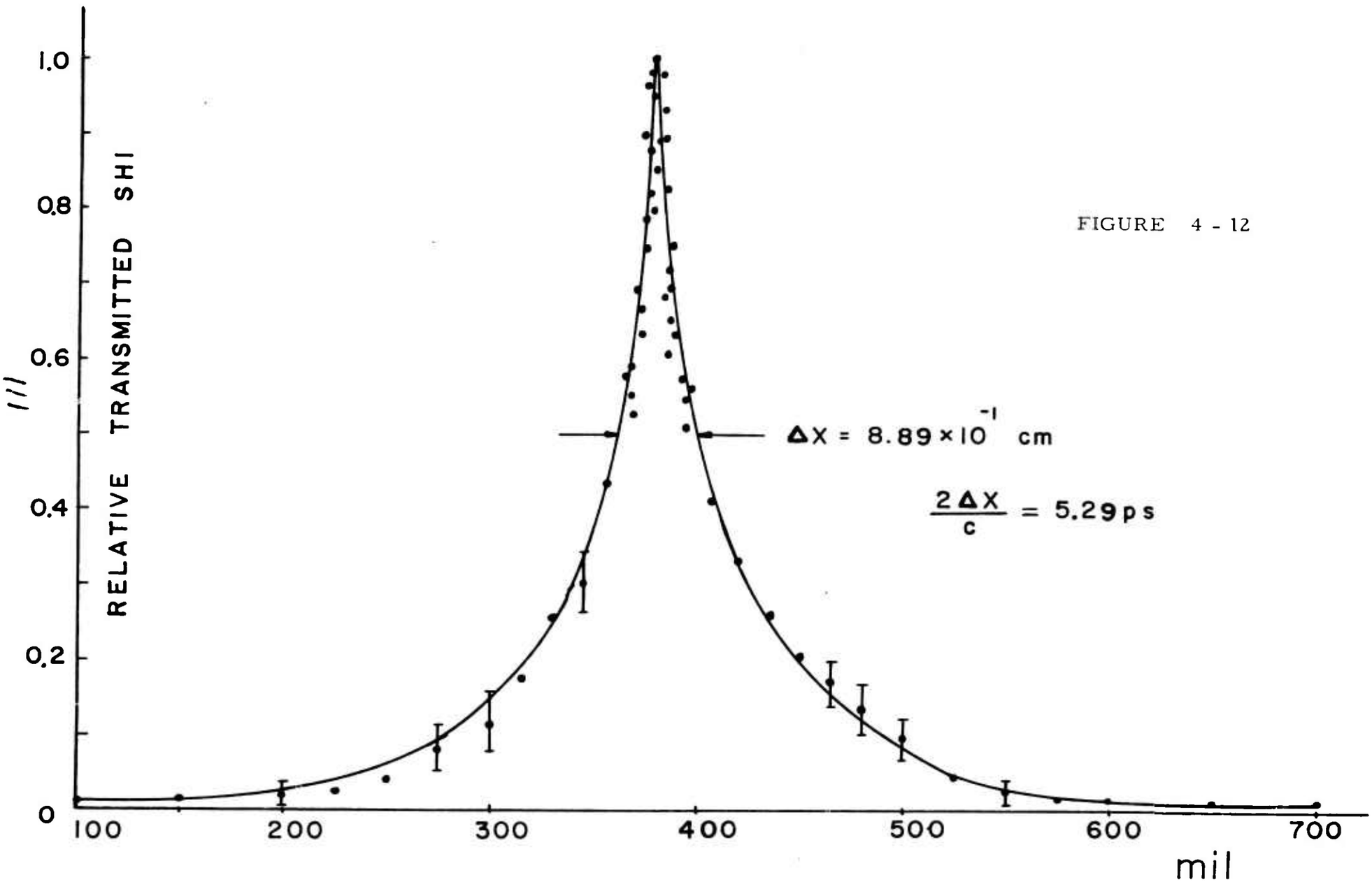
1.0
0.8
0.6
0.4
0.2
0
RELATIVE TRANSMITTED SHI
I/I
ΔX = 8.89×10⁻¹ cm
2ΔX/c = 5.29ps
100
200
300
400
500
600
700
mil

FIGURE 4 - 12

of the order of only 0.1 - 0.2 mm. Another factor that contributes to the larger pulsewidth is the characteristic of the laser system itself. It is an intrinsic problem of the system itself whether or not it can reproduce a perfectly mode locked pulse train . Any partially mode locked pulse train, which cannot be distinguishable by the fast oscilloscope, will yield a larger measured pulsewidth.

Apart from the resolution limitation, the principle of noncollinear phase matched technique via square law of SHG can be used for second order auto-correlation mapping and for picosecond pulsewidth measurement. The advantage of very high SHI by this method could be utilized in the future for the measurement of the pulsewidth via photographic methods which will be very convenient to operate.

CHAPTER V
DISCUSSION

During the course of the present study an attempt was made to extend the study and verification of the theory[12] to the third harmonic generation (THG) by using two beam spatial mixing (TBSM) technique The source of excitation was a Q-switched Nd:glass laser and a nonlinear optical medium immersed in an isotropic liquid consisting of fuchsin red dye molecules dissolved in hexafluoroacetone sesquihydrate. The concentration of the dye solution was set at 45 gm/liter. At this concentration the phase matchable THG in normal incidence and total reflection of a single Nd:glass laser beam was demonstrated earlier by Bey et al[30,50], and indices of refraction of the solution were given as

$$n(\omega) = n(3\omega) = 1.3205 \tag{5.1}$$

The experimental setup for this investigation is shown in Fig. 5-1. The monitor channel was similar to the previous setup except for the fuchsin pyrex cell and an interference filter of a transmission peak at 3500 A° were used instead of the quartz platelet and second harmonic interference filter respectively. The fundamental beam was split into two beams of equal intensity by the beam splitter. Subsequently the two beams were incident on the fuchsin cell with equal angle of incidence from the opposite side of a face normal of the cell. The signal channel, as indicated in Fig. 5-1 could be rotated around the vertical axis which was tangential to the entrance face of the fuchsin cell.

The signal arm was scanned through a large interval of angle by 1° for each step. Despite careful alignment of every optical component,

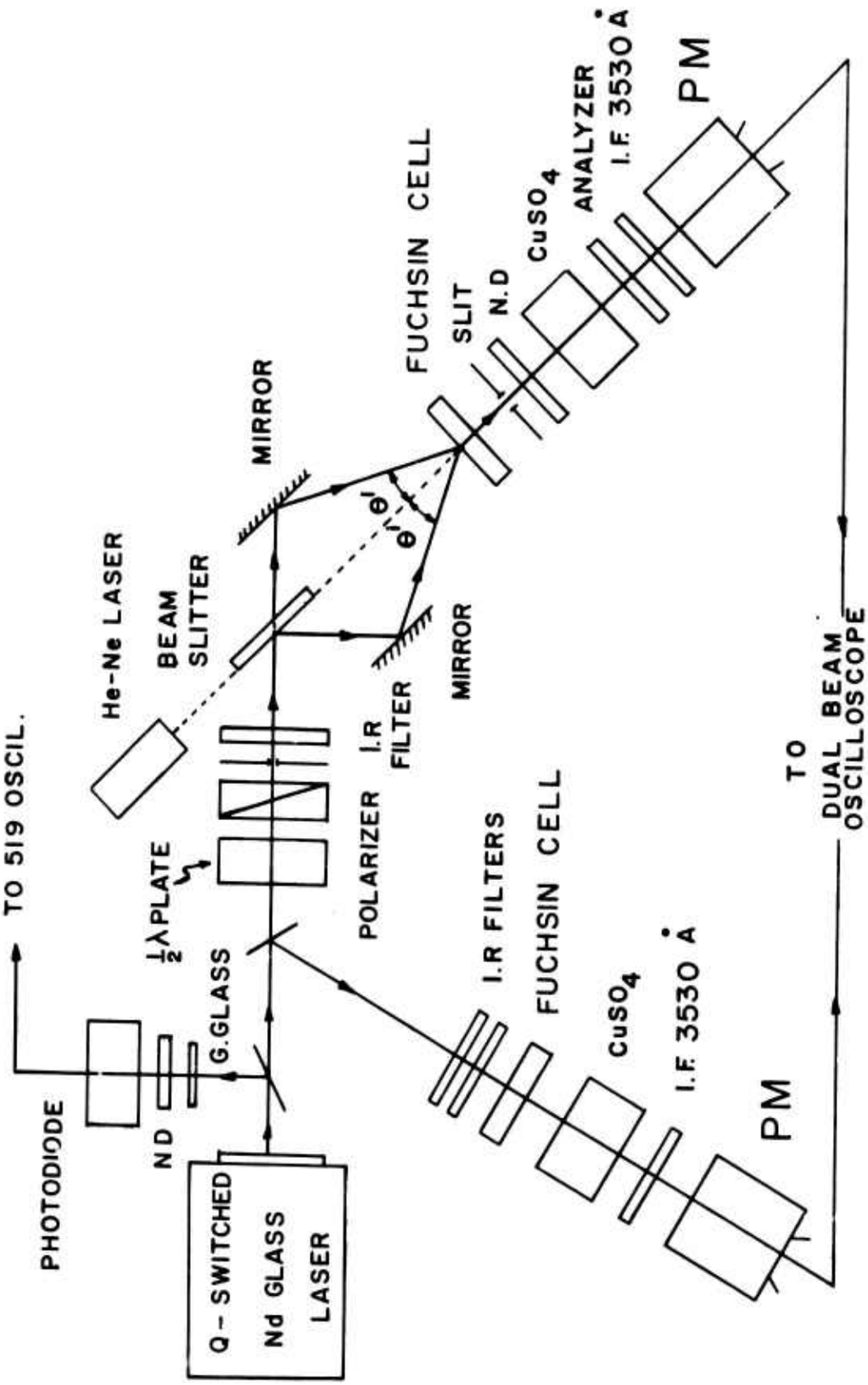
TO 519 OSCIL.
PHOTODIODE
ND
G.GLASS
Q - SWITCHED
Nd GLASS
LASER
½λ PLATE
He-Ne LASER
BEAM
SLITTER
POLARIZER
I.R
FILTER
MIRROR
MIRROR
FUCHSIN CELL
SLIT
N.D
CuSO4
ANALYZER
I.F 3530 Å
PM
I.R FILTERS
FUCHSIN CELL
CuSO4
I.F 3530 Å
PM
TO
DUAL BEAM
OSCILLOSCOPE

FIGURE 5 - 1

varying the angle of incidence θ_i and repeated scannings, the transmitted third harmonic intensity (THI) was not observed. The reasons that justify the result can be mathematically explained in terms of a noncollinear phase matched picture which will be given below.

The two incident beams of equal intensity are incident from quartz with $\theta_i^1 = \theta_i^2 = \theta_i$ as shown in Fig. 5-2. Since the dye fuchsin solution is an isotropic medium, the locus of transmitted third harmonic wave vector $\vec{k}_T$ will be a semicircle of radius $3|\vec{k}_t|$ inside the medium. The $\vec{k}_t$ is the transmitted fundamental wave vector. According to the phase matched condition given by several authors[33, 34, 43], the three transmitted fundamental wave vectors must add up so that the resultant vector is equal to $\vec{k}_T(3\omega)$. Here one assumes that one fundamental beam contributes the transmitted fundamental wave vector $2\vec{k}_t(\omega)$ whereas the other is $\vec{k}_t(\omega)$. Furthermore, boundary conditions given by Bloembergen and Pershan[12] require that the tangential components of those wave vectores must be conserved. By using equation (2.49) one obtains from Fig. 2-5 that

tangential component:

$$[2k_t(\omega) - k_t(\omega)] \sin\theta_1 = k_T(3\omega) \sin\theta_T \tag{5.2}$$

normal component:

$$[2k_t(\omega) + k_t(\omega)] \cos\theta_1 = k_T(3\omega) \cos\theta_T \tag{5.3}$$

Since $k_t(\omega) = \frac{\omega}{c} n(\omega)$ and $k_T(3\omega) = \frac{3\omega}{c} n(3\omega)$, equation (5.2) and (5.3) can be deduced to equation (5.4) and (5.5) respectively as

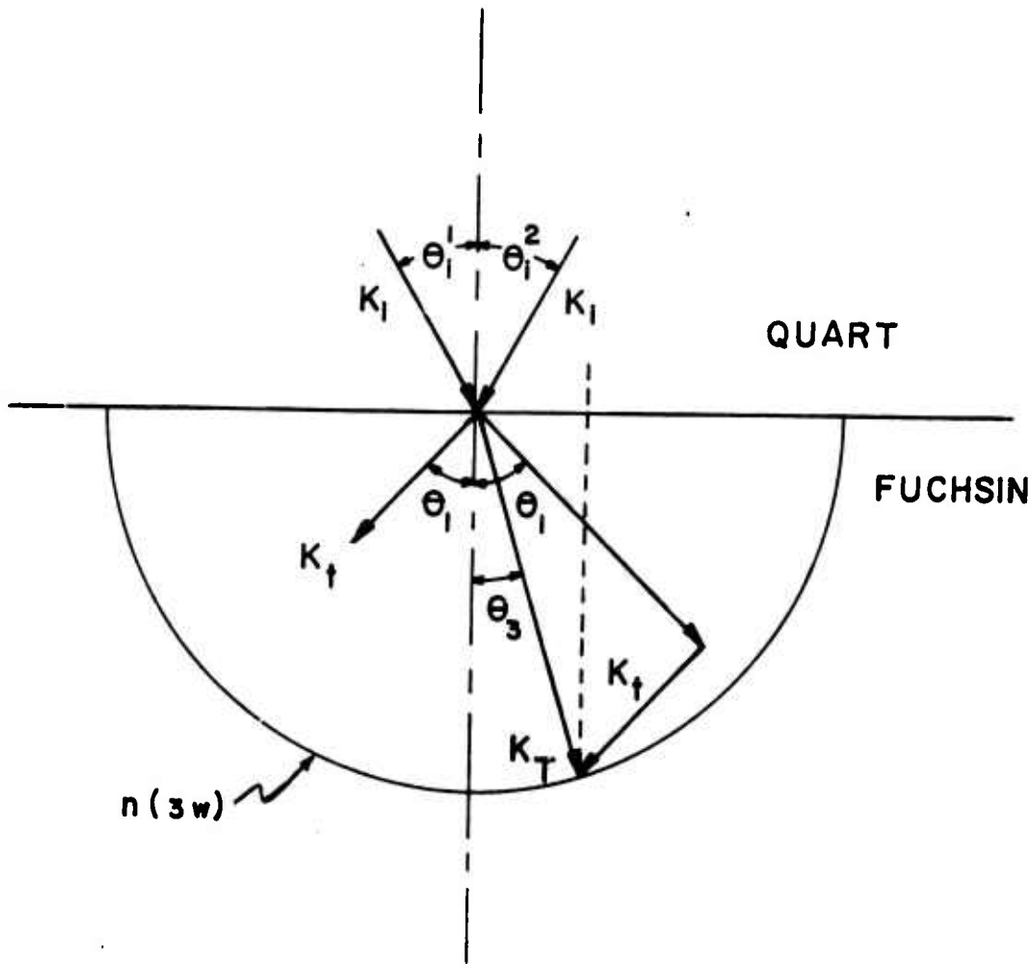
θ_i^1
θ_i^2
K_I
K_I
QUART
FUCHSIN
θ_t
θ_t
K_t
θ_3
K_t
K_T
n (3w)

FIGURE 5 - 2

$$\sin\theta_1 = \frac{3n(3\omega)}{n(\omega)} \sin\theta_T \tag{5.4}$$

$$\cos\theta_1 = \frac{n(3\omega)}{n(\omega)} \cos\theta_T \tag{5.5}$$

Since the dye fuchsin solution has a concentration such that $n(\omega) = n(3\omega)$, the solution of the simultaneous equations (5.4) and (5.5) becomes

$$\theta_1 = \theta_T = 0 \tag{5.6}$$

This is not a surprising result. It has the physical meaning that phase matched THG will be created if the fundamental beam is normally incident upon the dye fuchsin solution. Under this situation one obtains from equation (5.3) that $3\vec{k}_t = \vec{k}_T$ and the two fundamental beams will collapse into a single beam. This situation has already been investigated by Bey et al[50].

From the above analysis it is noted that when the dye fuchsin of concentration 45 gm/liter is employed as a nonlinear medium, the phase matched THG is produced under normal incidence of the fundamental beam. However, in the experimental investigation the angle of incidence was varied in 2° steps from 10° to 25°. This variation of the angle of incidence apart from 0° will yield phase mismatched condition and since the dye fuchsin solution is strongly absorbed at the third harmonic line (3530Å), a transmitted third harmonic intensity will not be observed in the experiment.

From equation (5.4) and (5.5), future analysis can be made if one selects a dye concentration different from 45 gm/liter. One has to

use higher dye concentration due to the fact that $n(\omega)$ is greater than $n(3\omega)$ in this region and the equation (5.4) and (5.5) will give physical solution. This can be mathematically demonstrated in the following example.

By using the dye concentration of 50gm/liter the indices of refraction at fundamental and third harmonic frequencies will be given as

$$n(\omega) = 1.3225 \qquad n(3\omega) = 1.3210 \tag{5.7}$$

From equation (5.4) and (5.5) one obtains

$$1 = (9\sin^2\theta_T + \cos^2\theta_T)\left\{\frac{n(3\omega)}{n(\omega)}\right\}^2$$

$$1 = (8\sin^2\theta_T + 1)\left\{\frac{1.3210}{1.3225}\right\}^2$$

$$\theta_T = 0.97^\circ \tag{5.8}$$

Thus, from equation (5.4) the corresponding angle of incidence in Fig. 5-2 will be

$$\theta_i^m = 2.88^\circ \tag{5.9}$$

This is the phase matched angle for a dye concentration of 50 gm/liter. One can use even higher dye concentration in order to achieve a relatively large phase matched angle. However, due to a lack of knowledge of the indices of refraction at hand, the experimental investigation has not been carried out. The above analysis will serve for future experiment involving TBSM for third harmonic generation from isotropic nonlinear media with $n(\omega) > n(3\omega)$.

Even though the experimental result for the case of dye concentration of 45 gm/liter, turned out to be negative, it can be explained by the theories developed by several authors[12, 33, 34, 43]. In a relatively new field it cannot be expected that experimental results always agree with theoretical predictions. However, to be able to ultilize theoretical knowledges to explain the phenomena observed in the experimental investigation will result a better understanding and direct contribution to the theory.

For this reason it is very important that experimental and theoretical go hand in hand for increase our knowledge of the field.

CHAPTER VI
CONCLUSION

The nonlinear optical interaction in a KDP prism in relation to second harmonic generation was investigated by means of Q-switched and mode-locked Nd:glass laser pulses and the results obtained from the investigation were subsequently utilized to measure the second order intensity auto-correlation function. The experimental results obtained from this investigation provide additional rather striking and detailed confirmation of the theory developed by Bloembergen and Pershan[12] on the behavior of the light waves at the boundary of a nonlinear crystalline KDP medium. Although the theory was developed for a homogeneous incident plane wave of infinite cross section, the results are well described by taking the field solution for the infinite plane wave and the cutting off the beam by modification of the aperture width expression and taking linear Fresnel factor into consideration. The recasted theoretical expressions given in chapter II have been well verified and are valid for an uniaxial crystal, e.g., KDP. The reasons that the modification of the infinite plane wave case works so well is due to the fact that the dimension of the relevant experimental parameters are large compared to the characteristic dimension of the physical problem. Detailed justification has been given by Simon[92].

The results obtained from the experiment of phase matched second harmonic generation at total reflection are in agreement with the other observations[88] under the same condition except different wave length and type of the fundamental beam. When the KDP crystal being phase matched along its surface was rotated about its face normal by 180° it

was found that the reflected second harmonic intensity in the neighborhood of critical angle was always lower . This phenomena can be qualitatively explained by an intrinsic property, the so called double refraction which results in a walk-off effect in the uniaxial crystal. However, an exact mathematical treatment that accounts for a detailed explaination of this phenomena remains for future investigations.

With good utilization of the advantages of mode locked Nd:glass laser pulses for the observation of reflected second harmonic intensity from a KDP crystal, the Nonlinear Brewster' s angle of the transparent medium (KDP) has been first demonstrated with an excellent agreement to the theoretical prediction.

For the transmitted second harmonic waves, the angular dependence of homogeneous, inhomogeneous as well as the total harmonic intensities emanated from KDP crystals were experimentally confirmed with the theory. The phenomena of phase matched SHG along the oblique direction by means of birefringence[33, 34] was investigated and the results were also in good agreement to the theory. The relative differences of SHI between the maximum and minimum as indicated in Fig. 4-8 and 4-9, were observed to be about ten orders of magnitude. The striking agreement of the experimental result of noncollinear phase matched SHG by means of two beam spatial mixing (TBSM) to the theoretical prediction was utilized to measure the second order intensity auto-correlation function of Nd:glass laser radiation. This,in principle, can be used for the construction of a device for picosecond pulsewidth measurement using simple

photographic techniques. This is due to the fact that the SHI emanating from the KDP crystal under noncollinear phase matched condition is so intense that it can be photographed.

Finally, the results obtained from this investigation confirm and extend the theory of Bloembergen and Pershan[12] for nonlinear optical interaction in an uniaxial crystal (KDP) in the regimes of reflected and transmitted second harmonic intensities.

APPENDIX

COMPUTER PROGRAMS FOR THEORETICAL CURVES

```
'RUN JB.305168.BHANTHUMNA.1.100
'PASSWD 17B9FI
'FOR.IS MAIN
      COMPLEX A1, A2, A3, A4,  A5, A6, A7, A8,  FNL, FLT, C, D
      C = (1.0,0.0)
      D = (0.0,1.0)
      READ (5,7)A
 7    FORMAT(F8.5)
 10   XINC = 0.1
      A = A+XINC
      PI = 3.1416
      IF ( A-75.0 ) 12, 12, 100
 12   AX = A*PI/180.0
      Z = SIN(AX)
      A1 = Z*C
      Z = COS(AX)
      A2 = Z*C
      B1 = 1.513122
      B2 = 1.47122
      B3 = 1.494305
      D1 = 1.6260
      D2 = 1.670
      Z = (D1/D2)*A1
      A3 = Z*C
      Z = SQRT( 1.0-(A3)**2.0)
      A4 = Z*C
 13   IF (A-64.797) 14, 14, 15
 14   Z = ( D1/B3) *A1
      A5 = Z*C
      Z = SQRT ( 1.0- (A5)**2.0)
      A6 = Z*C
      Z = (D1/B2)*A1
      A7 = Z*C
      Z = SQRT (1.0-(A7)**2.0)
      A8 = Z*C
      GO TO 80
 15   IF (A-66.781) 16, 16, 17
 16   Z = (D1/B3)*A1
      A5 = Z*C
      Z = SQRT ( 1.0- (A5)**2.0)
      A6 = Z*C
      Z = (D1/B2)*A1
      A7 = Z*C
      Z = SQRT ((A7)**2.0-1.0)
      A8 = Z*D
      GO TO 80
 17   Z = (D1/B3)*A1
      A5 = Z*C
      Z = SQRT((A5)**2.0-1.0)
      A6 = Z*D
      Z = (D1/B2)*A1
      A7 = Z*C
      Z = SQRT((A7)**2.0-1.0)
      A8 = Z*D
 80   FLT = ((2.0)*A2*A5)/(A1*A6 +A2*A5)
      FNL = (A5*A7*A7*A7)/(A3*(A7*A4 +A8*A3)*(A8*A4 + A7*A3)
     1*(A7*A6 + A8*A5))
      FLTR = REAL(FLT)
      FLTI = AIMAG(FLT)
      FNLR = REAL (FNL)
      FNLI = AIMAG (FNL)
      FNLM = SQRT ( FNLR*FNLR + FNLI*FNLI)
      FLTM = SQRT( FLTR*FLTR + FLTI*FLTI)
      SHI = (FNLM**2.0)*(FLTM**4.0)*(A4/A2)
      WRITE (6,90) A, SHI
 90   FORMAT (1HO, '  INC. ANGLE =  ',F6.3, '  REFLECTED SHI =  'F10.3)
      GO TO 10
 100  END
'XQT
59,9000
'FIN
```

Computer Program for the Theoretical Curve of Figure 4 - 1

```
*RUN VB,30516802,BHANTHUMNA,3,200
*FOR,IS MAIN
      COMPLEX F,A1,A2,A3,A4,A5,A6,F1,FNL,FL,C,D
      C=(1.0,0.0)
      D=(0.0,1.0)
      IF(A-75.0)12,12,50
 12   IF(A-66.615) 13,13,14
 13   X=SIN(A*PI/180.0)
      X= 1.0892*X
      X=X*X
      X=SQRT(1.0-X)
      F=X*C
      GO TO 15
 14   X=SIN(A*PI/180.0)
      X= 1.0892*X
      X=X*X
      X=SQRT(X-1.0)
      F=X*D
 15   AX=A*PI/180.0
      Z=SIN(AX)
      F1= 1.0892*Z*C
      A1=Z*C
      Z=COS(AX)
      A2=Z*C
      ALPHA=41.2*PI/180.0
      Z=SIN(ALPHA)
      A3=Z*C
      Z=COS(ALPHA)
      A4=Z*C
      R= ASIN(0.9746*SIN(AX))
      Z=SIN(R)
      A5=Z*C
      Z=COS(R)
      A6=Z*C
      FNL=(F1*F1*F1)*(2.0*F1*F*A4-A3+2.0*F1*F1*A3)/(A5*(2.0*F1*F)*(F1*A6
     1+F*A5)*(F*A6+F1*A5))
      FL=2.0*F1*A2/(A1*F+A2*F1)
      FNLR=REAL(FNL)
      FNLI=AIMAG(FNL)
      FLR=REAL(FL)
      FLI=AIMAG(FL)
      FNLM=SQRT(FNLR*FNLR+FNLI*FNLI)
      FLM=SQRT(FLR*FLR+FLI*FLI)
      SHI=(FNLM**2.0)*(FLM**4.0)
      WRITE(6,20)A,SHI
 20   FORMAT(1H0,' INCIDENT ANGLE =',F8.5,' INTENSITY OF SHG =',F10.3)
 50   END
59.90000
00
```

Computer Program for the Theoretical Curve of Figure 4 - 2

```
$RUN VB,30516802,BHANTHUMNA,3,200
$FOR,IS MAIN
      COMPLEX A1,A2,A3,A4,A5,A6,A7,A8,FNL,FL,C,D
      C= (1.0,0.0)
      D= (0.0,1.0)
      READ(5,7)A
    7 FORMAT(F8.5)
   10 XINC =0.1
      A = A+XINC
      PI = 3.1416
      IF (A-75.0) 12,12,100
   12 AX= A*PI/180.0
      Z= SIN(AX)
      A1= Z*C
      Z= COS(AX)
      A2= Z*C
      Z= (1.6277/1.670)*A1
      A3= Z*C
      Z= SQRT(1.0-((1.6277/1.670)*A1)**2.0)
      A4= Z*C
      IF (A-66.61) 13,13,14
   13 Z=(1.6277/1.4942)*A1
      A5= Z*C
      Z= SQRT(1.0-(((1.6277/1.4942)*A1)**2.0))
      A6= Z*C
      GO TO 15
   14 Z= (1.6277/1.4942)*A1
      A5= Z*C



      Z= SQRT((((1.6277/1.4942)*A1)**2.0)-1.0)
      A6= Z*D
   15 ALPHA= 48.8*PI/180.0
      Z= SIN(ALPHA)
      A7= Z*C
      Z= COS(ALPHA)
      A8= Z*C
      FNL= ((A5*A5*A5)*(A5*A8+A6*A7))/(A3*(A5*A6+A5*A5)*(A5*A4+A6*A3)
     1*(A6*A4+A5*A3))
      FL= 2.0*A5*A2/(A1*A6+A2*A5)
      FNLR= REAL(FNL)
      FNLI= AIMAG(FNL)
      FLR= REAL(FL)
      FLI= AIMAG(FL)
      FNLM= SQRT(FNLR*FNLR + FNLI*FNLI)
      FLM= SQRT(FLR*FLR + FLI*FLI)
      SHI =  (FNLM**2.0)*(FLM**4.0)
      WRITE (6,20) A, SHI
   20 FORMAT(1H0,' INCIDENT ANGLE =',F8.5,' INTENSITY OF SHG =',F10.3)
      GO TO 10
  100 END
$XQT
59.90000
$FIN
$FIN
```

Computer Program for the Theoretical Curve of Figure 4 - 3

```
RUN VB,30516802,BHANTHUMNA,3,200
'FOR,IS MAIN
      READ(5,7)A
    7 FORMAT(F8.5)
   10 XINC =0.1
      A = A+XINC
      PI = 3.1416
      IF (A-50.0) 12,12,100
   12 AX= A*PI/180.0
      Z=SIN(AX)
      A1= Z
      Z= COS(AX)
      A2= Z
      Z=(1.6277/1.670)*A1
      A3= Z
      Z=SQRT(1.0-((1.6277/1.670)*A1)**2.0)
      A4= Z
      Z= (1.6277/1.4942)*A1
      A5= Z
      Z=SQRT (1.0-(((1.6277/1.4942)*A1)**2.0))
      A6= Z
      ALPHA= 48.8*PI/180.0
      Z= SIN(ALPHA)
      A7= Z
      Z= COS(ALPHA)
      A8= Z
      Z= (1.6277/1.4716)*A1
      A9 = Z
      Z=SQRT(1.0-(((1.6277/1.4716)*A1)**2.0))
      A10= Z
      FNL=(A5*A9*A9*(A9*A8-A10*A7))/(A3*(A9*A6+A10*A5)*(A9*ADDA10*A3)
     1*(A10*A4+A9*A3))
      FL= (2.0*A2*A5)/(A1*A6+A2*A5)
      SHI = (FNL**2.0)*(FL**4.0)
      WRITE (6,20) A, SHI
   20 FORMAT(1H0,' INCIDENT ANGLE ='F8.5,' INTENSITY OF SHG ''F10.3)
      GO TO 10
  100 END
'XQT
34.90000
'FIN
```

Computer Program for the Theoretical Curve of Figure 4 - 6

```
'RUN VB,305168,BHANTHUMNA,1,100
'PASSWD 1789FI
'FOR,IS MAIN
      READ(5,7)A
  7   FORMAT(F8.5)
  10  XINC = 0.1
      A = A+XINC
      PI = 3.1416
      IF (A-90.0 ) 12,12,100
  12  AX = A*PI/180.0
      A1 = SIN(AX)
      A2 = COS(AX)
      B2 = 1.47122
      B1 = 1.513122
      B3 = 1.494305
      D1 = 1.6260
      D2 = 1.670
      A3 = (B1*A1)**2.0
      A4 = (B2*A2)**2.0
      A5 = SQRT(A4+A3)
      B4 = (B1*B2)/A5
      CX = AX
      C1 = SIN(CX)
      C2 = ASIN((B4*C1)/B3)



      C3 = (C2*180.0)/PI
      C4 = ASIN((B4*C1)/D1)
      C5 = (C4*180.0)/PI
      C6 = ASIN((B4*C1)/D2)
      C7 = (C6*180.0)/PI
      R1 = SIN(C4)
      R2 = COS(C4)
      R3 = SIN(C2)
      R4 = COS(C2)
      R5 = SIN(C6)
      FLT = (2.0*R2*R3)/(R1*R4+R2*R3)
      FNLS = ((R3)*(-1.0))/((B3)**2.0-(B4)**2.0)
      FNLT = ((1.0)/(D2*B4))*(R3*A1*A1*A1)/(R5*(SIN(AX+C6))*(COS(AX-C6)*
     1*(SIN(AX+C2))) - (FNLS)*(B3/B4)
      SHI1 = B3*(FLT**4.0)*(FNLS**2.0)*R4/R2
      SHI2 = B4*(FLT**4.0)*(FNLT**2.0)*A2/R2
      SHI = SHI1 + SHI2
      WRITE(6,90) A,C3,C5, SHI1, SHI2, SHI,B4
  90  FORMAT (1HO, '  ZETAT =  ',F6.3, '  ZETAS =  ',F6.3,
     1' INC.ANGLE=  ',F6.3,' SHI1= ',F10.3,' SHI2= ',F10.3,
     1' SHI = ',F10.3, ' INDEX E= ',F10.7)
      GO TO 10
 100  END
'XQT
0.000000
'FIN
```

Computer Program for the Theoretical Curve of Figure 4 - 7 and 4 - 8

```
'RUN VB,305168,BHANTHUMNA,1,100
'PASSWD 17B?FI
'FOR,IS MAI'I
      READ(5,7)A
  7   FORMAT(F8.5)
  10  XINC = 0.1
      A = A+XINC
      PI = 3.1416
      IF (A-66.8)12,12,100
  12  AX = A*PI/180.0
      A1 = SIN(AX)
      A2 = COS(AX)
      B3 = 1.494305
      B4 = 1.47125
      D1 = 1.6260
      A3 = ASIN((D1*A1)/B3)
      A4 = SIN(A3)
      A5 = COS(A3)
      FLT = (2.0*A2*A4)/(A1*A5 +A2*A4)
      FNLS = ((A4)*(-1.0))/((B3)**2.0 -(B4)**2.0)
      SHI1 = B3*(FLT**4.0)*(FNLS**2.0)*A5/A2
      WRITE (6,90) A, A3, SHI1
  90  FORMAT (1HO, '  INC.ANGLE =  ',F6.3, ' ZETAS =  ',F6.3,
     1'  SHI1  =    ',F10.3)
      GO TO 10
  100 END
'XQT
64,50000
```

Computer Program for the Theoretical Curve of Figure 4 -7 (partial)

```
'RUN VB,305168,BHANTHUMNA,1,100
'PASSWD 17B9FI
'FOR,IS MAIN
      READ(5,7)A
  7   FORMAT(F12.8)
      D1 = 1.4889679
      D2 = 1.4929732
      D3 = 1.4968934
      D4 = 1.5041322
      D5 = 1.5097313
      D6 = 1.5127767
      D7 = 1.5131219
      D8 = 1.5125449
  10  XINC = 0.1
      A = A+XINC
      PI = 3.1416
      B1 = 1.6260
      B2 = 1.494305
      B3 = 1.670
      B4 = (48.8*PI)/180.0
      IF (A-5.0)12,12,15
  12  YINC = 0.000079328
      D1 = D1+YINC
      DX = D1
      GO TO 80
  15  IF (A-10.0) 16,16,25
  16  YINC = 0.00007878
      D2 = D2 + YINC
      DX = D2
      GO TO 80
  25  IF (A-20.0) 26,26,35
  26  YINC = 0.00007256
      D3 = D3+YINC
      DX = D3
      GO TO 80
  35  IF (A-30.0) 36,36,45
  36  YINC = 0.00005881
      D4 = D4+YINC
      DX = D4
      GO TO 80
  45  IF (A- 40.0) 46,46,55
  46  YINC = 0.00003050
      D5 = D5+YINC
      DX = D5
      GO TO 80
  55  IF (A-44.3) 56,56, 65
  56  YINC = 0.00000793
      D6 = D6+YINC
      DX = D6
      GO TO 80
  65  IF (A-50.0) 66,66,75
  66  YINC = 0.00001034
      D7 = D7-YINC
      DX = D7
      GO TO 80
  75  IF (A-60.0) 76,76,100
  76  YINC = 0.00004607
      D8 = D8-YINC
      DX = D8
  80  AX = A*PI/180.0
      A1 = SIN(AX)
      A2 = COS(AX)
      A3 = (B1*A1)/B2
      A4 = SQRT(1.0-(A3*A3))
      A5 = (B1*A1)/DX
      A6 = SQRT(1.0-(A5*A5))
      A7 = (B1*A1)/B3
      A8 = ASIN((B1*A1)/B2)
      A9 = ASIN((B1*A1)/DX)
      A10 = ASIN((B1*A1)/B3)
      FLT = (2.0*A2*A3)/(A1*A4 + A2*A3)
      FNLS = (SIN(B4-A8))/((B2)**2.0-(DX)**2.0)
      FNLT = (1.0/(B1*DX))*(A3*A5*A5*SIN(A9+B4))/(A7*SIN(A9+A10)
     1*COS(A9-A10)*SIN(A8+A9)) -(B2/DX)*(SIN(B4-A8))/((B2)**2.0-
     1(DX)**2.0)
      SHI1 = B1*(FLT**4.0)*(FNLS**2.0)*A4/A2
      SHI2 = DX*(FLT**4.0)*(FNLT**2.0)*A6/A2
      SHI = SHI1 + SHI2
      WRITE (6,90) A,DX, SHI1, SHI2, SHI
  90  FORMAT (1H0, '   INC, ANGLE =  ',F6.3, '   INDEX ERAY =  ',F10.7,
     1'   SHI1 =  ',F12.3, '   SHI2 =  ',F12.3,'   SHI =  ',F12.3)
      GO TO 10
 100  END
'XQT
0.000000
'FIN
'FIN
```

Computer Program for the Theoretical Curve of Figure 4 - 9

```
'RUN VB,30516802,BHANTHUMNA,3,200
'FOR,IS MAIN
      READ(5,7)A
    7 FORMAT (F8.5)
   10 XINC = 0.1
      A = A+XINC
      PI = 3.1416
      IF(A-25.0)12,12,100
   12 AX=A*PI/180.0
      Z=SIN(AX)
      A1=Z
      Z=COS(AX)
      A2=Z
      Z=(1.0/1.4942)*A1
      A3=Z
      Z=SQRT(1.0-A3*A3)
      A4=Z
      FNLT =(1.4942/1.4712)*A4*(1.0/((1.4942*A4)**2.0-(1.4712)**2.0))
     1+(1.0/1.4712)
      FLT= (2.0*A2*A3)/(A1*A4+A2*A3)
      FNLS = (1.0/((1.4942*A4)**2.0-(1.4712)**2.0))
      SHI1 = (FLT**4.0)*(FNLT**2.0)/A2
      SHI2 = (FLT**4.0)*(FNLS**2.0)/A2
      SSHI = SHI1 + SHI2
      WRITE(6,20) A, SSHI, SHI1, SHI2
   20 FORMAT(1H0,' INCIDENT ANGLE ='F8.5,  'TOTAL INTENSITY OF SHG = '
     1F10.3,   'SHI1 = 'F10.3,   'SHI2 = ' F10.3)
      GO TO 10
  100 END
'XQT
0.00000
'FIN
```

Computer Program for the Theoretical Curve of Figure 4 - 10

References

1. T. H. Maiman, Nature, 187, 493 (1960).
T. H. Maiman, R. H. Hoski s, I.J. D'Haenens, C. K. Asawa and V. Evtuhov, Phys. Rev. 123, 1511 (1961).

2. P. A. Franken, A. E. Hill, C. W. Peters and G. Weinereich, Phys. Rev. Lett., 7, 118 (1961).

3. N. Bloembergen, "Nonlinear Optics", (W. A. Benjamin, New York, 1965).

4. P. N. Butcher, "Nonlinear Optical Phenomena", Ohio State University Press, 1965.

5. P. A. Franken and J. F. Ward, Rev. Mod. Phys., 35, 23 (1963).

6. N. Bloembergen, "Topics in Quantum Electronics", (Lecture in Theoretical Physics Vol. 5, 218, 1963 Interscience, New York).

7. P. S. Pershan, "Nonlinear Optics", Progress in Optics Vol. 5, 85, (1966). (Interscience, New York, Amsterdam North Holland).

8. R. W. Minck, R. W. Terhune and C.C. Wang, Appl. Opt. 5, 1595 (1966).

9. N. Blombergen, Amer. J. Phys. 35, 989 (1967).

10. J. Ducuing, "Nonlinear Optical Processes" in Proceedings of the International School of Physics "Enrico Fermi"Quantum Optics.

11. J. A. Armstrong, N. Bloembergen, J. Ducuing and P. S. Pershan, Phys. Rev. 127, 1918 (1962).

12. N. Bloembergen and P. S. Pershan, Phys. Rev. 128, 606 (1962).

13. S. A. Akhmanov and R. V. Khokhlov, "Problemy Nyelineynoy Optiki" (Akad. Nank USSR, Moscow, 1964).

14. D. A. Kleinman, Phys. Rev. 126, 1977 (1963); ibid 128, 1761, (1962).

15. P. S. Pershan, Phys. Rev. 130, 919 (1963).

16. J. A. Giordmaine, Phys Rev. A 138, 1599 (1965).

17. G. L. Lamb, Jr., Rev. Mod. Phys. 43, 99 (1971).

18. M. Born and E. Wolf, "Principles of Optics", 4th edition, Pergamon Press.

19. G. Mayer and F. Gires, C. R. Acad. Sc., Paris 258, 2039 (1964).

20. R. W. Terhune, P. D. Maker and C. M. Savage, Phys. Rev. Lett. 8, 404 (1962).

21. C. C. Wang, Phy. Rev. A. 152, 149 (1966).

22. S. L. McCall and E. L. Hahn, Phys. Rev. 183, 457 (1969).

23. S. R. Hartmann, "Generation and Relaxation of Photon Echo" Proceedings of International School of Physics "Enrico Fermi" Quantum Optics.

24. I. D. Abella, N. A. Kurnit and S. R. Hartmann, Phys. Rev., 141, 391 (1966).

25. J. Ducuing and N. Bloembergen, Phys. Rev. Lett., 10, 474 (1963).

26. N. Bloembergen and J. Ducuing, Phys. Rev. Lett., 6, 5 (1963).

27. R. K. Chang and N. Bloembergen, Phys. Rev., 144, 775 (1966).

28. N. Bloembergen and C. H. Lee, Phys. Rev. Lett., 19, 835 (1967).

29. N. Bloembergen, H. J. Simon and C. H. Lee, Phys. Rev. 181, 1261 (1969).

30. P. P. Bey, J. R. Giuliani and H. Rabin, Phys. Rev. 184, 849 (1969).

31. C. C. Wang and E. L. Baarden: Phys Rev. 185, 1079 (1969); ibid B 1, 2827 (1970).

32. W. K. Burns and N. Bloembergen, Phys. Rev., B. 4, 3437 (1971).

33. J. A. Giordmaine, Phys, Rev. Lett. 8, 19 (1962).

34. P. D. Maker, R. W. Terhune, M. Nisenoff, and C. M. Savage, Phys. Rev. Lett. 8, 21 (1962).

35. G. D. Boyd, A. Ashkin, J. M. Dziedzic, and D. A. Kleinman, Phys Rev. A 137, 1305 (1965).

36. R. C. Miller, D. A. Klienman and A. Savage, Phys. Rev. Lett. 11, 146-149 (1963).

37. G. D. Boyd, R. C. Miller, K. Nassau, W. L. Bond, and A. Savage, Appl. Phys. Lett. 5, 234 (1964).

38. J. E. Gensic, L. G. Vanuitast, S. Singh. H. J. Levinstein, and W. A. Bonner, Appl. Phys. Lett. 11, 161, (1967), ibid 12, 224 (1968).

39. S. K. Kurtz, T. T. Perry and J. G. Bagman Jr., Appl. Phys. Lett 12, 186 (1968).

40. G. Nath and S. Haussuhe, Appl. Phys. Lett. 14, 154 (1969). Phys. Lett. 294, 91 (1969).

41. A. Ashkin, G. D. Boyd, and J. M. Dziedzic, Phys. Rev. Lett. 11, 14 (1963).

42. R. C. Miller, G. D. Boyd and A. Savage, Appl. Phys. Lett. 6, 77 (1965).

43. P. K. Tier, Jour. Appl. Phys. 29, 1347 (1958).

44. G. D. Boyd, R. C. Miller, K. Nassau, W. L. Bond and A. Savage, Appl. Phys. Lett. 11, 234 (1964).

45. A. Askin, G. D. Boyd, and D. A. Klienman, Appl. Phys. Lett. 6, 179 (1965).

46. Shinsuke Umegaki, Seiichi Yabumoto, and Shun-ichi Tanaka, Appl. Phys. Lett. 21, 400 (1972).

47. R. L. Aggrawal, B. Lax, and G. Favrot, Appl. Phys. Lett. 22, 329 (1973).

48. P. D. Maker and R. W. Terhune, Phys. Rev. A 37, 801 (1965).

49. P. D. Maker, R. W. Terhune, and C. M. Savage, Third Conference on Quantum Electronics, Paris, 1963 (Columbia University Press, 1964).

50. P. P. Bey, J. F. Giuliani, and H. Rabin, Phys. Rev. Lett. 19, 819, (1967). IEEE Jour. Quant. Electr. QE-4, 932, (1968).

51. R. K. Chang, and L. K. Galbraith, Phys. Rev., 171, 993, (1968).

52. P. P. Bey, J. F. Giuliani and H. Rabin, Phys. Lett. 26A, 128, (1968).

53. J. F. Ward and G. H. C. New, Phys. Rev., 185, 57 (1969).

54. J. F. Young, G. C. Bjorklund, A. H. Kung, R. B. Miles, and S. E. Harris, Phys. Rev. Lett., 27, 1551 (1971).

55. R. B. Miles and S. E. Harris, IEEE Jour. Quant. Electr. QE-9, 470 (1973).

56. A. J. DeMaria, D. A. Stetser, and H. Heynau, Appl. Phys. Lett., 8, 174 (1966).

57. A. J. DeMaria, D. A. Stetser, and W. H. Glenn, Jr., Science, 156, 1557 (1967).

58. A. J. DeMaria, "Picosencond Laser Pulse", Progress in Optics, Vol. 9, 33 (1971).

59. A. J. DeMaria, W. H. Glenn, Jr., M. J. Brienza, and M. E. Mack, Proc. IEEE, Vol. 57, 2 (1969).

60. P. E. Smith, Proc. IEEE, Vol. 58, 1342 (1970).

61. H. W. Mocher and R. J. Collins, Appl. Phys. Lett. 7, 270 (1965).

62. J. A. Armstrong, Appl. Phys. Lett. 10, 16 (1967).

63. J. A. Giordmaine, D. M. Rentzpis, S. L. Shapiro and K. W. Wecht, Appl. Phys. Lett. 11, 216 (1967).

64. P. M. Rentzepis and M. A. Dugnay, Appl. Phys. Lett. 11, 218 (1967).

65. H. P. Weber, Phys. Lett., 274, 321 (1968).

66. J. R. Klauder, M. A. Dugnay, J. A. Giordmaine and S. L. Shapiro, Appl. Phys. Lett. 13, 174 (1968).

67. N. G. Basov, P. G. Kryukov, V. S. Letokhov and Yu V. Senatskii, IEEE Jour. Quant. Electr. QE-4, 606, (1968).

68. V. S. Letokhov, Sov. Phys. - JETP, 28, 1026 (1969).

69. T. I. Kuznetosova, Sov. Phys. - JETP, 28, 1303 (1969).

70. H. E. Rowe and T. Li, IEEE Journ. Quant. Electr. QE-6, 49 (1970).

71. R. H. Picard and P. Schweitzer, Phys. Rev. A 1, 1803 (1970).

72. S. L. Shapiro and M. A. Dugnay, Phys. Lett. 284, 698 (1969).

73. P. M. Rentzepis, C. J. Mitschele and A. C. Saxman, Appl. Phys. Lett. 17, 122, (1970).

74. M. A. Duguay, J. W. Hansen and S. L. Shapiro, IEEE Journ. Quant. Electr. QE-6, 725 (1970).

75. H. P. Weber, Journ. Appl. Phys., 39, 6041 (1968).

76. J. A. Giordmaine, M. Maier, and W. Kaiser, Phys. Rev. Lett. 17, 1275 (1966).

77. E. B. Treacy, Appl. Phys. Lett. 14, 112 (1969).

78. R. C. Eckardt and C. H. Lee, Appl. Phys. Lett. 15, 425 (1969).

79. S. Jayaraman and C. H. Lee, Appl. Phys. Lett. 20, 392 (1972).

80. S. Jayaraman and C. H. Lee, Bull. Am. Phys. Soc., Series II Vol. 18, No. 1, p. 91 (1973). (To be published in Journ. Appl. Phys.).

81. S. Jayaraman, Thesis, University of Maryland (1972).

82. A. Yariv, "Introduction to Optical Electronics", Holt, Rinehart, and Winston, Inc., New York, (1971).

83. R. J. Glauber, Phys. Rev. 131, 2766 (1963).

84. S. Singh, "Hand Book of Laser", Nonlinear Optical Material, 1971.

85. W. E. Forsythe, Smithsonian Physical Tables, (Smithsonian Institute, Washington, D. C., 1965), 8th. rev. ed. p. 468.

86. F. A. Jenkins and H. E. White, Fundamentals of Optics (McGraw-Hill Book Co., Inc., New York, 1957), 3rd. ed., p. 468.

87. J. Ducuing and N. Bloembergen, Phys. Rev., 133, A1493 (1964).

88. C. H. Lee Thesis, Harvard University (1967)

89. R. Fisher, Phys. Stat. Sol. 19, 757 (1967)

90. A. Savage, Jour. Appl. Phys 36, 1469 (1967)

91 H. Shih and N. Bloembergen, Phys. Rev. A. 3, 412, (1971)

92. H. J. Simon Thesis, Harvard University (1969)